Informes Técnicos Ciemat 1535
Septiembre, 2024

THERMO-HYDRAULIC TESTS WITH WYOMING BENTONITE AT HIGH TEMPERATURE (PROJECT EURAD-HITEC)

Villar Galicia, M.ª V.
García Herrera, G.
Iglesias Martínez, R.J.
Gutiérrez Álvarez, C.
Martín Martín, P.L.
Barcala Riveira J.M.

GOBIERNO DE ESPAÑA
MINISTERIO DE CIENCIA, INNOVACIÓN Y UNIVERSIDADES
Ciemat
Centro de Investigaciones Energéticas, Medioambientales y Tecnológicas

Publication available in catalog of official publications

ISSN: 2695-8864
NIPO: 152-24-009-2

Edition and Publication:
Editorial CIEMAT
Avda. Complutense, 40 28040-MADRID
e-mail: editorial@ciemat.es
Editorial news

ACKNOWLEDGEMENTS

This work has been financed by the European Union's Horizon 2020 Research and Innovation Programme under grant agreement No 847593 and by ENRESA through the ENRESA-CIEMAT agreement 10522.

TABLE OF CONTENTS

LIST OF FIGURES

LIST OF TABLES

1 INTRODUCTION

The thermo-hydraulic tests described in this report aimed at simulating in the laboratory the conditions of barrier materials during operation. These tests provide online and postmortem results that are very useful for the verification and validation of models of thermo-hydro-mechanical (THM) behaviour. The new tests started in the framework of HITEC had the particularity that the heater temperature was set at 150 °C. Two tests were carried out with the same initial and boundary conditions, except that one of them was saturated with glacial water (cell HT1) and the other one with saline water (cell HT2). The buffer material used was the Wyoming-type bentonite Bara-Kade.

These tests were performed in the same setup used in a previous research, the MAB (Mineralogical Alteration of Bentonite) project, carried out in collaboration with Amphos 21 for Posiva, the Finnish nuclear waste agency. In the framework of this project several THM tests were performed, some of them with Wyoming bentonite and using as hydration water the same solutions as in cells HT1 and HT2. However, in those tests the heater temperature was set to 110 °C. In particular, two of these tests, one of them in which glacial water was used as saturating fluid (cell C5) and another one with saline water (cell C4), had the same duration as tests HT1 and HT2 (Villar et al. 2020), hence the only difference between the two sets of tests (C4-C5 and HT1-HT2) was the heater temperature. Accordingly, the information provided by tests C4 and C5 can be used as a baseline to assess the effect of elevated temperature on the hydro-mechanical behaviour of compacted bentonite.

2 EXPERIMENTAL SETUP

The two tests, HT1 and HT2, were mounted in an experimental setup (Figure 1) previously prepared for a research financed by Posiva and carried out in collaboration with Amphos 21 (Idiart et al. 2017). The bentonite was compacted in stainless steel cells instrumented with four capacitive sensors (measuring relative humidity and temperature, RH/T sensors) placed at three different levels inside the bentonite and three radial stress sensors (PT sensors) placed at the bentonite/cell contact. The temperatures on the cells' surface were measured with thermocouples. At the bottom of the cells a stainless steel plane heater was placed. The upper part of the cell included a cooling chamber through which a cooling fluid circulated at a temperature of 20 °C. Hydration took place through a stainless steel porous filter placed on top of the sample. The hydration solution came from flasks hanged 1 m above the cells. The weight of the flask was continuously measured, which allowed to assess the cell water intake. A detailed description of each of these components, modified from Martín et al. (2017), is given in the following sections. The appearance of the cells during operation is shown in Figure 2.

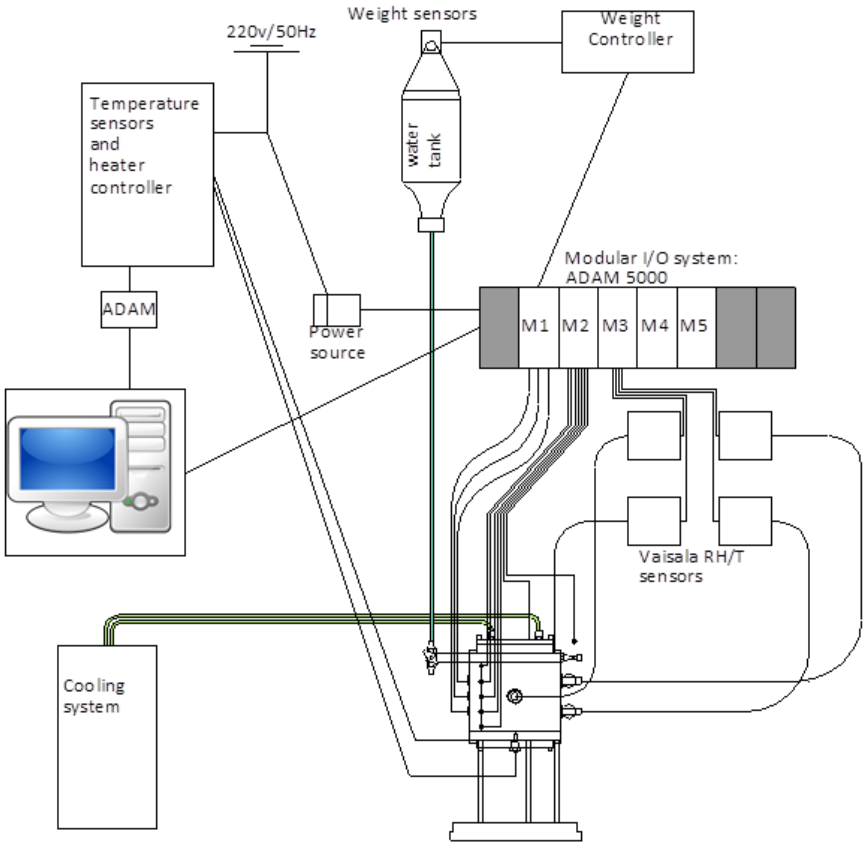

Figure 1. Experimental setup for the TH tests

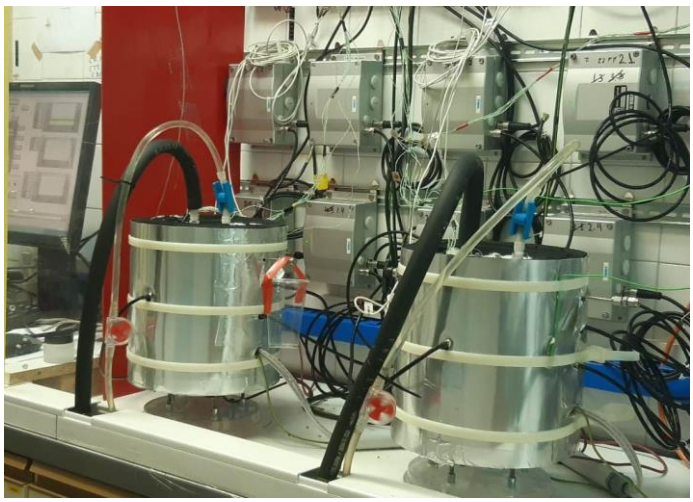

Figure 2. HT-1 and HT-2 cells wrapped with isolating material during operation

2.1 CELLS

The cylindrical cells were made out of stainless steel, with internal dimensions of 10x10 cm (HxD). Figure 3 and Figure 4 show blueprints of the cells, in which the location of the RH/T and PT sensors is indicated. Before assembling the cells, the material was cleaned with soap and water. The disposition of the cells during operation was vertical, with the system of hydration and refrigeration in the upper part, and the heater at the bottom. Hence, to keep the cells upright a system was designed in which the bottom of the cell was fixed to a methacrylate disc by means of equally-spaced threaded rods. These threaded rods also allowed the horizontal levelling of the cells.

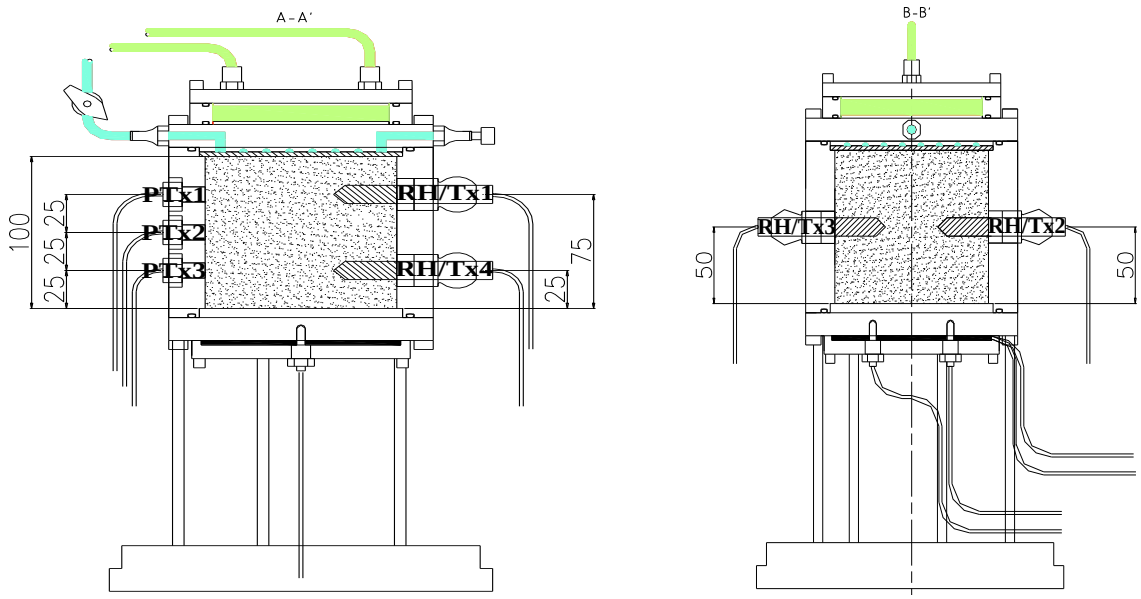

Figure 3. Longitudinal cross-sections of the cells with the sensors installed (x stands for the cell number: 1 or 2)

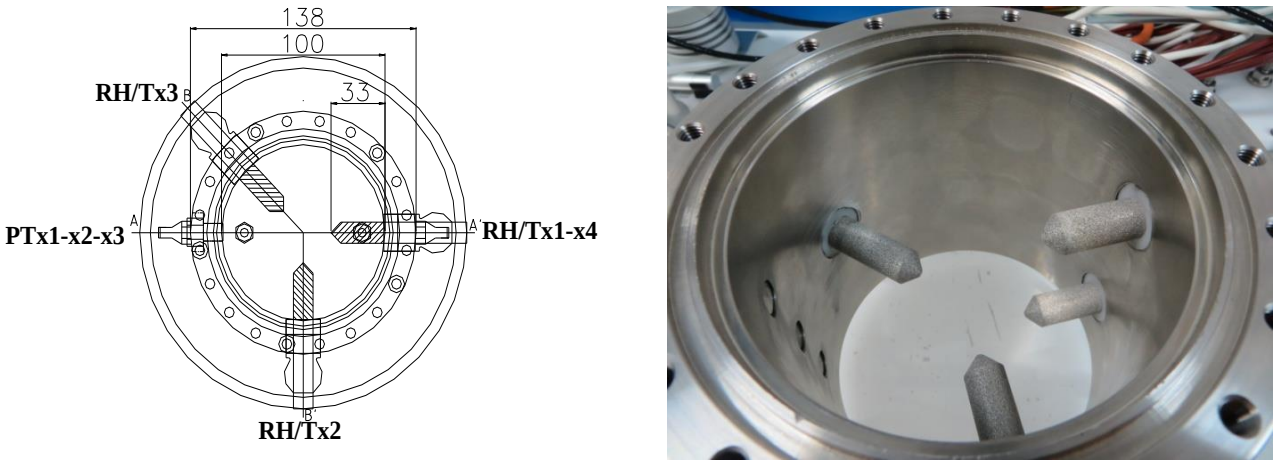

Figure 4. Cross-section of a cell, with indication of the location of the RH/T and pressure sensors (left), and internal view of the cell with the sensors inserted through the acetal rings (x stands for the cell number: 1 or 2)

Threaded hollow pieces of white acetal were installed in the RH/T sensors' inlets (Figure 5). These pieces were aimed to ensure a horizontal sensor socket and a good connection between the inner walls of the cell and the area where these sensors were located, giving continuity to the internal walls of the cell and providing thermal insulation.

Figure 5. Acetal threaded ring once inserted in the sensors' inlet

2.2 SENSORS

Each cell was instrumented with four RH/T transmitters inserted at three different levels inside the bentonite block and three total pressure sensors (PT) placed at the contact between the cell wall and the bentonite at the same levels as the RH/T sensors (Figure 3). These parameters (i.e. RH, T and PT) were measured as a function of time during the experiments. Additionally, the external temperatures (T, thermocouples), the mass of injected water and the temperature/power supplied at the heating surface was also measured. Table 1shows the names given to the sensors and their exact location.

INSIDE THE CELL			CELL SURFACE		
Reference	Distance to heater (cm)	Distance to cell axis (cm)	Reference	Distance to heater (cm)	Distance to cell axis (cm)
RH/T-x1	7,5	1.5-5.0	Tx5	10,0	6,9
RH/T-x2	5,0	1.5-5.0	Tx6	7,5	6,9
RH/T-x3	5,0	1.5-5.0	Tx7	5,0	6,9
RH/T-x4	2,5	1.5-5.0	Tx8	2,5	6,9
PT-x1	7,5	5,0	Tx9	1,2	6,9
PT-x2	5,0	5,0	Tx10	0,0	6,9
PT-x3	2,5	5,0	Tx11	14,5	2,5

Table 1. References and location of sensors in the cells (x stands for the cell reference: HT1 or HT2) inside de cell (left) and in cell surface (right)

2.2.1 RH/T TRANSMITTERS

The cells were instrumented with capacitive-type sensors placed inside the clay at three different levels (25, 50 and 75 mm from the heater, Figure 4). The transmitters used were VAISALA HMT337 (Figure 6), which include a humidity sensor (HUMICAP®) that changes its dielectrical characteristics with extremely small variations in humidity (capacitive-type RH sensor). They include also a temperature sensing element (Pt 100). The accuracy of the humidity sensor is ±1 % over the range 0-90 percent RH and ±2 % over the range 90-100 percent RH. The sensors are protected by cylindrical stainless steel filters (HM47280SP, length 41.5 mm). The Vaisala sensors integrate the measurement in a volume of 3.6 cm^3, 1.2 cm in the axial direction of the cell.

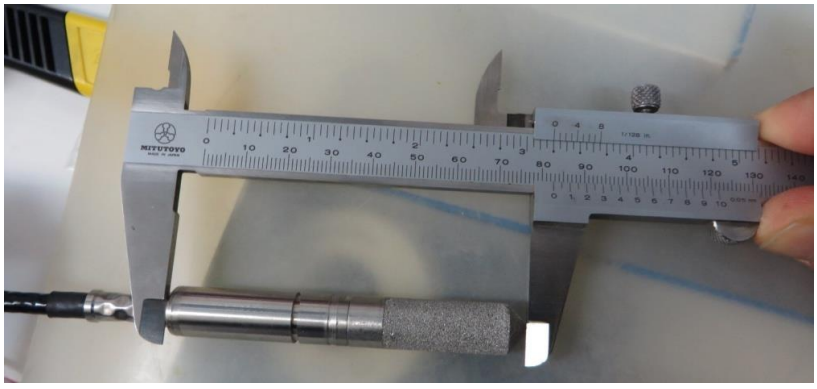

Figure 6. Vaisala HMT337 relative humidity sensor

In order to fit the RH/T sensors in place, cable glands from high-grade stainless steel SKINTOP® INOX were used (Figure 7). These cable glands (SS-316L: gland body and cap nut; silicone: sealing ring and O-ring; M20x1: connecting; IP68-10 bar; temperature range -40 °C

up to +100 °C) allowed to modify the installation and fix subsequent location problems (Figure 8).

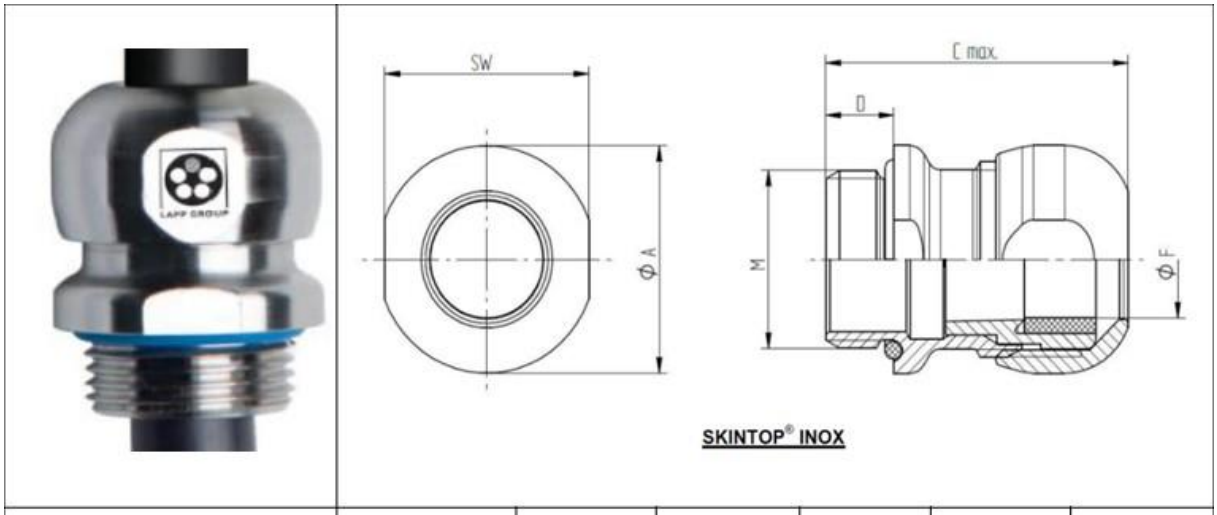

Dimensions in mm	SW	Ø A	C max.	D	Ø F	O-ring
	20	25.6	35.5	7	7.0-13.0	17x2

Figure 7. SKINTOP® INOX M20x1.5 cable gland

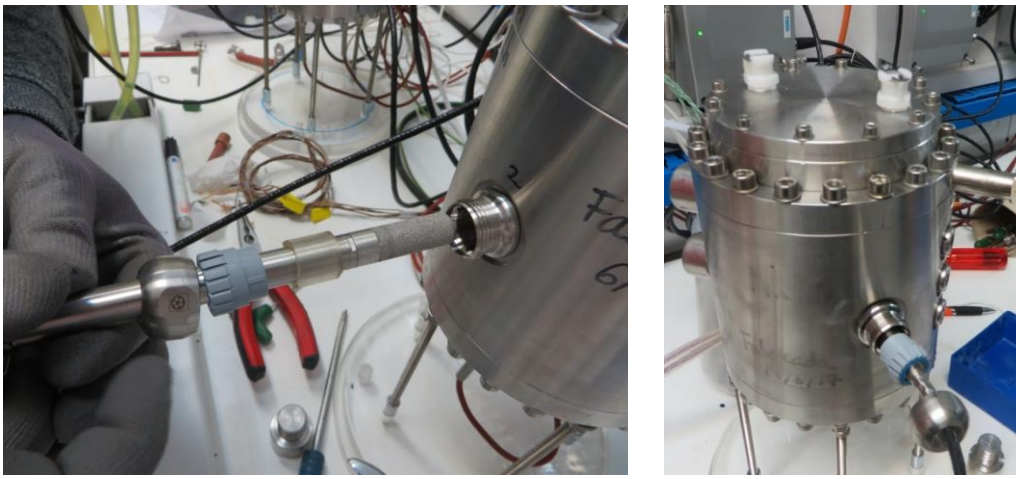

Figure 8. Insertion of RH/T sensor with cable gland

2.2.2 PRESSURE SENSORS

Radial pressures on the lateral surface of the bentonite block were measured at the same distances from the heater as those for the RH/T transmitters (i.e. 25, 50 and 75 mm, Figure 4). Two types of miniature pressure sensors with isolated diaphragm were installed, depending on the distance to the heater. The closer one was a XPC10 high temperature sensor, the two others were XPM10. Their characteristics are shown in Table 2 and their cross-section and dimensions are shown in Figure 9.

Both types are designed to measure static and dynamic pressure under a wide variety of conditions and are suitable for corrosive liquids and gases in a wide variety of harsh environments. They are made of stainless steel SS316L and their range is 0-100 bar with amplified outputs.

Sensor	XPC10-M-A1-100BS-/Z35	XPM10-A2-100BS-/ET1
Power supply	10 to 30 Vdc	±12 to ±18 Vdc
Sensitivity “FSO”	4 V ±0.2 V	5 V ±0.2 V
Zero Offset	0.5 V ±0.2 V	0 V ±0.2 V
Non-Linearity	±0.25%FS	±0.25%FS
Hysteresis	-	±0.25%FS
Repeatability	-	±0.2%FS
Operating Temperature (OTR)	-40°C to 220°C	-40 to 80°C
Compensated Temperature (CTR)	20 to 120°C	-20 to 100°C

Table 2. Characteristics of the pressure sensors

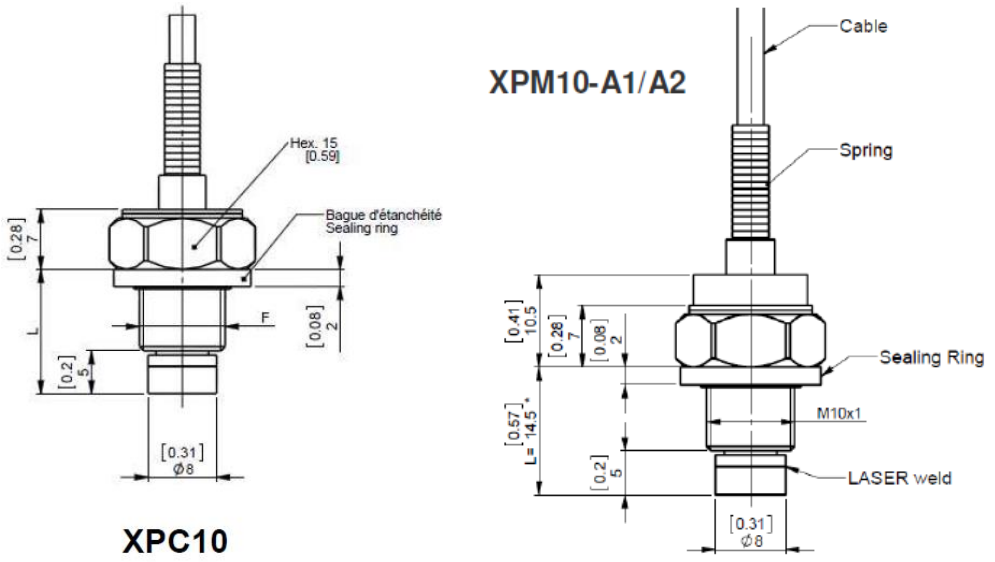

Figure 9. Blueprints of the pressure sensors

2.2.3 EXTERNAL THERMOCOUPLES

The external surface temperatures of the cell were measured by thermocouples fitted by an adhesive film. The thermocouples were welded on a cupper disk (6.3 mm Ø). Seven thermocouples were placed on the external surface of the cell, in contact with metallic elements (Figure 10). Their exact location is given in Table 1. Another thermocouple was placed between the two cells, at about 10 cm above them, with the aim of measuring the temperature of the laboratory close to where the cells were located. All thermocouples were type "K" class

1 (standard tolerance, -40 °C<*T*<375 °C, ±1.5 °C). They were connected to the data acquisition system through a thermocouple input module (ADAM-5018) that applied the cold junction compensation (CJC). The CJC temperature was measured by a thermistor in the lower channel of the module.

The thermocouples were not calibrated before installation but they were under specifications.

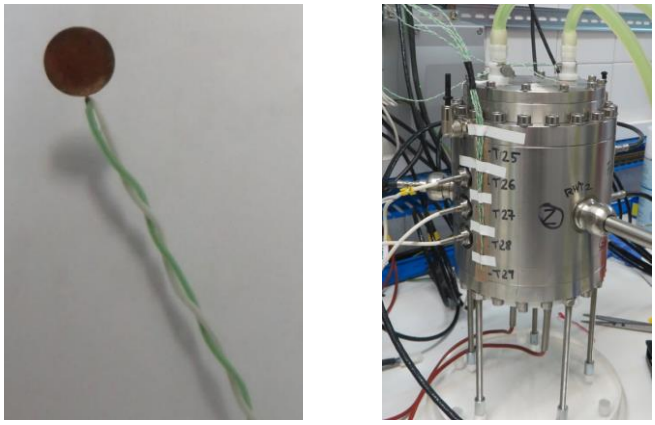

Figure 10. Appearance of the thermocouples (left) and of them stuck to the cell surface with their references marked on it (right)

2.3 HYDRATION SYSTEM

The hydration system was designed to supply water for hydration of the bentonite and at the same time measure the water intake. Each cell had its own independent hydration system. The hydration water was injected to the cells through the upper hydration line (blue lines in Figure 3) that crossed the upper lid of the cell. This lid has a continuous groove machined on its down surface to help a better water distribution (Figure 11), which was further facilitated by the use of a stainless steel porous filter placed on top of the sample. The filters were ultrasound-cleaned before their use.

Figure 11. Bottom surface of the upper lid of the cell with machined groove and water inlets

The water was taken from a low-pressure bladder accumulator manufactured in stainless steel by OLAER (EBV 1L-40B/00). The deposit had 1 L of capacity and could be recharged and pressurized with nitrogen up to 40 bar (Figure 12). The accumulator was filled by counter-pressure and the bladder (filled with air) was deformed elastically. Initially the injection pressure came from the elastic behaviour of the rubber bladder. This value was approximately 0.1 bar, since no additional pressure was applied. The hydration circuit was equipped with valves that allowed cutting off the water supply to the cell in order to avoid the system discharge in case of failures or modifications. All the parts of the system in contact with water were made of stainless steel AISI 316, including the tube connecting the accumulator to the cell.

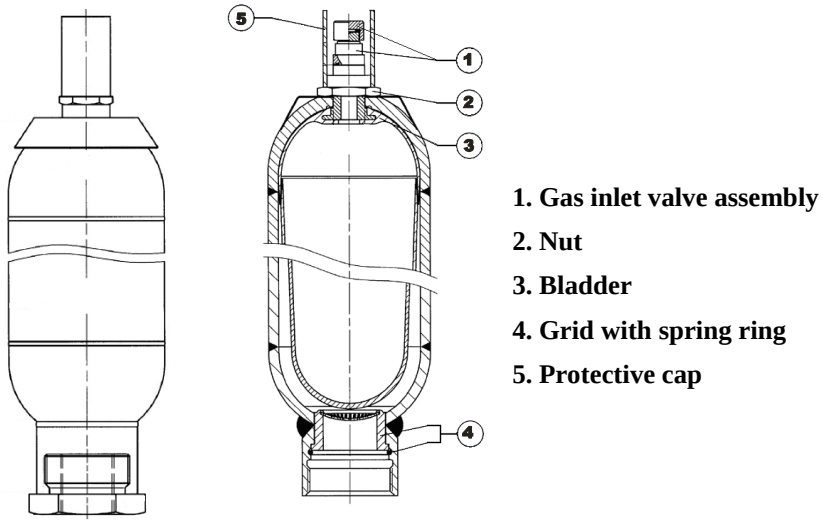

Figure 12. Pressure bladder accumulator used as deposit and pressurising system for the hydration water

Figure 13. Hydration system: accumulators, load cells and amplifiers

The amount of water entering the system was measured by weighing the accumulators. The accumulators hanged from load cells to control the mass of the water supplied to the cells. The weighing system for each cell consisted of the following elements (Figure 13):

- A 7-kg load cell HBM SP4MC6MR/7 (6-wire, 2 mV/V, precision 0.0001 kg C6MR, protection IP67).
- Measurement amplifier/indicator HBM MVD2510 (0.1 % precision) with analogue output (from 0 to 10 VDC) directly connected to the data acquisition system. The water intake was measured from the analogue output of the weighing amplifier of the hydration system.

2.4 HEATING SYSTEM

The heating system for each cell consisted of a circular heater and corresponding monitoring and control systems (HCS). The heater maintained a constant temperature (150 ˚C) as homogeneous as possible. The system was designed in such a way that, if a failure happened during operation, it would be possible to perform repairs/replacements of the heating elements once the system cooled down.

2.4.1 HEATER

The heater was in direct contact with the lower lid of the cell. The electric heating element (Figure 14a), a metal shielded resistance MEYER 0816 (225 W, 230 V, 100 mm Ø, 3.5 mm max thick, with silicone rubber lids), was sandwiched between a Teflon cover, which protected it, and the lower lid of the cell. The electrical supply was grounded.

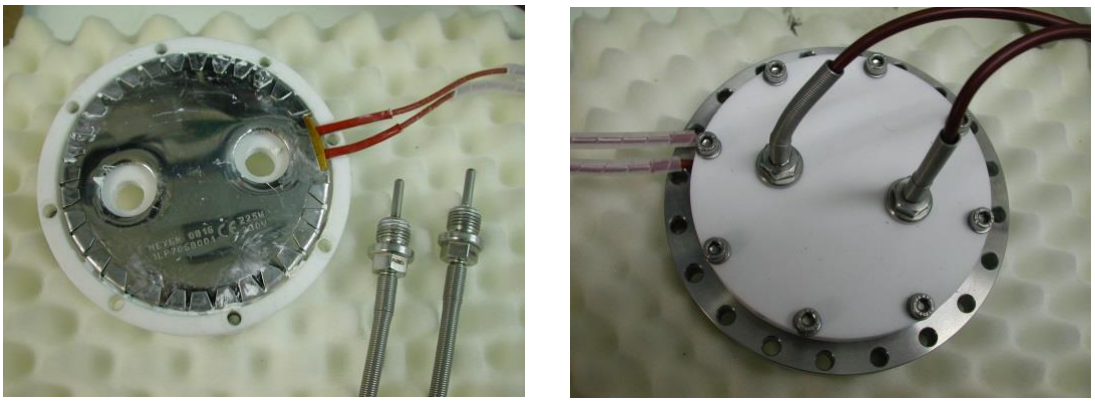

Figure 14. Heater: a) heating elements, temperature sensors and cover; b) assembled set

Two temperature sensors were inserted in the heating surface, through holes in the heating element and in the Teflon cover (Figure 14). One sensor provided the temperature value for the loop control modules, the other one did the same for the redundant individual controller. They were Graff 4-wire Pt100, with SS body (1/4G, 6mm Ø, 30 mm length) and silicone rubber lids. Its maximal working temperature was 200 ˚C.

The heating surface in contact with the cell was treated with a conductive paste to better transmit the heat towards the steel in contact with the bentonite. Sensor inserts received a similar treatment.

Connections of the power supply and of the signals from sensors, as well as the assemblage, were performed carefully and sequentially: 1) installation of the resistances in the protective cover, 2) application of the conductive paste, 3) cover bolted to the cell, 4) installation of the temperature sensors, 5) connection of the sensors to the HCS and 6) connection of the power supply. In each step, the functioning of the assembled components was verified.

The ends of the resistors and temperature sensor signal cables, each appropriately identified, were prolonged and passed through protective conducts to the connection box of the HCS.

2.4.2 HEATING CONTROL SYSTEM (HCS)

It was based on a controller (with 2 loops) that measured the temperatures in each cell (at the control point) and controlled that the temperature value was equal to the set-point value. The controller made the calculations, regulated the power by the auxiliary electronics and sent the temperature and instantaneous power data as demanded by the data acquisition system (Figure 15).

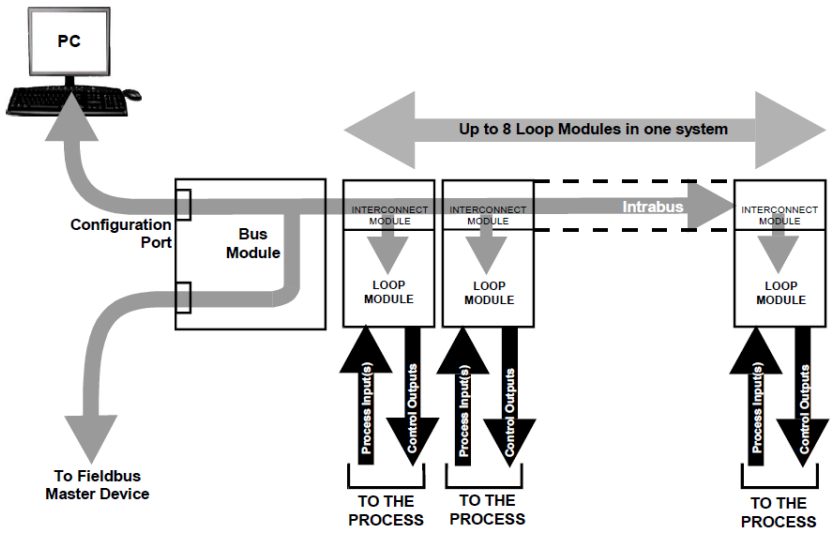

Figure 15. Typical MLC 9000+ system block diagram

The HCS consisted of a main controller, a secondary controller, a cabinet, temperature sensors, an electronic power regulation system and a heater protection system that are described below.

2.4.2.1 MAIN CONTROLLER

The temperature of the heaters was controlled by a WEST MLC9000+, a DIN-rail-mounted multi-loop PID control system that consisted of a single Bus Module and any combination of up to 8 Loop Modules (only 2 used in this setup). The Bus Module was a supervisory module that provided power to the Loop Modules and contained a back-up of the system configuration data. It also managed the communications with external devices. The Loop Modules were independent control modules managed by the Bus Module.

The WEST MLC9000+ controller used was composed by three modules: a bus module BM220-MB (24V supply, PC port and RS485 port installed with Modbus firmware, Figure 16 a) and two multiple loop modules Z4620 (four loops, universal inputs, six SSR outputs, Figure 16 b, c). The controller WEST MLC-9000+ (Figure 15) received the set-point values from the test control (through the configuration port) and switched to operation in an autonomous mode, transforming the nominal control parameters to the power supplied to the heater during automatic operation. The MLC9000+ sent data of temperature and power consumed to the computer of the experiment through an RS485 line with Modbus protocol.

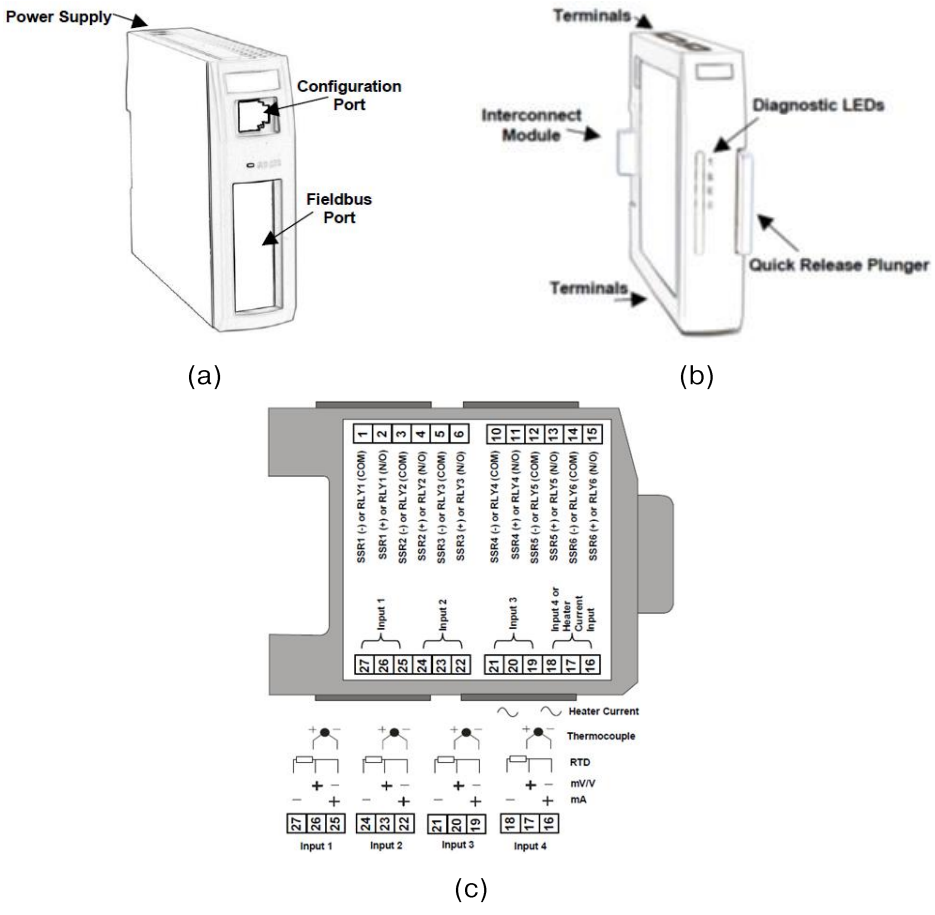

Figure 16. MLC9000+ modules: a) Bus module BM220; b) multiple loop module Z4620 and c) electrical connections

2.4.2.2 SECONDARY CONTROLLER

In addition, a WEST CAL ET2011 controller (PT100 input, Output 230VAC, 8A relay) was installed as backup in case of main controller failure (in order to prevent the temperature to go down below 80 ˚C).

2.4.2.3 CABINET

These controllers, along with their power supply (24 VDC), 16 relays (CG, model RGS1A23D25KKE, output 230 VAC, control voltage 3-32 VDC, operational current 25 AAC), fuses (1 and 16 A) and switches were arranged in an instrumentation cabinet fixed on the laboratory wall (Figure 17). All signals from heater temperature sensors (16) and power supply lines (8) were connected through this cabinet (Figure 18). This setup allows to operate 8 cells simultaneously, but only 2 of them were used in the setup for these tests.

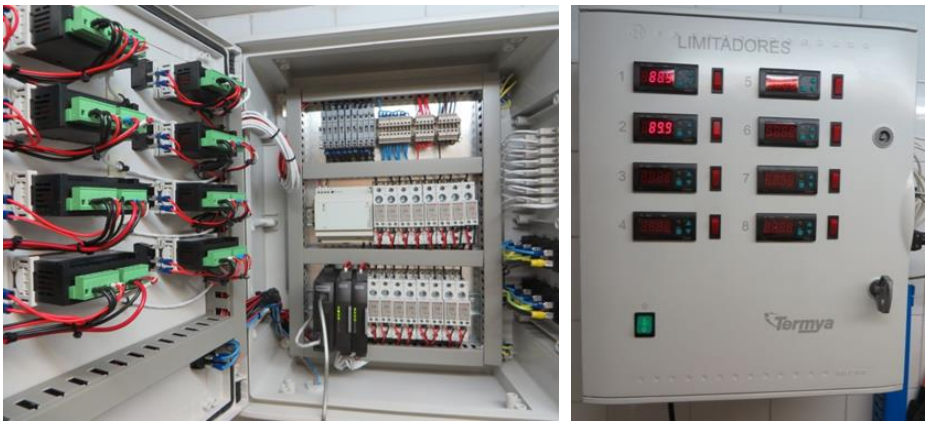

Figure 17. HCS cabinet: internal and external views

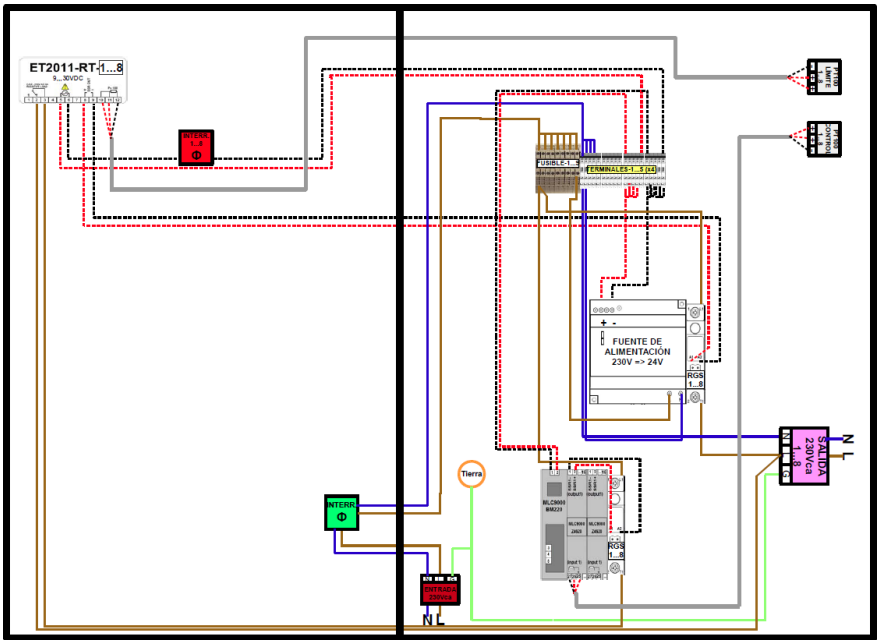

Figure 18. Schematic design of each cell connection in the HCS cabinet

2.4.2.4 TEMPERATURE SENSORS

The sensors on the heating surface provided the temperature value for the loop control modules and individual controllers. They were 4-wire Pt100 (from GRAFF), with SS body (1/4G, 6 mm Ø, 30 mm length) and silicone rubber leads. Although they were 4-wire type, they were connected to the HCS as 3-wire type. Its maximal working temperature was 200 °C.

2.4.2.5 ELECTRONIC POWER REGULATION SYSTEM

This system was designed to control the electric power supplied to the resistor. The MLC 9000+ controlled a solid state relay, which acted as interrupter for the resistor, regulating conduction time and, consequently, the power supplied to the heater (to the process, Figure 15).

2.4.2.6 HEATER PROTECTION SYSTEM

There was only a heating element per heater. This element was over-dimensioned (225 W), preventing excessive load, in view of the anticipated duration of the tests and the expected lifetime of these resistors. This scheme also allowed for an instantaneous increase in power, but could induce an excessive increase in temperature in the resistor. This behaviour was carefully controlled during the first stage of heating.

There was an alarm system designed to detect the possible failure of either the heating elements or the critical elements of the power electronics. This was accomplished by detecting variations in the power consumption of the heating element. In the event of failure of the resistor, the system would activate an alarm.

2.4.3 CONTROLLER CONFIGURATION

Proprietary software MLC 9000+ WORKSHOP defined which Bus Module and Loop Modules were used and then configured the control characteristics of the Loop Modules and the standard communication parameters of the Bus Module. The output configuration was used to allocate the outputs, an output has to be assigned to each control loop. This secured program allowed access only by authorised persons.

2.5 COOLING SYSTEM

The upper part of the cell includes a cooling chamber of an approximate volume of 93 cm^3, closed by a bolted cover (Figure 19).

Figure 19. Cooling chamber

The cooling fluid, water at 20 °C, was impelled and circulated by a Huber Minichiller 600 OLÉ (-20/+40 °C, ±0.5 °C, 600 W at 15 °C, 18 L/min) through two lines, connected to two drills in the cooling chambers, inlet and outlet, by two quick-couplings (green lines in Figure 3). The arrangement of the system for cooling fluid circulation is shown in Figure 20. This minichiller was used for several cells in addition to the two HITEC cells. The chiller had to be changed on September 2021 by a Huber Minichiller 300-NR (-20/+40 °C, 300 W at 15 °C, 14 L/min) that was subsequently used only for the two HITEC cells.

Figure 20. System for cooling fluid circulation: minichiller (left), inlet/outlet to the cells (right)

2.6 DATA ACQUISITION SYSTEM (DAS)

The data acquisition of the instrumentation signals were done by Advantech ADAM-5000E (Figure 21). After placing the sensors in their housings, the cables were carried to terminal blocks placed in a DIN rail. These terminal blocks served to organise the wiring and to distribute the power required by the sensors. The signals were then carried to the input screw terminals of each ADAM-5000E. These devices communicated with the experiment computer through an

RS485 serial line and a driver supplied by the manufacturer. The values recorded by the DAS were: water outlet, heater power supply and temperatures, external cell temperatures (including room and cooling circuit), RH and temperature values within bentonite and radial pressures on the cell wall.

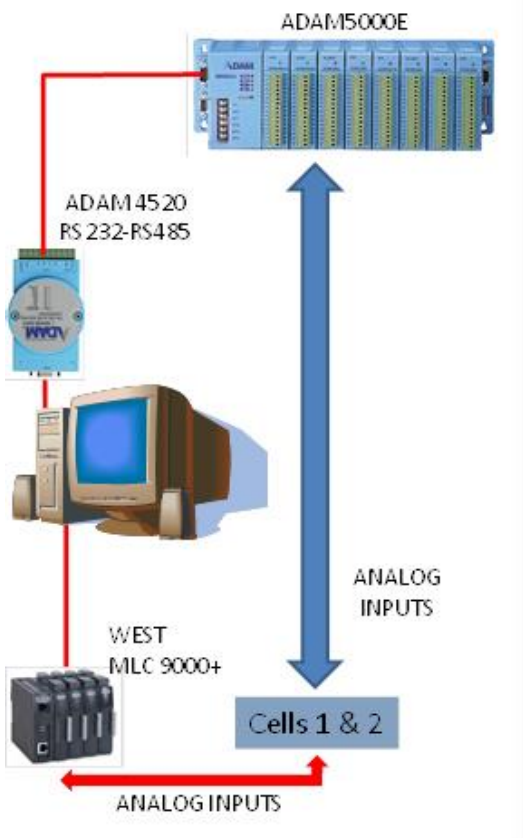

Figure 21. Data Acquisition System (DAS) overall scheme

2.6.1 ADAM-5000E

It was a DIN-rail-mounted 8-slot Distributed DA&C System for RS-485 that could be configured with any combination of up to 8 modules. It supervised and provided power to the modules and managed the independent external input/output modules.

The ADAM-5000E had five modules: two ADAM-5018 (7-ch thermocouple module) and three ADAM-5017 (8-ch analogue input module). Their characteristics are shown in

REFERENCE	No. CHANNEL	INPUT TYPE	ACCUARICY	RESOLUTION	SAMPLE/SEC
ADAM-5018	7 differential	thermocouple	± 0.1%	16-bit	10
ADAM-5017P	8 differential	±150 mV ±500 mV ±1 V ±5 V ±10 V	± 0.1%	16-bit	10

Table 3. The distribution of the analogue inputs for the modules is shown in Figure 22, Figure 23 and Figure 24.

REFERENCE	No. CHANNEL	INPUT TYPE	ACCUARICY	RESOLUTION	SAMPLE/SEC
ADAM-5018	7 differential	thermocouple	± 0.1%	16-bit	10
ADAM-5017P	8 differential	±150 mV ±500 mV ±1 V ±5 V ±10 V	± 0.1%	16-bit	10

Table 3. Characteristics of the analogue I/O modules in the DAS

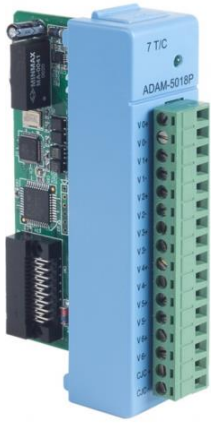

Ch0: cell 1: Pressure sensor close to hydration

Ch1: cell 1: Pressure sensor medium zone

Ch2: cell 1: Pressure sensor close to heater

Ch3: cell1: Mass of water flask

Ch4: cell2: Mass of water flask

Ch5: cell 2: Pressure sensor close hydration

Ch6: cell 2: Pressure sensor medium

Ch7: cell 2: Pressure sensor close heater

Figure 22. Channel distribution of the 1st I/O analogue module

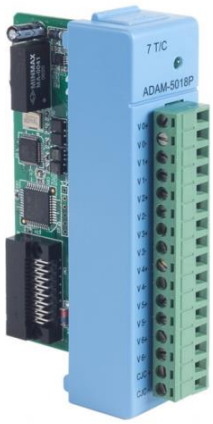

Ch0: T#1: External temperature at heater

Ch1: T# 2: External temperature at 25 mm

Ch2: T# 3: External temperature at 50 mm

Ch3: T# 4: External temperature at 75 mm

Ch4: T# 5: External temperature at hydration

Ch5: T# 6: External temperature at cooling exit

Ch6: T# 6: Room temperature

Ch7: CJC

Figure 23. Channel distribution of the 2nd (cell 1) and 4th (cell 2) I/O analogue modules

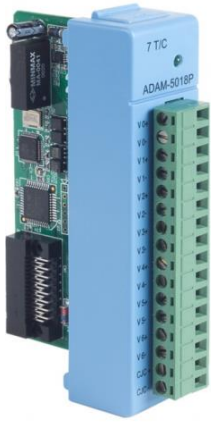

Ch0: Temperature from Vaisala 1

Ch1: RH from Vaisala 1

Ch2: Temperature from Vaisala 2

Ch3: RH from Vaisala 2

Ch4: Temperature from Vaisala 3

Ch5: RH from Vaisala 3

Ch6: Temperature from Vaisala 4

Ch7: RH from Vaisala 4

Figure 24. Channel distribution of the 3rd (cell 1) and 5th (cell 2) I/O analogue modules

2.6.2 LABVIEW APPLICATION

LabVIEW was used to develop the data acquisition application (Figure 25). This program used two RS-485 serial lines to communicate with a West MLC9000+ temperature controller and four ADAM5000E data acquisition chassis (Figure 21). This application allowed the configuration of different parameters for each experiment, asked for the data to the different nodes, showed the data in screen and recorded them in files. A different file for each cell was generated.

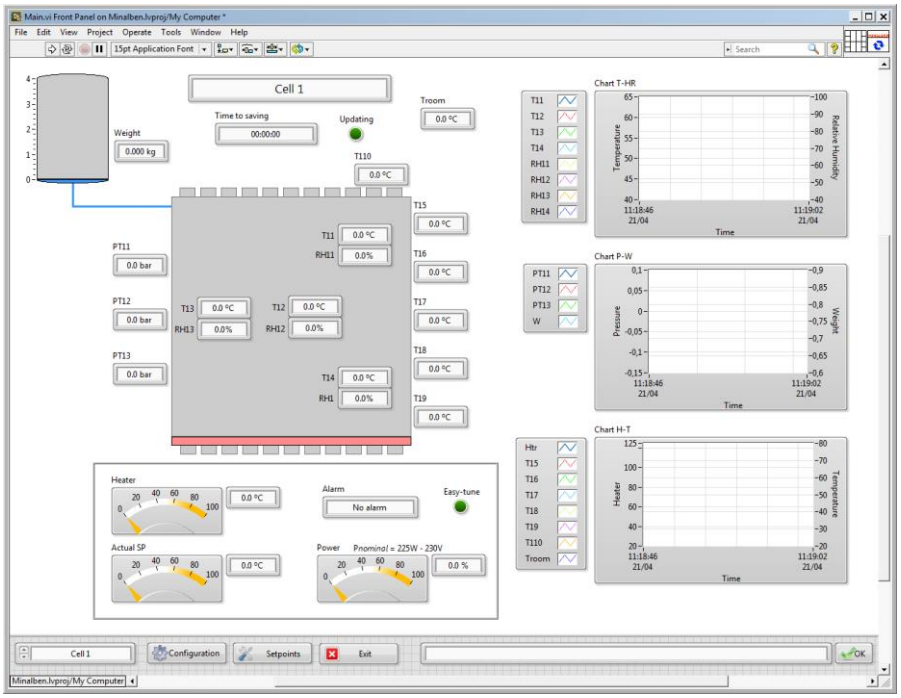

Figure 25. Interface of program LabVIEW

This program displayed an interface which recognised the location of each sensor, with values in real time, as well as a series of graphs showing the evolution of the different parameters over time. Data for water content, pressure, humidity, temperature, weight of the flask of water, power and temperature of the heater recorded for each cell. The data collection frequency for each cell could be configured as desired.

The program also showed the target temperature for each cell, which could be modified by the user.

2.7 EXTERNAL INSULATION

In order to prevent as much as possible external heat losses, the cells were laterally and beneath surrounded with thermal insulation. The insulation material used was a specific high-temperature material. Rock wool and two 25-mm thick insulation layers of foamed synthetic elastomer were used. This kind of material was chosen because is easy to install and does not require any additional covering as a vapour barrier (Figure 26):

- The inner layer was made of ceramic fibre insulation (rock wool), a high-temperature thermal insulation material (thermal conductivity of 0.24 W/m·K at 800 ˚C).
- The 25-mm thick middle layer was made of HT/Armaflex, a high-temperature thermal insulation material (thermal conductivity of 0.045 W/m·K at 40 ˚C) with closed cell structure that remains flexible at temperatures of up to 150 ˚C.
- The 25-mm thick external layer is made of Arma-Chek Silver, similar to HT/Armaflex with lower service temperature (110 ˚C). Covered with double layer laminate of UV-protected aluminium and a PVC backing, it is specially designed for cladding of Armaflex, offers resistance to mechanical impact and assists in the prevention of under insulation corrosion.

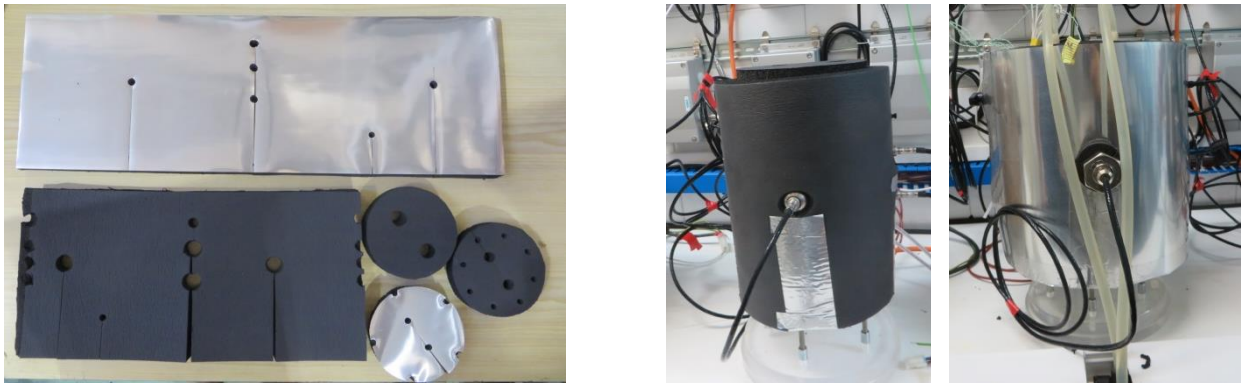

Figure 26. Template used to cut the insulation material and appearance of it once installed

The insulation thickness required was calculated using an external surface coefficient of 5 $W/(m^2 \cdot K)$, which is the one recommended. A template was designed so that the material fit perfectly the cells, with the necessary perforations for sensors and cables (Figure 26, left).

3 MATERIAL

The material with commercial name ‘Bara-Kade’ is Wyoming sodium bentonite similar to MX-80. Its use was proposed by Posiva in June 2020, although it had not been initially foreseen. Approximately 6 kg were received at CIEMAT in September 2020 sent by Posiva. The as-received water content was 8.2 %.

The density of the solid particles, needed to compute the degree of saturation, was determined using pycnometers and deionised water as suspension liquid. The value obtained was 2.82 g/cm^3.

4 PREPARATORY ARRANGEMENTS

4.1 CALIBRATION OF SENSORS

4.1.1 VAISALA SENSORS

All new VAISALA sensors were calibrated by the manufacturer, only the refurbished Vaisala sensors (they were used ones with replaced new capacitive elements) were calibrated for both humidity and temperature (four refurbished sensors were placed in Cell 1 and one in Cell 2). For this purpose, a Vaisala humidity calibrator HMK15 was used (Figure 27) and the following procedure was applied:

1. In HMK15, three solutions of $MgCl_2$, NaCl and K_2SO_4 were prepared according to instructions of the HMK15 user's manual.

2. The sensor filter was removed, the sensor was attached to an adapter supplied with the HMK15 and inserted into the $MgCl_2$ tank taking care that it did not touch the liquid.

3. The thermometer supplied with the HMK15 was placed in another hole in the adapter.

4. The adapter has four holes so three sensors could be calibrated simultaneously (the 4th hole is for the thermometer).

5. A PC was connected to the Vaisala electronics service port using the RS232 serial cable.

Figure 27. Setup for calibration of the RH/T Vaisala sensors

6. The PTTY program was used as a terminal.

7. The "RCH" command was issued to Vaisala to start the calibration sequence.

8. Calibration instructions from the HMT330 user's manual were followed.

9. This procedure was repeated for the dissolution of K_2SO_4.

4.1.2 PRESSURE SENSORS

The calibration of the pressure sensors consisted in measuring the main source of variation in their signals, i.e. the offset under different conditions: at room temperature before and after being tightened, and then at different temperatures (30, 40, 50, 60 and 70 ˚C). Sensitivity values were obtained from the specifications provided by the manufacturer.

4.2 BENTONITE COMPACTION

The target dry density and water content values for the bentonite blocks were 1.55 g/cm^3 and 17 %. The quantity of material necessary to compact each block was calculated by taking into account these target values and the internal volume of the cells (internal diameter and height of 10 cm). This gives a block volume of 785.40 cm3 and a necessary dry bentonite mass of ~1,217 g, which corresponds approximately to 1,425 g of bentonite with 17 % water content. Since the initial water content of the bentonite was 8.2 %, the necessary quantity of deionised water was slowly added to the bentonite, mixed thoroughly and let homogenise in a close plastic bag for several days.

In a previous investigation (Martín et al. 2017), several compaction methods were tested with the goal of obtaining initial conditions in terms of dry density as homogeneous as possible throughout the bentonite block. The one selected then was used in this work, consisting in the uniaxial compaction in five 2-cm high bentonite layers of the same bentonite mass each. During compaction, bolts were used to avoid material losses through the holes for sensors in the cell body. The surface of each layer was scraped before pouring and compacting the next portion of material. The last two layers were compacted using another cell as a collar, to avoid loss of material. During compaction, the cells were placed upside down. As a result, the layer compacted first, i.e. the bottom one during compaction, was the one on top (closest to the hydration surface) during operation of the tests.

A trial block was compacted following this procedure. It was extracted from the cell (Figure 28) and the water content and dry density along the block were determined. Four pieces of each layer of a volume of between 16 and 22 cm^3 were cut (Figure 28, right). The dry density was determined in two of these subsamples by immersing them in mercury to estimate their actual volume, and the water content was obtained in the four subsamples by drying them in the oven at 110 ˚C for 48 h. It was observed that, except for the first compacted layer, the dry density of

the external sample was higher than that of the internal sample of each layer. Additionally, the overall dry density of each layer was computed by taking into account the mass of bentonite used and the resulting height of the layer after compaction. The results obtained are shown in Figure 29.

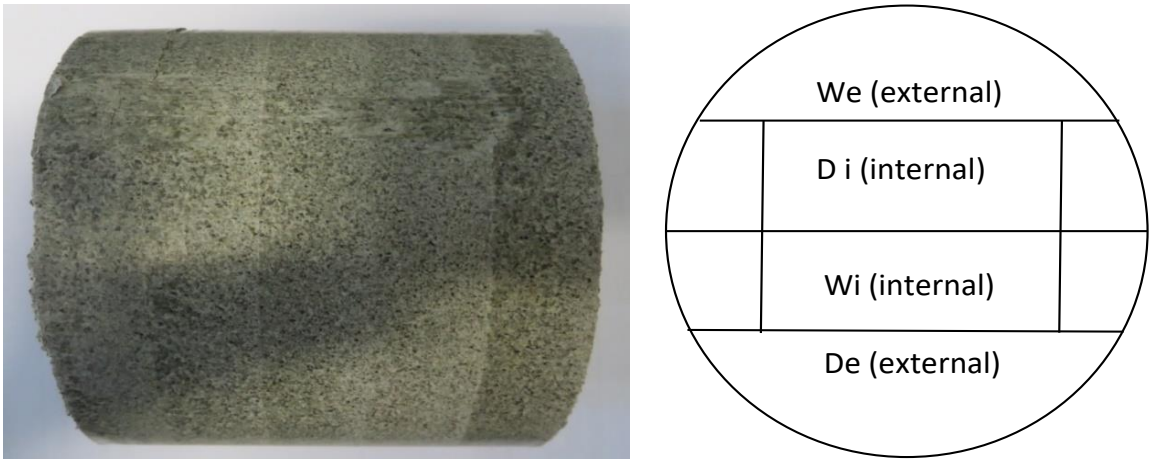

Figure 28. Trial compacted block and sectioning of each layer to determine dry density and water content

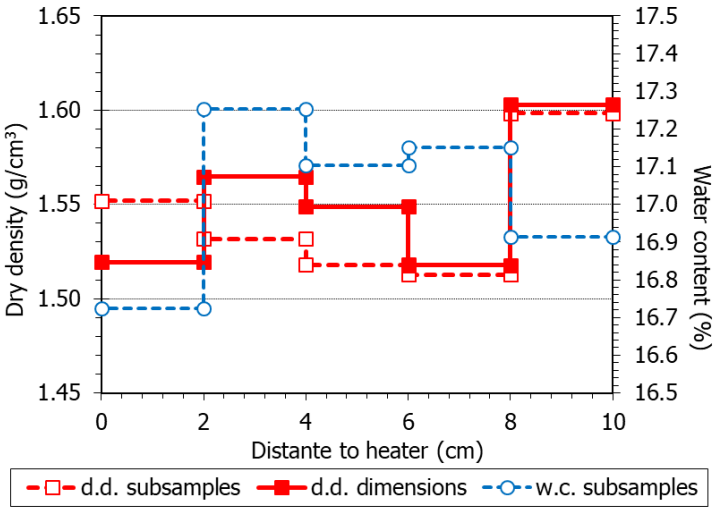

Figure 29. Dry density and water content along the trial block (the layer to be closest to the heater was the last compacted)

Following the same procedure, the two blocks of cells HT1 and HT2 were compacted, and the dry densities estimated for each layer are shown in Figure 30.

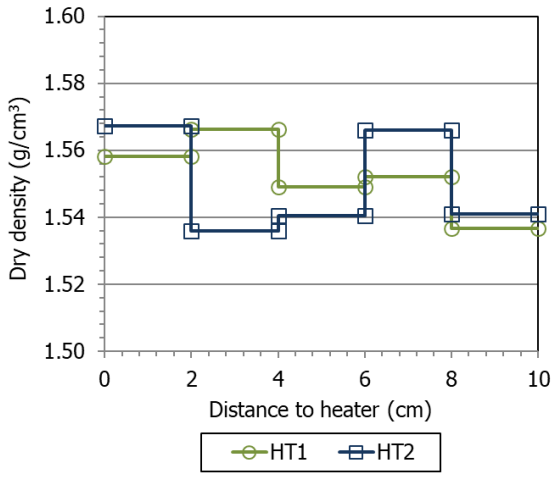

Figure 30. Dry density along the blocks of cells HT1 and HT2 as computed from the layers' weight and dimensions

4.3 SYNTHETIC WATER PREPARATION

Recipes to prepare a synthetic glacial meltwater, used in cell HT1, and a saline groundwater, used in cell HT2, were developed based on the information from Hellä et al. (2014) and Schatz (2011), as agreed with POSIVA for the MAB project (Martín et al. 2017). The saline water corresponds to the Reference 2 solution in Schatz (2011), with TDS= 10 g/L.

The salts used to prepare the synthetic water should be of the highest purity available ("reagent grade") and the anhydrous state will be assured by drying at 105-110 °C at least for two hours taking into account the physical characteristics of the reagents. Deionized water (Millipore Milli-Q water purification system) was used as aqueous medium.

The procedure used to prepare the glacial meltwater was as follows:

1. Weigh 0.19075 g of $CaCl_2 \cdot 2H_2O$
2. Weigh 0.25094 g of $MgCl_2 \cdot 6H_2O$
3. Weigh 0.08337 g of KCl
4. Weigh 0.13307 g of NaCl
5. Weigh 0.03628 g of K_2SO_4
6. Weigh 0.0473 g of $Na_2SiO_3.9H_2O$

7. Add to a 1000 mL glass vessel with ≈ 700 mL of deionised water the reagents in the same order as from step 1 to 6. The order in which the salts are added to the water is important in order to avoid precipitations.

8. After each addition pH must be measured.

9. Then, 10 mL of this dissolution was taken per litre of water.

10. Make up the solution to 1000 mL with deionised water.

The saline water was prepared by dissolving $CaCl_2$ and NaCl in dionised water at a Ca^{2+}/Na^+ mass ratio of 1:2 to a total dissolved solids (TDS) content of 10 g/L. For every litre of desired solution, 6.4739 g NaCl and 3.5261 g $CaCl_2$ (or 4.6700 g $CaCl_2$-$2H_2O$) should be added to the deionised water in an appropriate vessel or container. It should be ensured that the added salts are completely dissolved prior to use (Schatz 2011).

Once prepared, the ions in the water were analysed by ionic chromatography, except silicon which was analysed by ICP-OES. Table 4 compares the theoretical composition and the analysed one for the two types of water.

ION	GLACIAL - HT1. Hellä et al. (2014)	GLACIAL - HT1 EXPEERIMENTAL	SALINE – HT2 Schatz (2011)	SALINE – HT2 EXPERIMENTAL
Na^+	0,66	0,83	2.545	2.542
K^+	0,60	0,74	-	-
Ca^{2+}	0,52	0,86	1.271	1.628
Mg^{2+}	0,30	0,68	-	-
SiO_2	0,10	-	-	-
Cl^-	3,00	2,94	6.184	6.689
SO_4^{2-}	0,20	0,12	-	-
pH	5,80	5,73	7	6,87
TDS (ppm)	5,44	6,18	10.000	10.859
E.C. (mS/cm)	0,0085	0,0097	15,6	17,0
I.S. (mol/L)	$1.2 \cdot 10^{-4}$	$1.7 \cdot 10^{-4}$	0,21	0,23
E.N. (%)	3,2	28,7	-0,09	0,82

Table 4. Comparison of the theoretical solution composition and the experimental water composition obtained in this work (units in mg/L, TDS: total dissolved solids, E.C.; electrical conductivity, I.S.: ionic strength; E.N.: electronegativity)

5 CELL AND SETUP ASSEMBLAGE

According to the experience gained in previous investigations (Martín et al. 2017, Idiart et al. 2017), the following protocol was followed to start the tests:

1. Preparation of the clay mass by adding water to the bentonite and preservation of it in a plastic bag for 9 days in the case of HT1 and 3 days in the case of HT2.

2. Two days before compaction, the water content of the clay was checked.

3. Every component of the cell was weighed and photographed. Bolts were screwed into the inlets of the cell prior to compaction.

4. Compaction of the bentonite as described in section 4.2.

5. The cell with the compacted clay was weighed again and wrapped in plastic film to avoid water losses.

6. Configuration of the data acquisition file for the particular cell, selecting the channels corresponding to the appropriate sensors.

7. Two weeks before the insertion of sensors in the cell, recording of data started. This allowed to check the values measured under the same conditions (RH and T in the laboratory) and compare initial differences among sensors in offset values.

Figure 31. Drilling of holes through a threaded nut with a 12-mm drilling bit for insertion of the RH/T sensors

8. The bolts placed in the inlets of the cell for inserting the Vaisala RH/T sensors were removed one at a time and replaced immediately by a threaded nut through which a

12-mm drilling bit was used. The depth to which the bit was pushed inside the bentonite was that of the sensor. During drilling, as much material as possible was recovered and weighed (Figure 31). The dry density of the bentonite block was then recalculated taking into account the volume occupied by the sensors and the material extracted during drilling.

9. Once the four holes were drilled, the cell was weighed again.

10. The cell was placed on the methacrylate support.

11. The RH/T sensors were inserted and fixed.

12. The pressure sensors were installed applying a tightening torque in the range recommended by the manufacturer.

13. The thermocouples were stuck to the cell wall (Figure 10).

14. The cell was wrapped with the insulation material.

Once the cell was ready with the sensors installed, the program started recording data every 4 h, in order to check the influence of the laboratory temperature fluctuations (controlled to 21±1 ˚C) on the values measured (Figure 32, Figure 33).

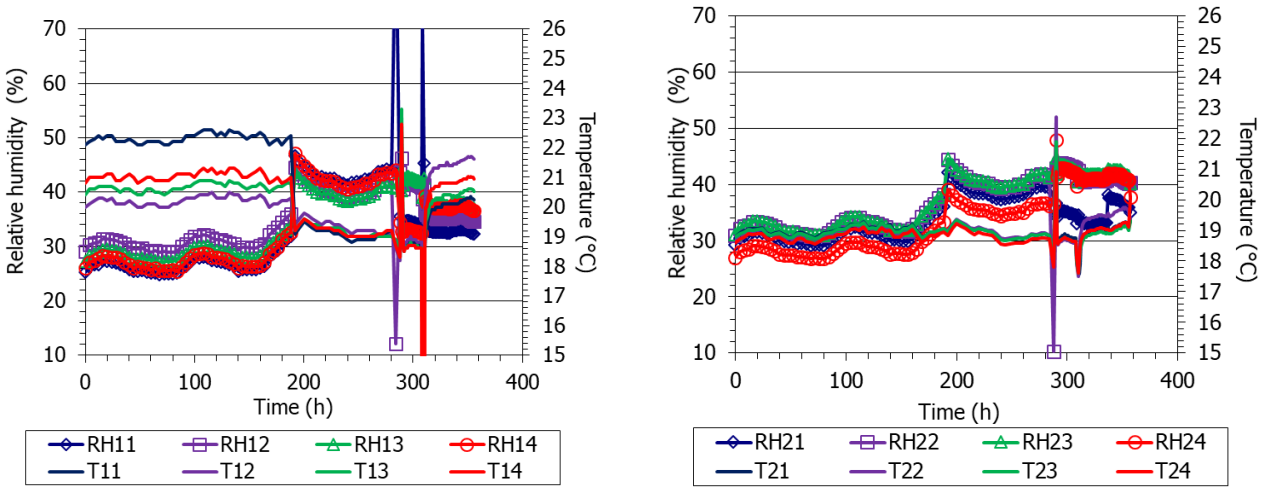

Figure 32. Values measured by RH/T sensors before installation in cell HT1 (left) and cell HT2 (right)

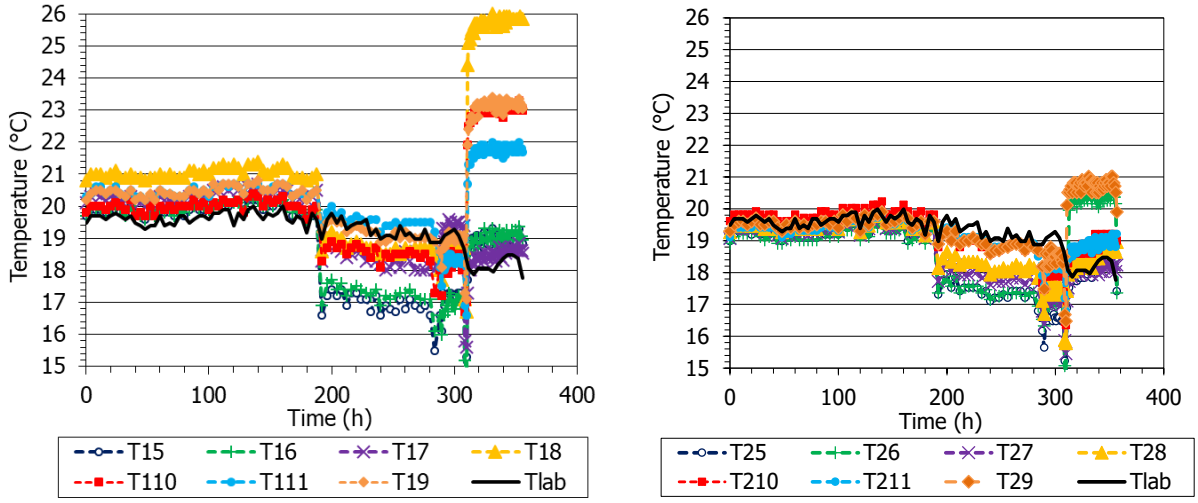

Figure 33. Values measured by external thermocouples before installation in cell HT1 (left) and cell HT2 (right)

Table 5 summarises the characteristics of the bentonite in each cell. For the computation of dry density, the internal volume of the cell has been taken to be 785.40 cm^3, considering the internal dimensions of 10 x 10 cm and the volume of the sensors inserted in the bentonite as 13.57 cm^3.

CELL #	HT1	HT2
Initial water content (%)	17,1	17,2
Sample mass (g)	1.421,9	1.425,0
Compaction pressure[a] (MPa)	8,50	8,20
Sample mass after drilling (g)	1.398,7	1.400,4
Theoretical dry mass (g)	1.194,9	1.194,4
Dry density (g/cm^3)	1,55	1,55
Porosity	0,449	0,451
Void ratio	0,816	0,822
Degree of saturation (%)	59	59

Table 5. Characteristics of the bentonite samples after compaction ([a] Average value for the five layers)

6 TESTS INITIATION

The cooling system on top was connected to the cells a week before switching on the heater. The heater temperature started to be increased two months after the cells were mounted. Before starting to increase the heater temperature the reading interval of the data acquisition file was set to 1 minute. The heater temperature was initially set at 70 ˚C and then was increased by steps to 150 ˚C over a period of nine days (Figure 34). When the steady state for temperature and relative humidity inside the bentonite was approximately reached, which took three months, hydration was launched. A summary of the main dates for both cells is given in Table 6.

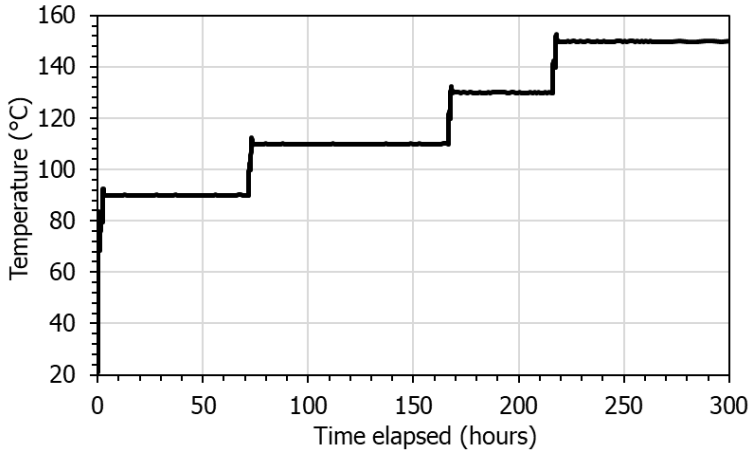

Figure 34. Temperature increase sequence in cells HT1 and HT2

CELL	BENTONITE PREPARATION	COMPACTION	SENSOR INSTALLING	HEATING	HYDRATION
HT1	01/12/2020	09/12/2020	18/12/2020	15/02/2021	17/05/2021
HT2	13/12/2020	17/12/2020	18/12/2020	15/02/2021	25/05/2021

Table 6. Dates of cells installation and beginning of the different phases

7 ONLINE RESULTS

Table 7 and Table *8* detail the dates of every milestone for each cell, as well as unforeseen events affecting the cells that took place during operation. Among them, an overheating episode took place after the cells had been hydrating for three months. As a result of an air conditioning failure on August 13th 2021, concurrent with a heat wave in Madrid, the temperature in the laboratory reached values of 42 ˚C. The chiller reached its upper limit (40 ˚C) and stopped, resulting in a significant increase of the temperatures in the cells. When the failure was realised, and to avoid damaging of the sensors, the heater temperature was decreased to 100 ˚C and remained in this value for 7 days before increasing it again to 120 and then to 150 ˚C. For some days in September the chiller kept going on and off and the temperatures experienced sudden changes. Afterwards, the chiller was replaced and the temperatures came back to normal, but increases in the water uptake rates, as well as drops in radial pressure were observed. The repercussion on the systems is detailed in sections 7.1.3.1 and 7.2.3.1.

Date	Time heating (days)	Time hydration (days)	Relevant events
18/12/2020	-	-	Cell assemblage and sensors installation
09/02/2021	-	-	Launching of cooling system
15/02/2021	0	-	Launching heating at 70°C and progressive increment of temperature
24/02/2021	9	-	Setting of heater temperature at 150°C
17/05/2021	91	0	Launching hydration
13/08/2021	179	88	Air conditioning failure during heatwave (lab temp reached 42°C)
15/08/2021	181	90	Failure of chiller, followed by cell overheating
16/08/2021	182	91	Heater temperature set to 100°C
23/08/2021	189	98	Heater temperature set to 120°C
24/08/2021	190	99	Heater temperature set to 150°C
6/9/21 – 9/9/21	194 – 197	112 – 115	Repeated failure of chiller: cell overheating episodes
10/09/2021	198	116	Chiller replacement
30/01/2022	349	258	Failure of air conditioning: room temperature rise for ~2 weeks
09/03/2022	387	296	RH/T sensors sealing (hydration and heating switched off and on: temporary cooling)
28/04/2022	438	347	Sudden drop of radial pressures
11/05/2022	450	359	Scheduled blackout (temperature of heater temporarily changed)
30/5/22 – 31/5/22	469 – 470	378 – 379	Removing of RH/T11&14 sensors (hydration and heating switched off and on: temporary cooling)
12/07/2022	513	421	Scheduled blackout (temperature of heater temporarily changed)
02/08/2022	534	443	Short air conditioning failure
20/10/2022	612	521	Short air conditioning failure
22/11/22– 23/11/22	646 – 647	554 – 555	Removing of RH/T12 sensor (hydration and heating switched off and on: temporary cooling)
13/12/22-25/2/23	666 – 741	~575 – 650	The external temperatures of the cell slightly increased, particularly in the upper part. They come back to normal without any action
25/04/2023	800	708	Scheduled blackout (temperature of heater temporarily changed)
13/11/2023	1,001	909	Scheduled blackout (temperature of heater temporarily changed)
09/01/2024	1,058	967	Dismantling

Table 7. Summary of main events in cell HT1

DATE	TIME HEATING (days)	TIME HYDRATION (days)	RELEVANT EVENTS
18/12/2020	-	-	Cell assemblage and sensors installation
09/02/2021	-	-	Launching of cooling system
15/02/2021	0	-	Launching heating at 70 °C and progressive increment of temperature
24/02/2021	9	-	Setting of heater temperature at 150 °C
25/05/2021	99	0	Launching hydration
13/08/2021	179	80	Air conditioning failure during heatwave (lab temp reached 42 °C)
15/08/2021	181	82	Failure of the chiller, followed by cell overheating
16/08/2021	182	83	Heater temperature set to 100 °C
23/08/2021	189	90	Heater temperature set to 120 °C
24/08/2021	190	91	Heater temperature set to 150°C
6/9/21 – 9/9/21	194 – 197	104 – 107	Repeated failure of chiller: cell overheating episodes
10/09/2021	198	108	Chiller replacement
04/10/2021	231	132	PT22 sensor failure
30/01/2022	349	250	Failure of air conditioning: room temperature rise for ~2 weeks
05/03/2022	383	284	PT21 sensor failure
07/03/2022	385	286	RH/T sensors sealing (hydration and heating switched off and on: temporary cooling)
11/05/2022	450	351	Scheduled blackout (temperature of heater temporarily changed)
24/05/2022	463	364	Sensor PT21 disconnected. Heater failure and repair (temperature temporarily changed)
12/07/2022	512	413	Scheduled blackout (temperature of heater temporarily changed)
19/07/2022	519	420	Removing of RH/T sensors (hydration and heating switched off and on: temporary cooling)
02/08/2022	534	435	Short air conditioning failure
20/10/2022	612	513	Short air conditioning failure
26/12/2022	679	580	The external temperatures of the cell slightly increased, particularly in the upper part. They come back to normal without any action
25/04/2023	799	700	Scheduled blackout (temperature of heater temporarily changed)
25/09/2023	952	853	Dismantling

Table 8. Summary of main events in cell HT2

7.1 CELL HT1 – GLACIAL WATER

7.1.1 STABILISATION PHASE

Sensors were installed in the cell and started recording values for 59 days before the initiation of the heating phase. The average values for relative humidity and temperature during this initial phase are shown in Figure 35 (left). The relative humidity and temperature inside the bentonite were of 76.7±0.2 % and 22.7±0.9 °C, respectively, with the RH on top being slightly lower, which can be related to a different behaviour of sensor RH/T11, already observed while the sensors were measuring on air (Figure 32). The external temperatures were lower than the inner ones and softly increased from the top to the bottom of the cell (in a range <1 °C). After the cooling system on top of the cell was switched on, the internal and external temperatures decreased and the gradient of temperatures between top and bottom of the cell surface increased (Figure 35, right). Once the different offsets corrected, the total pressures did not change when the cooling system was launched. They remained around 0.0 MPa.

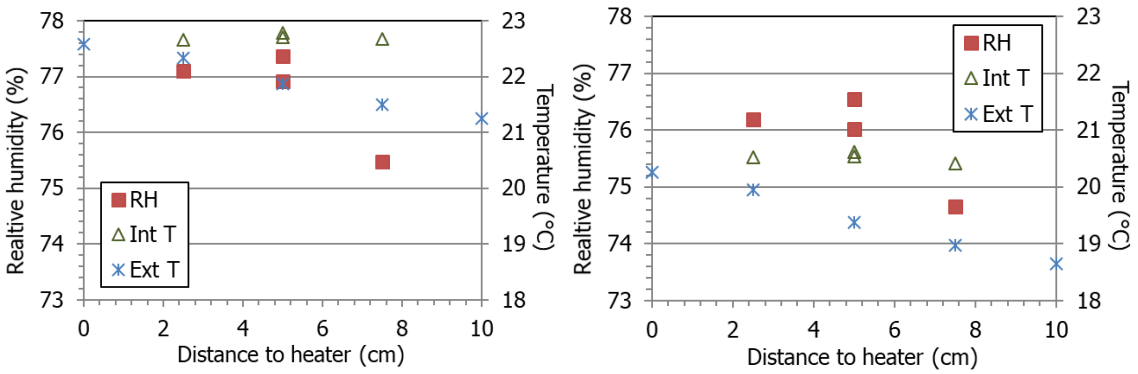

Figure 35. Steady relative humidity and temperature values during the stabilisation phase in cell HT1 (left) and after cooling on top was switched on (right)

7.1.2 HEATING PHASE

The following figures show the evolution of relative humidity, temperature and pressure during the heating phase (Figure 36 to Figure 38) and the steady values at the end of this phase (Figure 39). The temperatures were increased from 70 °C to 150 °C over a period of 9 days. To keep the final target temperature a power of 10 W was necessary. After each temperature step, thermal equilibrium was quickly reached. The water vapour moved towards the upper part of the cell, where the relative humidity started to increase first at the bottom sensor location and then in locations upwards. At 2.5 cm from the heater (sensor RH/T14) the RH reached 100 % in less than 1 h and in the middle part of the column in 4-8 days. After just four days the bottom of the sample started to dry out (sharp decrease in relative humidity) and some days later the

middle part of the sample also experienced a decrease in relative humidity. At the location of sensor RH/T11 (7.5 cm from the heater), the RH reached 100 % seven days after the beginning of heating (before the heater temperature reached the target value of 150 °C) and the sensor was flooded before hydration started. The upper radial pressure sensor recorded an increase up to 2 MPa after 20 days of heating and then a slow decrease. At the end of the heating phase only this pressure sensor recorded a significant value. The thermal gradient measured inside the bentonite and on the external surface of the cell was similar.

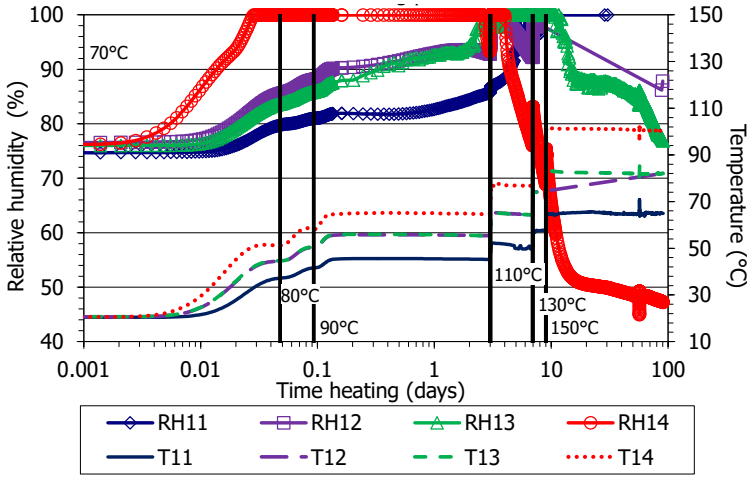

Figure 36. Evolution of relative humidity and temperature inside the bentonite during the heating phase of cell HT1 (the vertical lines indicate the successive target temperatures of the tablaheater)

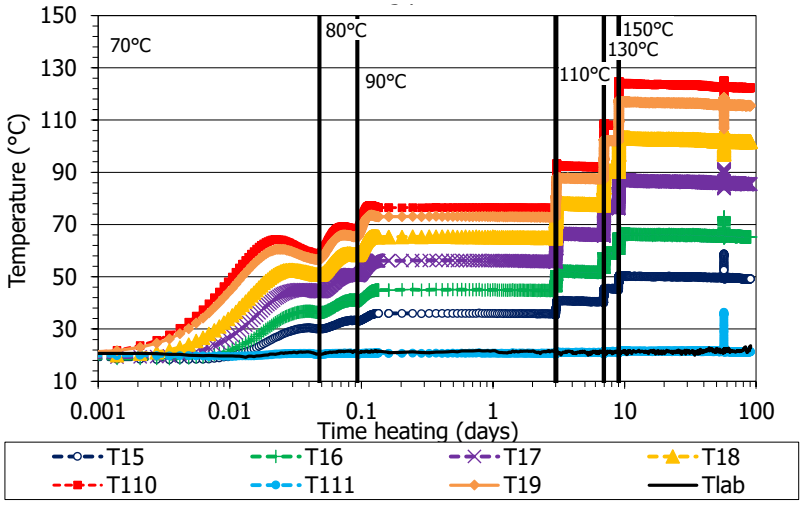

Figure 37. Evolution of external temperatures during the heating phase of cell HT1 (the vertical lines indicate the successive target temperatures of the heater)

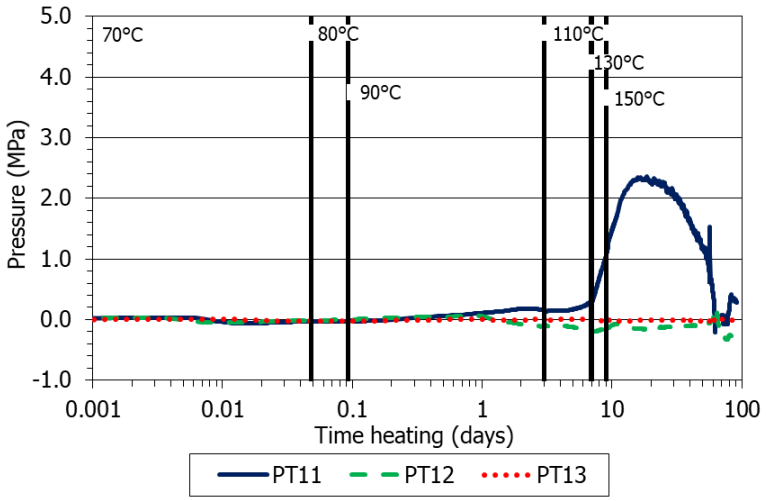

Figure 38. Evolution of lateral pressure between the bentonite and the cell wall during the heating phase of cell HT1 (the vertical lines indicate the successive target temperatures of the heater)

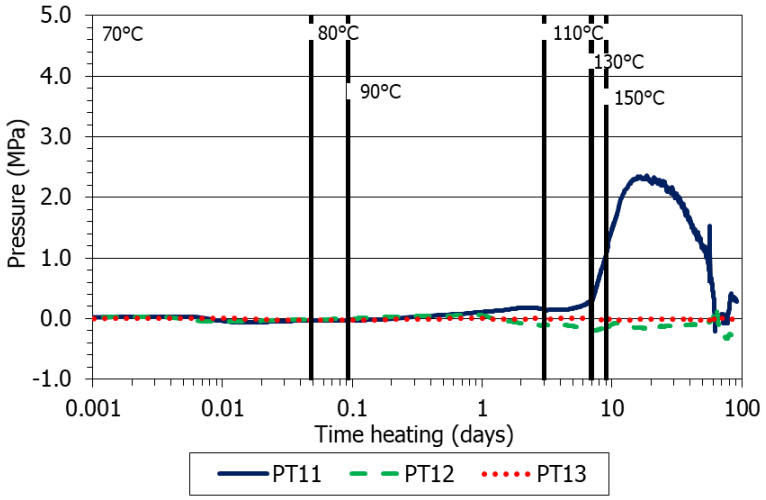

Figure 39. Steady values of relative humidity and temperature at the end of the heating phase in cell HT1

7.1.3 HEATING+HYDRATION PHASE

After the three initial months of heating, leading to quasi-steady hydraulic conditions, hydration started in May 2021. The evolution of relative humidity and internal and external temperatures during the heating+hydration phase is presented in Figure 40 and Figure 41. The temperatures were not affected by the beginning of hydration, and both the internal and the external sensors recorded constant temperatures until they failed. The RH/T sensor on top was already flooded when hydration started. In the middle part of the column the relative humidity started to increase about one day after the beginning of hydration and in the bottom part after about ten days. The two sensors in the middle of the column were flooded in less than 25 days. After three months of hydration there was an overheating episode (described below) which caused the

flooding of sensor RH/T14. From this time on no information about the RH or T inside the bentonite was provided, except for sensor RH/T14.

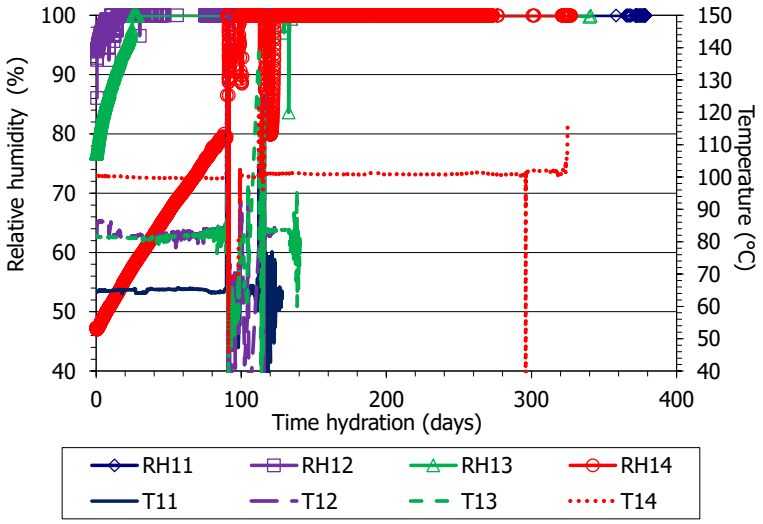

Figure 40. Evolution of relative humidity and temperature inside the bentonite during the heating+hydration phase of cell HT1 (hydration lasted 967 days)

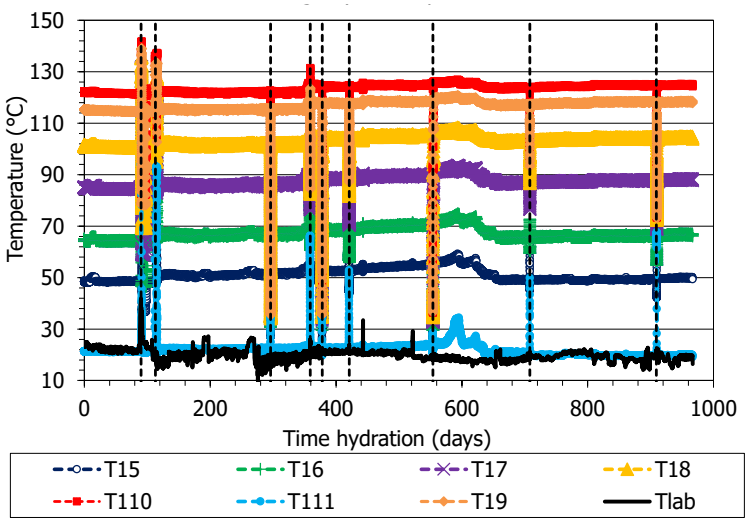

Figure 41. Evolution of laboratory and external temperatures on cell HT1 during the heating+hydration phase

The evolution of radial pressures and water intake during the heating+hydration phase is shown in Figure 42. The radial pressure sensors in the upper and middle parts of the cells had recorded increasing trends since the beginning of hydration, while the bottom sensor did not record any change. The pressure and water intake evolutions were greatly affected by the overheating and heating/cooling cycles described below.

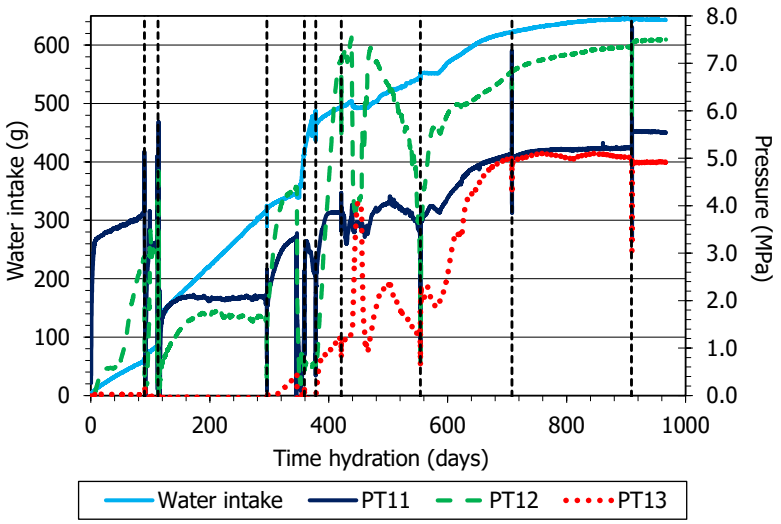

Figure 42. Evolution of radial pressure and water intake during the heating+hydration phase of cell HT1 (the dotted vertical lines indicate blackouts and other events)

7.1.3.1 OVERHEATING EPISODE AND CHILLER REPLACEMENT

As a result of an air conditioning failure on August 13th 2021 (day 88 of hydration), concurrent with a heat wave in Madrid, the temperature in the laboratory reached values of 42 °C (Figure 43, where the temperatures on the surface of the cell are also shown). The chiller system on top of cells failed and the temperatures in cell HT1 reached 123 °C in the bentonite upper part and 148 °C at 2.5 cm from the heater (Figure 44). When the failure was realised, and to avoid damaging the sensors, the heater temperature was decreased to 100 °C and remained in this value for 7 days before increasing it again to 120 and then to 150 °C. These changes can be observed in the Figures. The radial pressures dropped as a result of the overheating and then recovered, although the pressure on top was not as high as before (Figure 45).

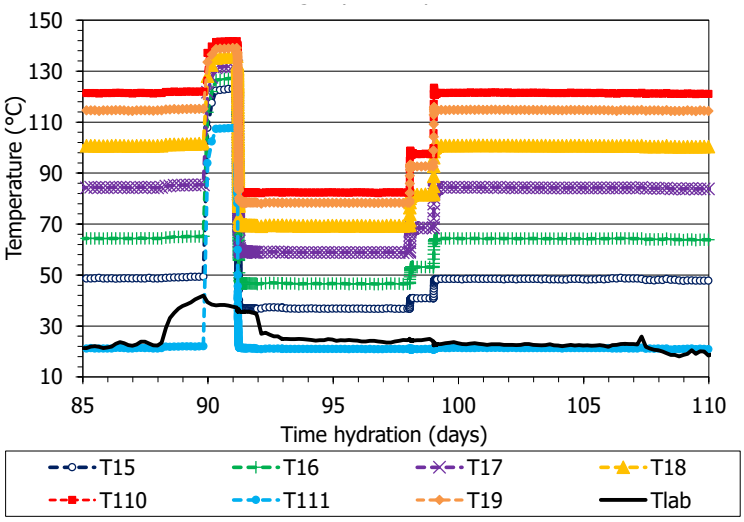

Figure 43. Evolution of laboratory and external temperatures on cell HT1 around the overheating episode

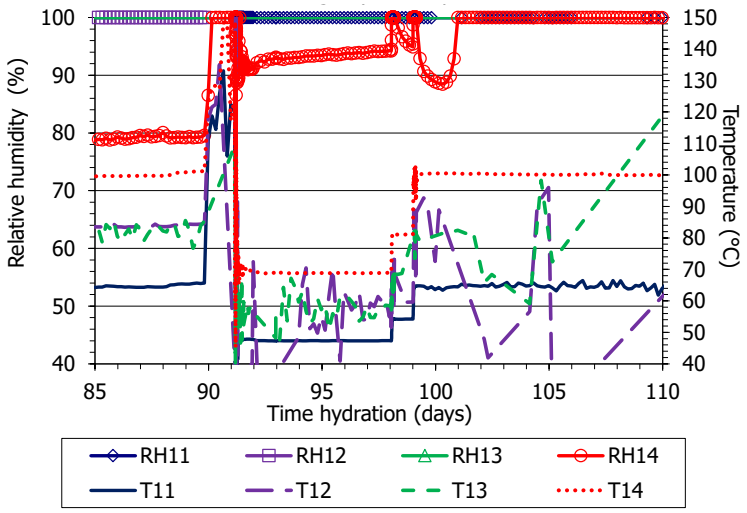

Figure 44. Evolution of relative humidity and temperature inside the bentonite of cell HT1 around the overheating (day 90 of hydration)

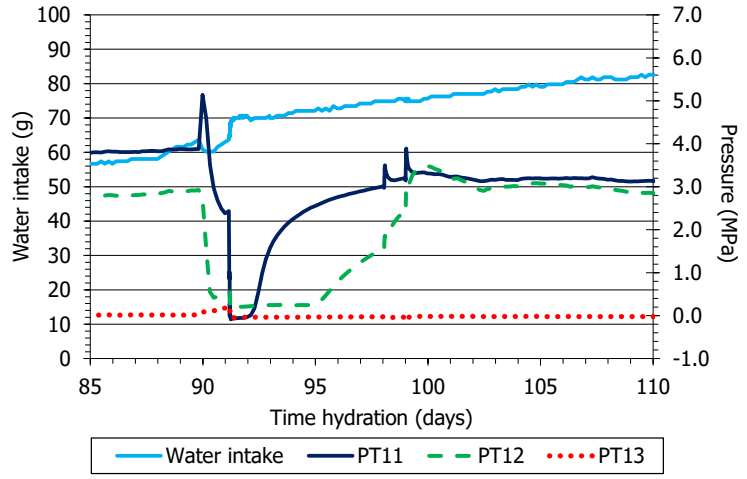

Figure 45. Evolution of radial pressure and water intake of cell HT1 around the overheating (day 90 of hydration)

After the heater temperature had been set again to 150 °C, the chiller kept going on and off for some days, and the external and internal temperatures experienced sudden changes (Figure 46, Figure 47). Afterwards, the chiller was replaced (see subchapter 2.5) and the temperatures came back to normal, but increases in the water uptake rates, as well as drops in radial pressure were observed (Figure 48). All the RH/T sensors, except RH/T14 that apparently resumed normal behaviour, stopped providing any information after 130-140 days of hydration.

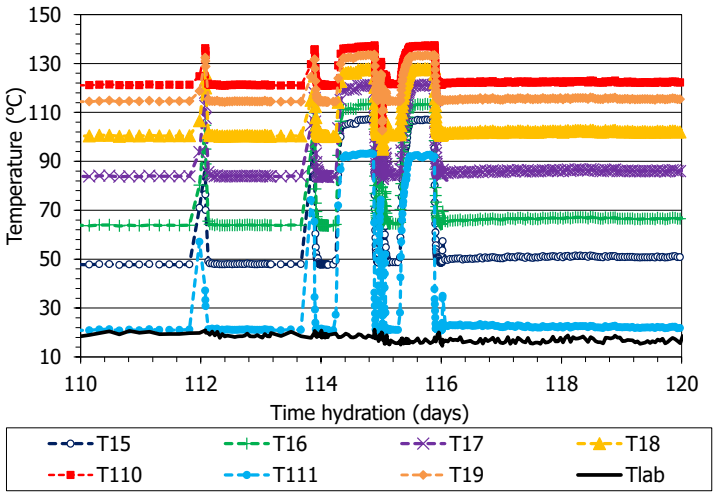

Figure 46. Evolution of laboratory and external temperatures of cell HT1 in the period between the overheating and the chiller replacement

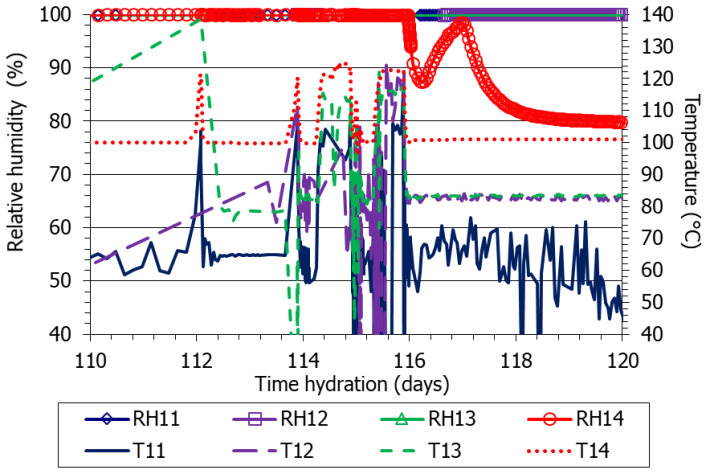

Figure 47. Evolution of relative humidity and temperature inside the bentonite of cell HT1 in the period between the overheating and the chiller replacement

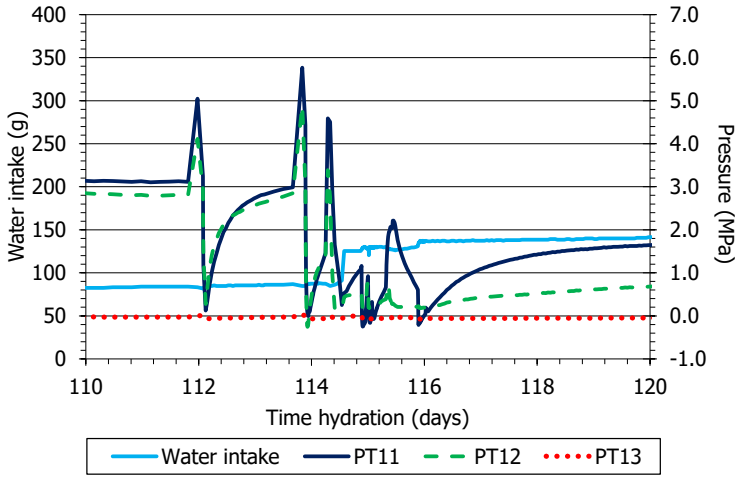

Figure 48. Evolution of radial pressure and water intake of cell HT1 in the period between the overheating and the chiller replacement

7.1.3.2 RESEALING OF SENSORS' INLETS

The increase in water intake rate and the pressure drop mentioned above were attributed to some water leak resulting from alternating thermal expansion and contraction of the cell elements resulting from the chiller failures detailed above, and/or deterioration of some of the cell elements because of the excessive temperatures. The leaks took possibly place through the sensors' openings. Hence, it was decided to try and see if this was the case and reseal these openings. The actions taken for that are summarised below. The whole process described took less than 5 hours:

On day 296 of hydration the heater was switched off, the hydration inlet was closed and the insulating material around the cell was removed. The cooling system was switched off.

After a cooling period of 60-90 minutes, the relative humidity sensors were inspected. In some of them the sealing elements were clearly broken or deteriorated. Water drops and even bentonite were observed in some of them, which confirmed that these openings were leaking points (Figure 49).

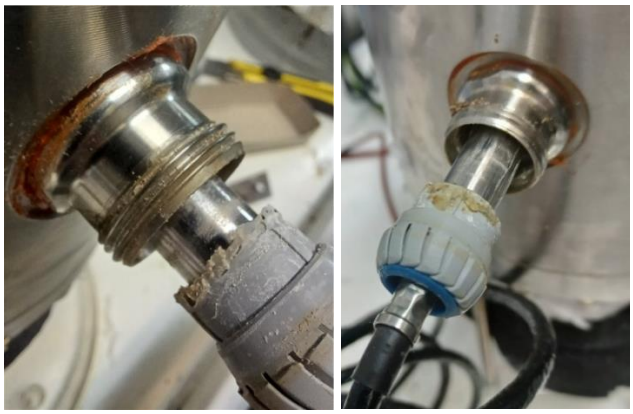

Figure 49. Deteriorated cable gland (left) and bentonite around sensor RH/T13 in cell HT1 (right)

The RH sensors' inlets were sealed with Nural 28 silicone at all possible places (Figure 50).

The pressure sensors were inspected and checked to be tightly fastened, so no further actions were taken.

The isolating material was again wrapped around the cell, the cooling system was launched and the heater temperature was increased in steps (70, 100, 120, 140 and 150 °C) in one hour.

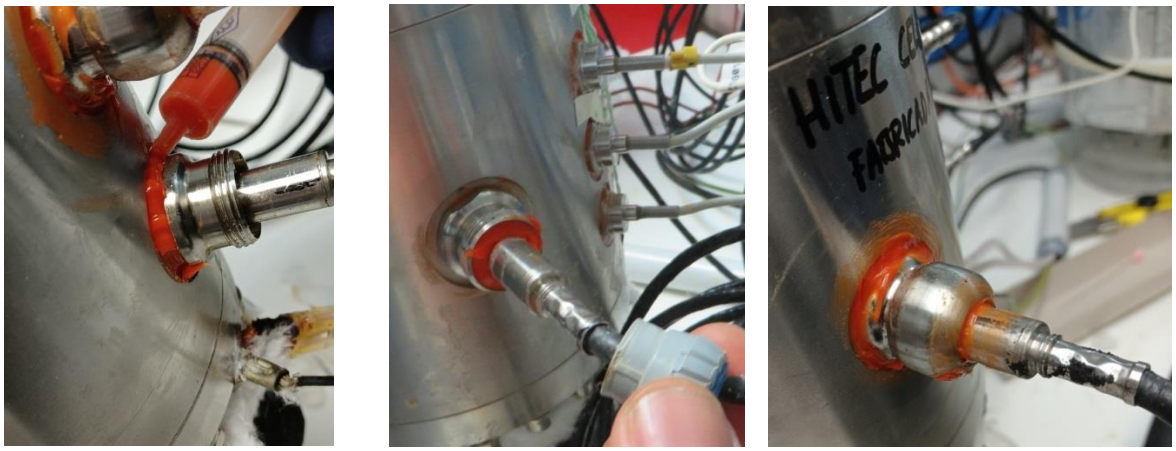

Figure 50. Resealing of RH/T sensors

Figure 51 shows the evolution of radial pressure and water intake in cell HT1 just before and after sensors' sealing (hydration time: 296 days). The radial pressure sensors started to record increases (including the bottom one PT13 that had not recorded any pressure previously) and the water intake rate decreased.

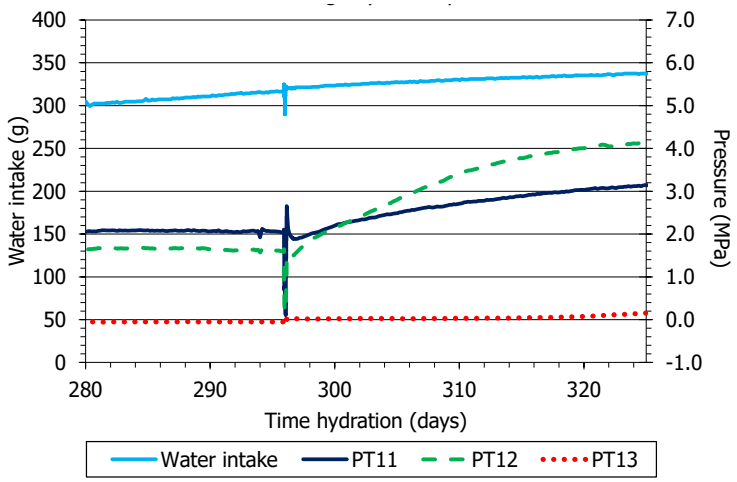

Figure 51. Evolution of radial pressure and water intake before and after sensors' sealing in cell HT1

7.1.3.3 REMOVING OF SENSORS AND OTHER MINOR EVENTS

Despite having sealed the RH/T sensors' inlets as described in the previous subchapter, a sudden drop of the pressures measured on the cell wall along with an increase of water intake took place some weeks afterwards, day 347 of hydration (Figure 52).

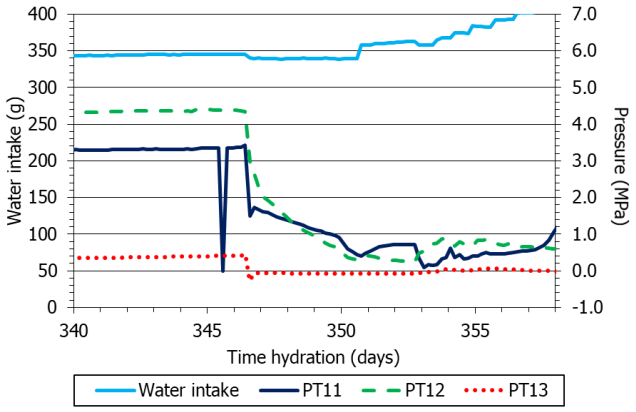

Figure 52. Evolution of radial pressure and water intake in a period around a drop of pressure in cell HT1

It was considered that this behaviour could only be explained by new leaks through the sensors' inlets. Additionally, on day 372 from the beginning of hydration, bentonite and water were identified inside the electronic box of sensor RH/T12. Furthermore, sensor RH/T14 had been expelled from the cell and sensor RH/T11 was halfway out of the cell (Figure 53). Hence it was decided to completely remove these two sensors, since they were not providing data, and plug the inlets with bolts. To accomplish this the heater was switched off, the insulation material was removed, the sealing elements of the sensors were unscrewed, sensor RH/T11 was extracted and finally the two inlets were closed with bolts sealed with Nural 28 (Figure 54). Afterwards the insulation material was put in place again, the cooling system on top was switched on, the heater temperature was set to 70 °C and the hydration line was open. From the moment the heater was switched off until the hydration line was open 4 hours elapsed. The heater temperature was increased in steps up to 140 °C in 4 additional hours and the next day the target temperature of 150 °C was set again.

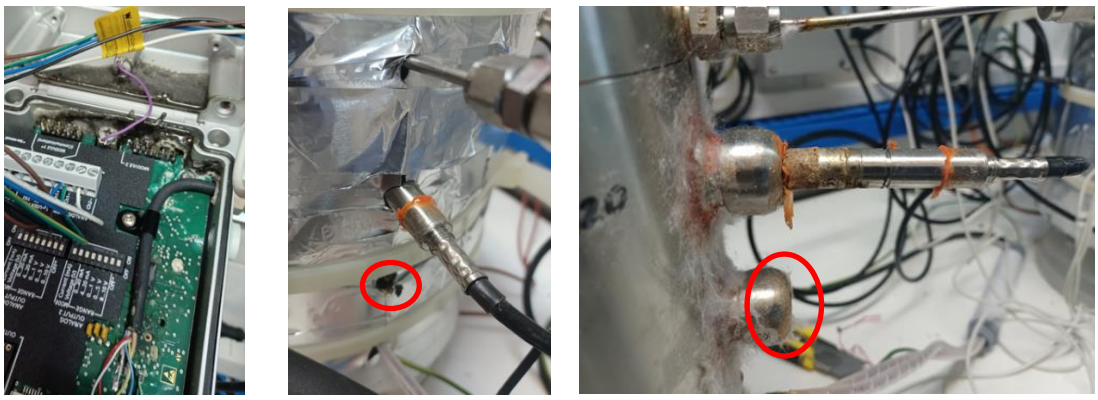

Figure 53. Bentonite and water inside the electronic box of sensor RH/T12 (left), sensor RH/T11 halfway outside the cell (middle and right) and empty inlet of sensor RH/T14 (encircled)

Figure 54. Empty housing of sensor RH/T14 (left), appearance of sensor RH/T11 once extracted (middle), sensors inlets closed with bolts (right)

The temperatures outside the cell just before and after the sensors' removal are shown in Figure 55. Figure 56 shows the evolution of radial pressures and water intake along a period comprising the initial sealing of sensors described in 7.1.3.2 and the removal of sensors RH/T11 and 14 (indicated by black dotted vertical lines). The pressures clearly increased after these two actions, while the water intake rate decreased. Ten days before the sensors removal there was a scheduled blackout (indicated with an orange dotted line) and shortly before it, the drop of pressures shown in Figure 52 had taken place. Another blackout took place on day 421 of hydration (indicated with an orange dotted line). Just before this blackout the pressure sensors had reached values as high as 7 MPa in the middle part and 1 MPa at the bottom. The scheduled blackouts lasted less than 1 h and did not have major impacts on the radial pressures.

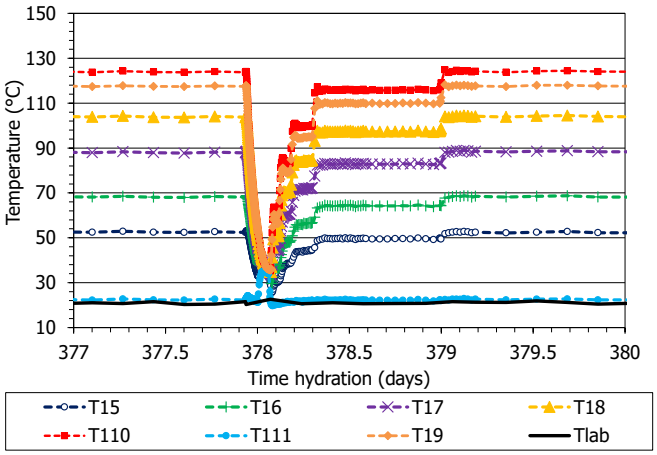

Figure 55. Evolution of external temperatures before and after removal of sensors RH/T11 and 14

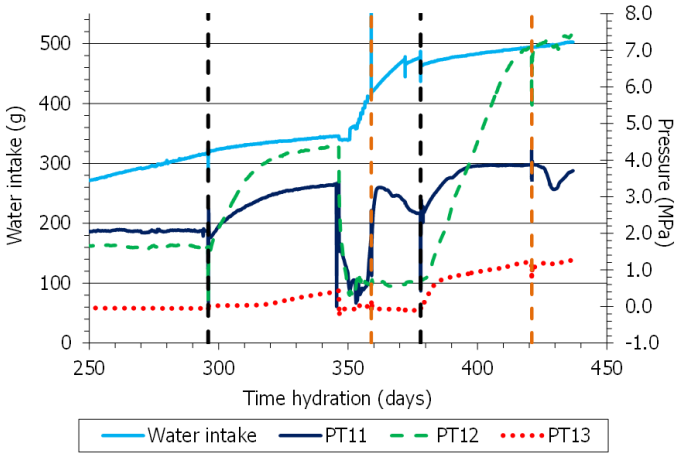

Figure 56. Evolution of radial pressure and water intake in a period where blackouts (orange dotted vertical lines) and actions to seal and remove sensors (black dotted vertical lines) took place

On hydration day 438 sensor PT12, which had reached a value of 7.6 MPa, started to record decreasing values down to a minimum of 3.8 MPa (on ~443 hydration day) and then resumed again an increasing trend, reaching a new peak of 7.3 MPa on hydration day 471. Afterwards it recorded a continuous decrease. In this period the other two sensors also peaked and eventually showed a decreasing trend (Figure 57). It was considered that this behaviour resulted from a new leak taking place through sensor RH/T12. Hence, it was removed and the inlet closed with a bolt on hydration day 554, following the same procedure described above for the other sensors' removal. The sensing element was completely corroded and the stainless filter could not be extracted (Figure 58). Afterwards the pressures increased again and the sensors on top and bottom reached approximately steady values of ~5 MPa while the pressure recorded by the middle sensor continued slightly increasing until the end of the test (Figure 42). Before the end of the test, two more scheduled blackouts took place, as detailed in Table 7.

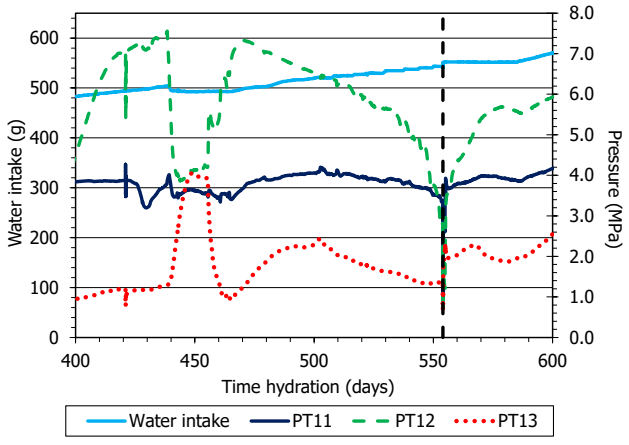

Figure 57. Evolution of radial pressure and water intake before the removal of sensor RH/T12 (dotted vertical line)

Figure 58. Extraction of sensor RH/T12 and sensing element once extracted

7.2 CELL HT2 – SALINE WATER

7.2.1 STABILISATION PHASE

Sensors were installed in the cell and started recording values for 59 days before the initiation of the heating phase. The average values for relative humidity and temperature during this initial phase are shown in Figure 59 (left). The relative humidity and temperature inside the bentonite were of 78 % and 22 ˚C, respectively, with the RH increasing from top to bottom, which can be partly related to a different behaviour of sensor RH/T21, already observed while the sensors were measuring on air (Figure 32). The external temperatures were lower than the inner ones and increased from the top to the bottom of the cell in a range ~1 ˚C. After the cooling system on top of the cell was switched on, the internal and external temperatures decreased and the gradient of temperatures between top and bottom of the cell surface slightly increased (Figure 59, right). Once the different offsets corrected, the total pressures did not change when the cooling system was launched and remained around 0.0 MPa.

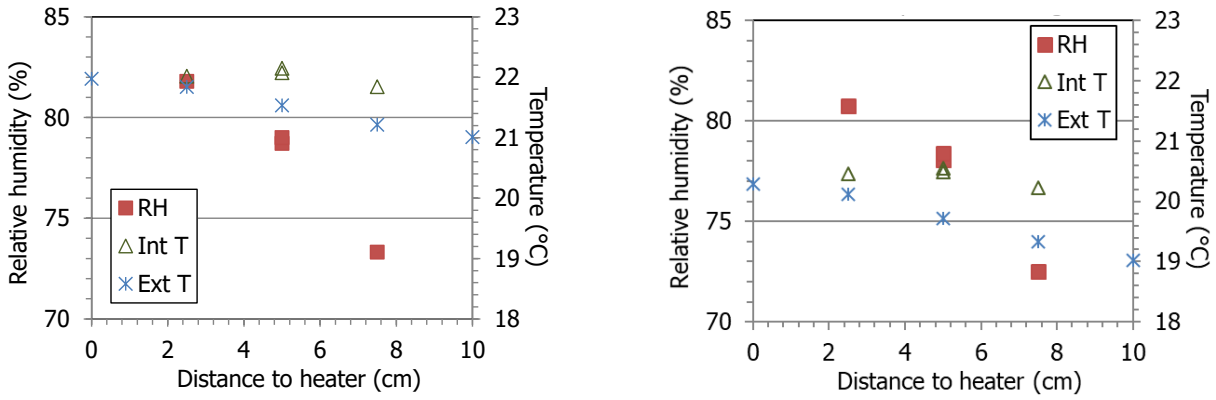

Figure 59. Steady relative humidity and temperature values during the stabilisation phase in cell HT2 (left) and after cooling on top was switched on (right)

7.2.2 HEATING PHASE

The following figures show the evolution of relative humidity, temperature and pressure during the heating phase (Figure 60 to Figure 62). The temperatures were increased from 70 ˚C to 150 ˚C over a period of 9 days. To keep the final target temperature a power of 10.5 W was necessary. After each temperature step, thermal equilibrium was quickly reached. The water vapour moved towards the upper part of the cell, where the relative humidity started to increase first at the bottom sensor location and then in locations upwards. At 2.5 cm from the heater (sensor RH/T24) the RH reached 100 % in 20 minutes and in the middle and upper part of the column when the heater temperature was increased to 110 ˚C. The two middle sensors (which behaved similarly) started to record a relative humidity decrease shortly afterwards, whereas the upper sensor (at 7.5 cm from the heater) remained flooded until the end of heating. The sensor at the bottom of the sample started to dry out one day after the heater temperature reached the target value of 150 ˚C. The upper radial pressure sensor recorded an increase up to 2 MPa after 20 days of heating and then a slow decrease. At the end of the heating phase none of the pressure sensors were recording a significant value. The thermal gradient measured inside the bentonite and on the external surface of the cell was similar. The steady values at the end of this phase are shown in Figure 63.

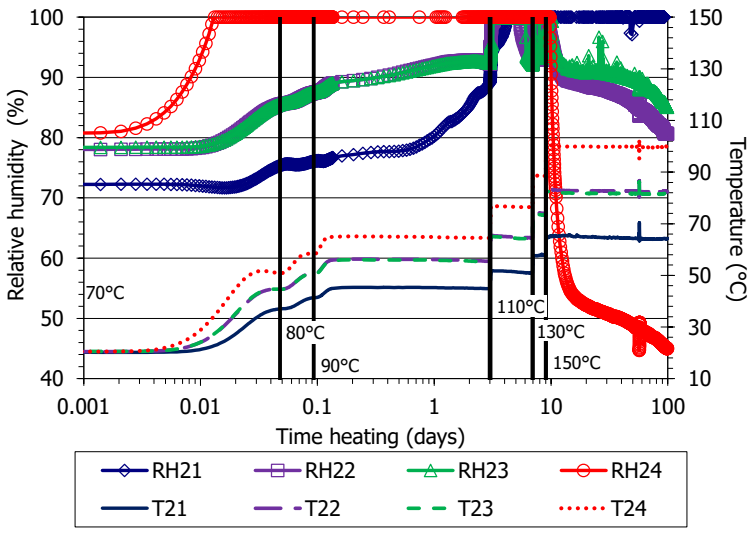

Figure 60. Evolution of relative humidity and temperature inside the bentonite during the heating phase of cell HT2

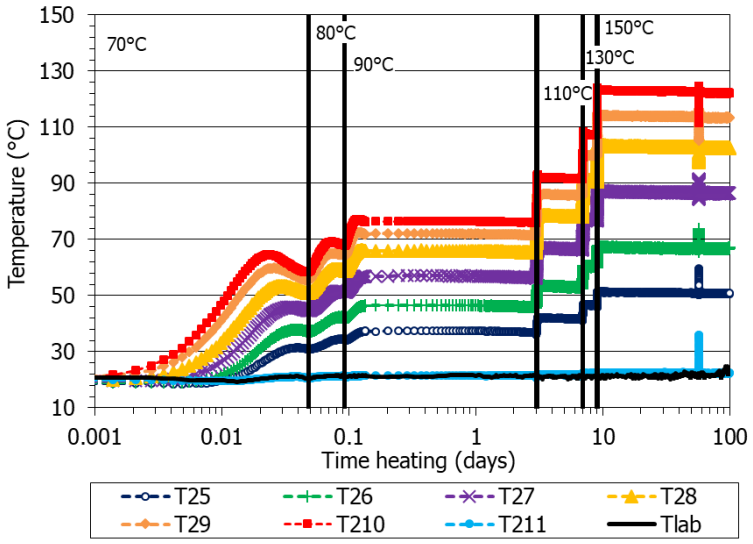

Figure 61. Evolution of external temperatures during the heating phase of cell HT2 (the vertical lines indicate the successive target temperatures of the heater)

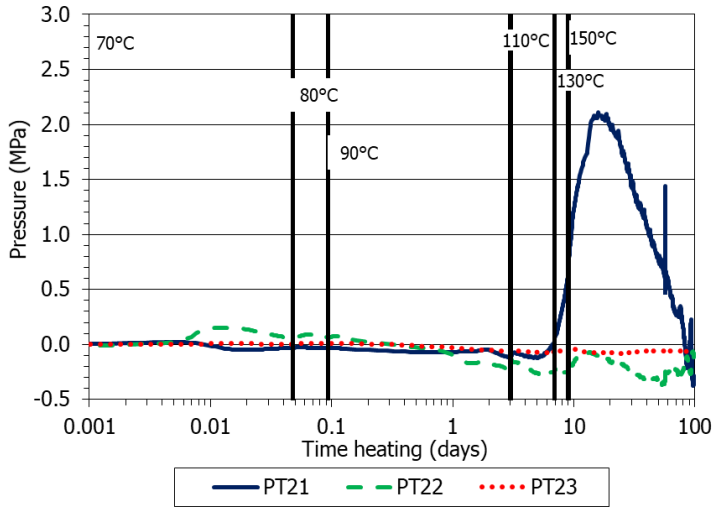

Figure 62. Evolution of radial pressure during the heating phase of cell HT2

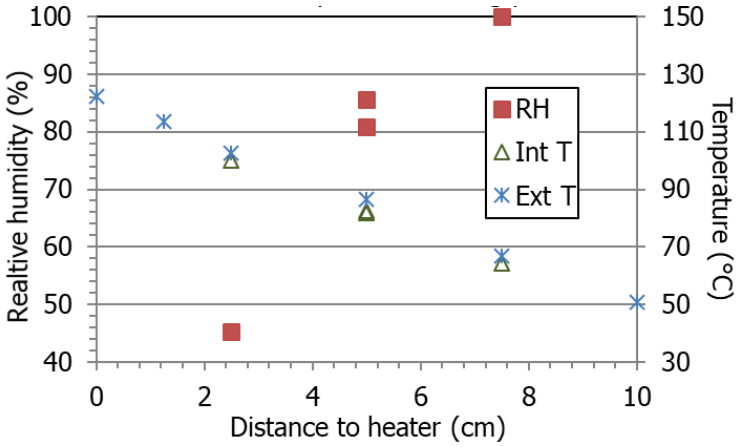

Figure 63. Steady values of relative humidity and temperature at the end of the heating phase in cell HT2

7.2.3 HEATING+HYDRATION PHASE

After the three initial months of heating, leading to quasi-steady hydraulic conditions, hydration started in May 2021. The evolution of relative humidity and internal and external temperatures during the heating+hydration phase is presented in Figure 64 and Figure 65. The temperatures were not affected by the beginning of hydration, and both the internal and the external sensors recorded constant temperatures until they began to fail. The RH/T sensor on top was already flooded when hydration started. In the middle part of the column the relative humidity started to increase about one day after the beginning of hydration and in the bottom part almost at the same time. The two sensors in the middle of the column were flooded in less than 25 days. After three months of hydration there was an overheating episode (described in 7.1.3.1 and below) which caused the flooding of sensor RH/T24. From this time on no reliable information about the RH or T inside the bentonite was provided, except for sensor RH/T24.

The evolution of radial pressures and water intake during the heating+hydration phase is shown in Figure 66. The radial pressure sensors in the upper and middle parts of the cells had recorded increasing trends since the beginning of hydration, while the bottom sensor did not record any change. The pressure and water intake evolutions were much affected by the overheating and heating/cooling cycles described below.

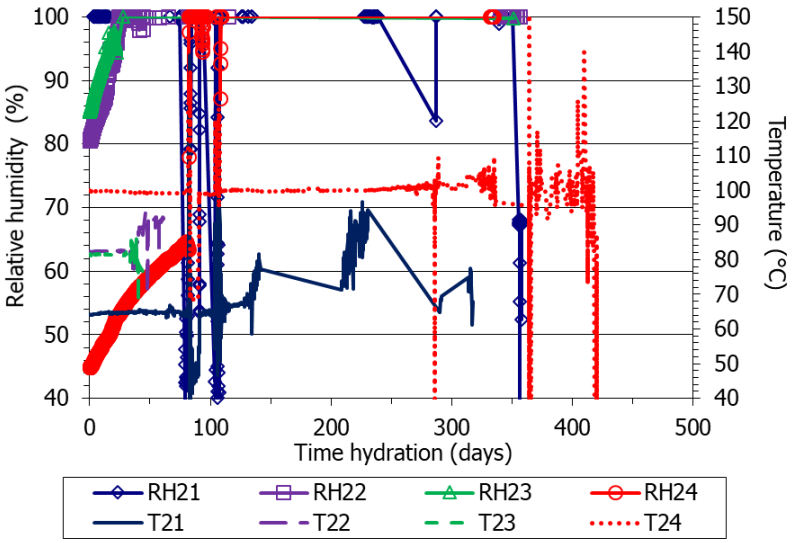

Figure 64. Evolution of relative humidity and temperature inside the bentonite during the heating+hydration phase of cell HT2 (hydration lasted 853 days)

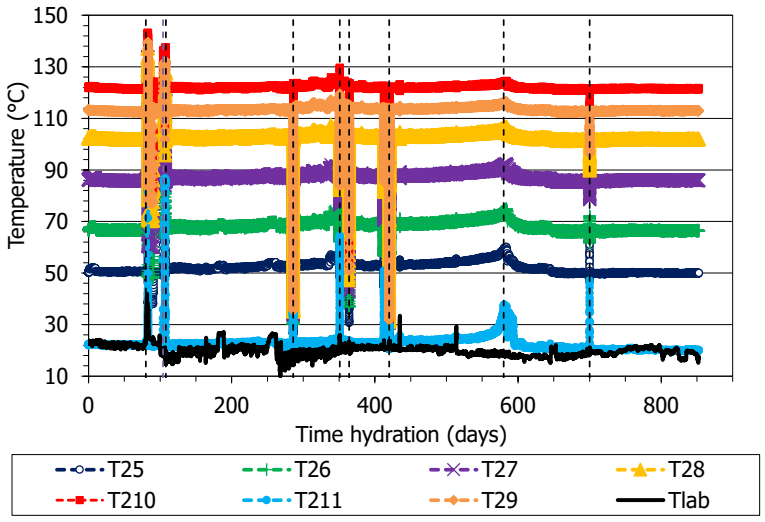

Figure 65. Evolution of external temperatures during the heating+hydration phase of cell HT2

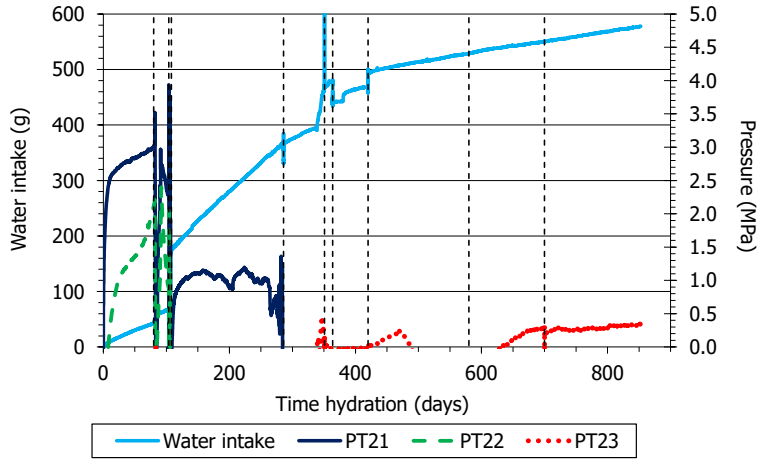

Figure 66. Evolution of radial pressures and water intake during the heating+hydration phase of cell HT2

7.2.3.1 OVERHEATING EPISODE AND CHILLER REPLACEMENT

As a result of an air conditioning failure on August 13th 2021 (day 80 of hydration), concurrent with a heat wave in Madrid, the temperature in the laboratory reached values of 42 °C (Figure 67, where the temperatures on the surface of the cell are also shown). The chiller system on top of cells failed (day 82 of hydration) and the temperatures in cell HT2 reached 125 °C in the bentonite upper part and 137 °C at 2.5 cm from the heater (Figure 68). When the failure was realised, and to avoid damaging the sensors, the heater temperature was decreased to 100 °C and remained in this value for 7 days before increasing it again to 120 and then to 150 °C. These changes can be observed in the Figures. The radial pressures dropped to 0 MPa as a result of the overheating and increased again when the heater temperature was set to 100 °C. When it was set again to the target value of 150 °C, the pressures decreased again, particularly in the

middle of the block. The pressure sensor at the bottom of the column did not react during the whole process and kept in 0.0 MPa (Figure 69).

After the heater temperature had been set again to 150 °C, the chiller kept going on and off for some days (hydration days 104-107), and the external and internal temperatures experienced sudden changes (Figure 70, Figure 71). Increase in the water uptake rate, as well as drops and subsequent increases in radial pressure were observed (Figure 72). Afterwards, the chiller was replaced (hydration day 108) and, although the water intake rate reduced, the radial pressures were almost suppressed. After these events, no more RH information was provided and only the temperatures recorded by sensors RH/T21 and RH/T24 seem reliable.

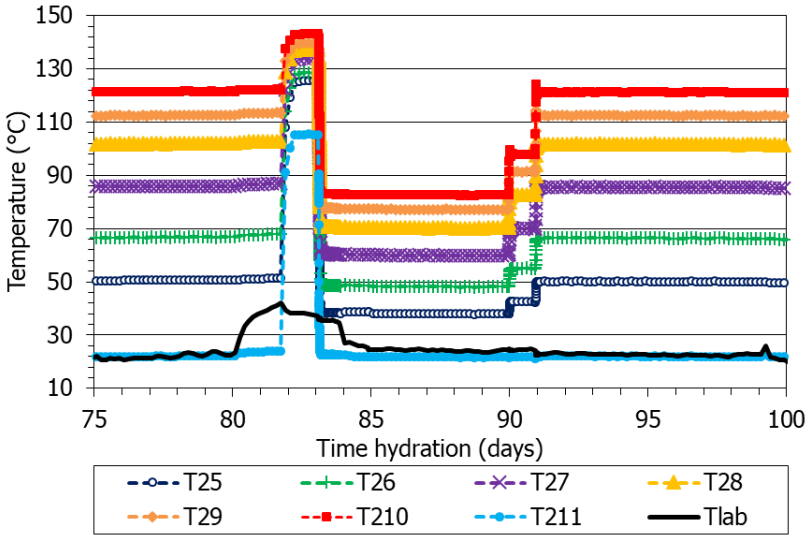

Figure 67. Evolution of laboratory and external temperatures on cell HT2 around the overheating episode

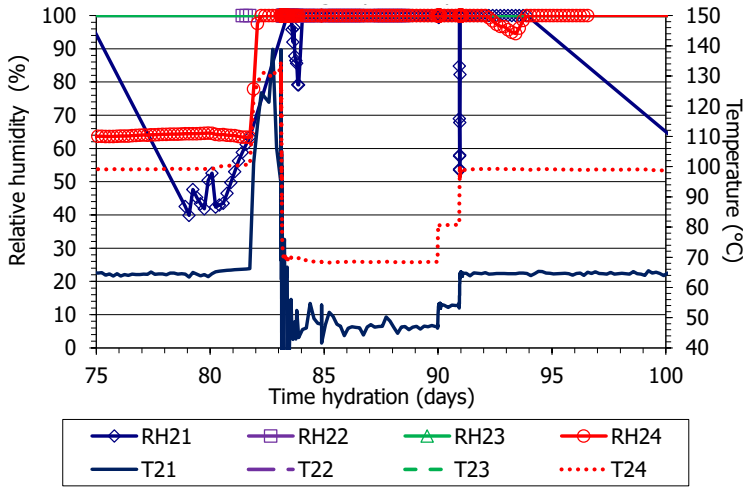

Figure 68. Evolution of relative humidity and temperature inside the bentonite of cell HT2 around the overheating (day 80 of hydration)

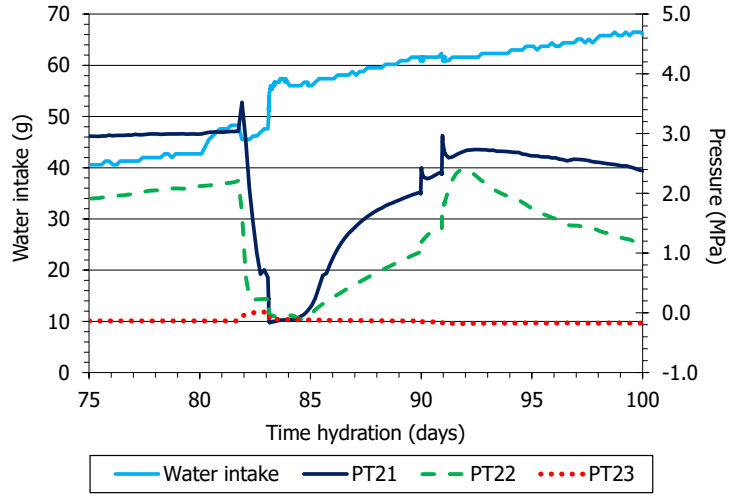

Figure 69. Evolution of radial pressure and water intake of cell HT2 around the overheating (day 80 of hydration)

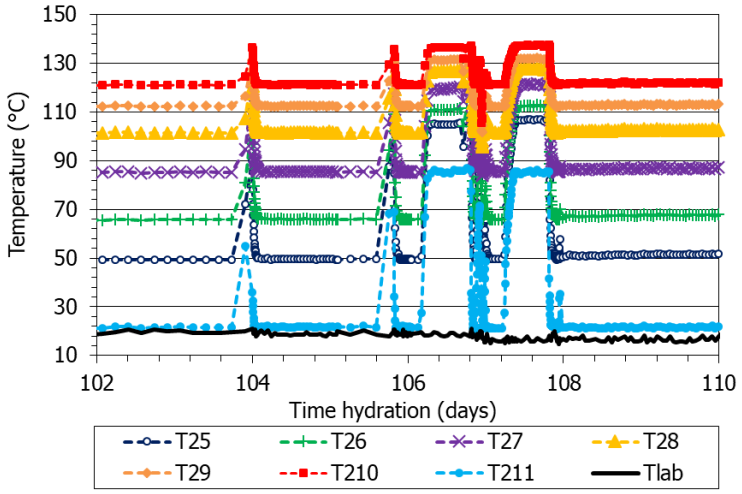

Figure 70. Evolution of laboratory and external temperatures of cell HT2 in the period between the overheating and the chiller replacement

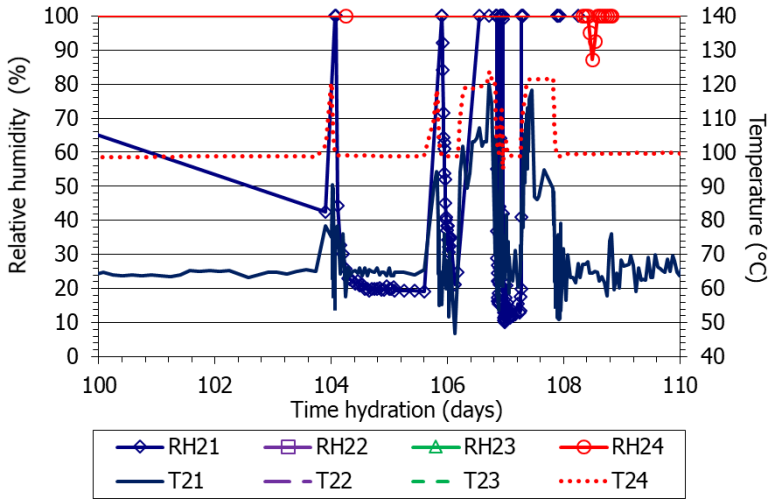

Figure 71. Evolution of relative humidity and temperature inside the bentonite of cell HT2 in the period between the overheating and the chiller replacement

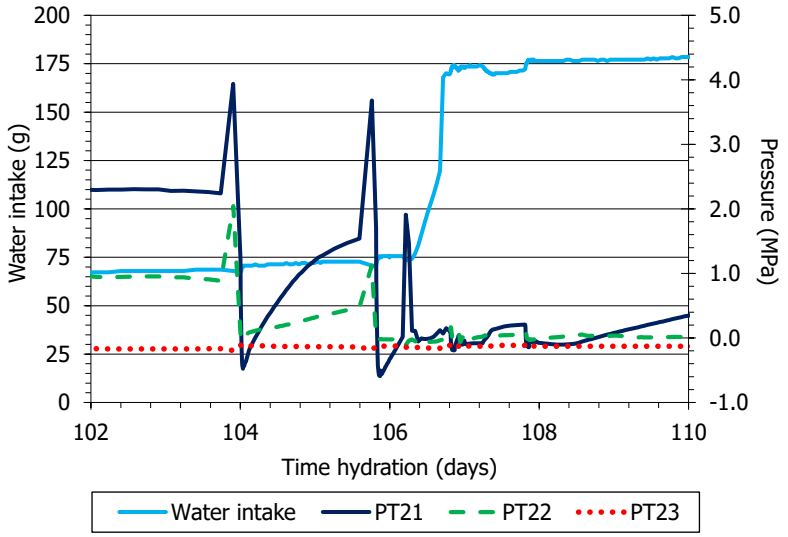

Figure 72. Evolution of radial pressure and water intake of cell HT2 in the period between the overheating and the chiller replacement

7.2.3.2 RESEALING OF SENSORS' INLETS

Once the chiller was replaced and the temperatures had come back to normal, an increased water uptake rate was observed, as well as a persistent drop in the radial pressure measured by sensor PT21 and the eventual failure of sensor PT22 (Figure 73).

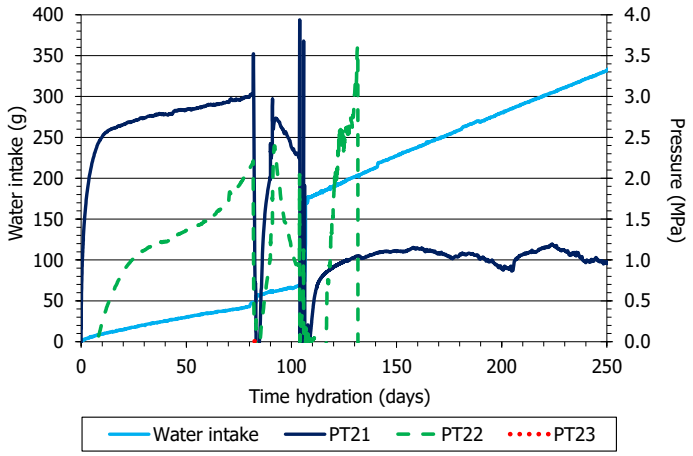

Figure 73. Evolution of radial pressure and water intake rate before and after the chiller replacement (day 108 of hydration)

This behaviour was attributed to some water leak resulting from alternating thermal expansion and contraction of the cell elements resulting from the chiller failures detailed above, and/or deterioration of some of the cell elements because of the excessive temperatures and salinity. The leaks took possibly place through the sensors' openings. Hence, it was decided to try and see if this was the case and reseal these openings. The resealing process was the same described in subchapter 7.1.3.2 and took place simultaneously. It started on day 286 of

hydration and took less than 5 hours. As with cell HT1, water drops, bentonite and what seemed salt precipitates were observed when the RH/T sensors were inspected (Figure 74).

Figure 74. Water drops and bentonite around sensor RH/T22

Figure 75 shows the evolution of radial pressure and water intake in cell HT2 just before and after sensors' sealing (hydration time: 286 days). The pressure sensors in cell HT2 did not resume any proper functioning (and in the case of sensor PT21 the behaviour even worsened) and the water intake rate was not clearly suppressed.

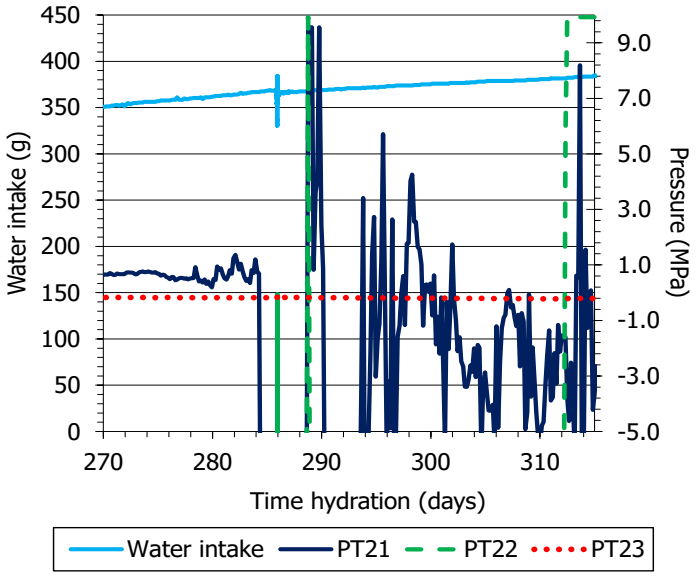

Figure 75. Evolution of radial pressure and water intake before and after sensors' sealing in cell HT2

7.2.3.3 REMOVING OF SENSORS AND OTHER MINOR EVENTS

In May 2022 (hydration day 364), a few weeks after the sealing of the RH/T sensors' inlets, bentonite was identified on the electronic boxes of sensors RH/T22 and RH/T24 (Figure 76). Sensor PT21, which had not been providing reliable information, had to be disconnected. As a

result of an electronic failure the heater temperature had inadvertently decreased to 70 °C. All those aspects were fixed on the same day.

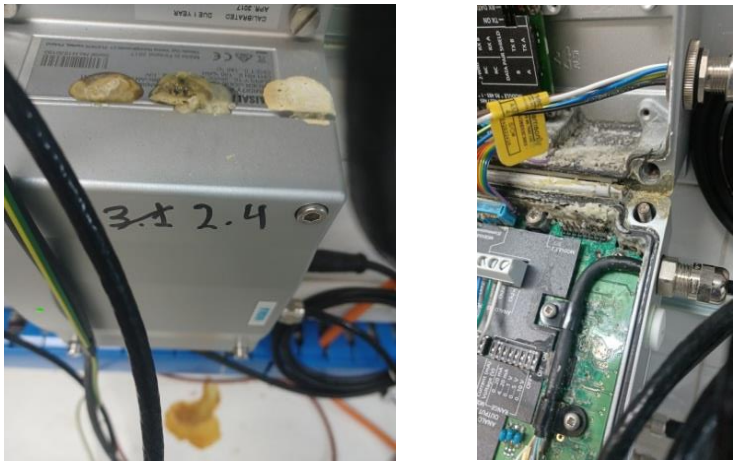

Figure 76. Box of sensor RH/T24 with bentonite on its surface (left) and box of sensor RH/T21 with bentonite inside (right)

In an attempt to reduce the high water intake rate (presumably triggered by leaks through the cell elements), it was decided to completely remove the RH/T sensors and plug the inlets with bolts. This was accomplished on hydration day 420. Only the external temperatures, heater power and temperature, and water intake were being correctly measured by then. Even though there were no conclusive indications of faulty behaviour of sensor PT23, it only started to record noticeable values (but <0.5 MPa) towards the end of the test (Figure 66).

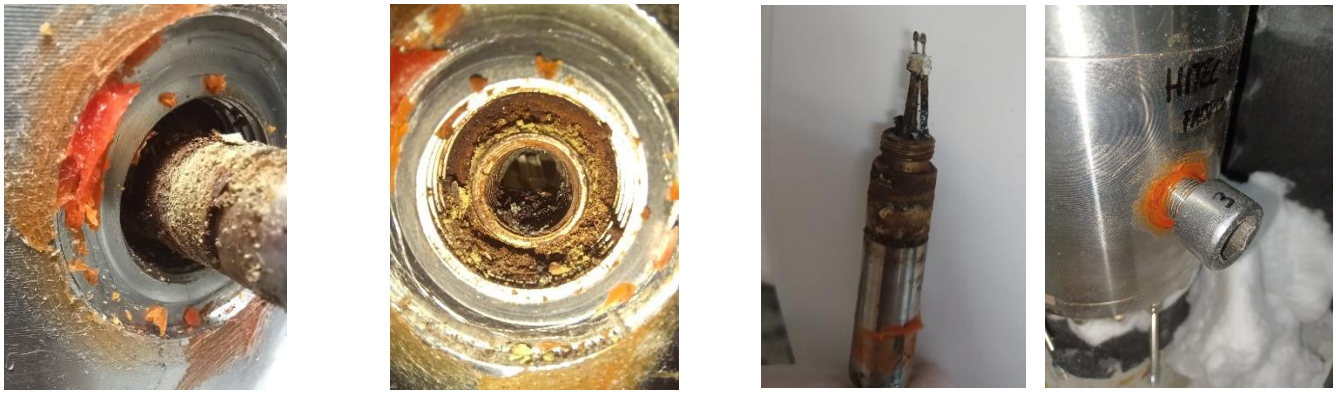

Figure 77. Removing of RH/T sensors in cell HT2 and sealing of inlet with bolts

The heater was disconnected, the insulation material was removed, the sealing elements of the sensors were unscrewed, the sensors were extracted and the inlets were closed with bolts sealed with Nural 28 (Figure 77). The heater temperature decreased to 31 °C. Afterwards the insulation material was put in place again, the cooling system on top was switched on, the heater temperature was set to 70 °C and the hydration line was open. From the moment the heater was switched off until the heater was switched on again 3 hours elapsed. The heater

temperature was increased in steps up to 120 ˚C in 2 additional hours and the next day the target temperature of 150 ˚C was set again. The temperatures outside the cell just before and after the sensors' removal are shown in Figure 78.

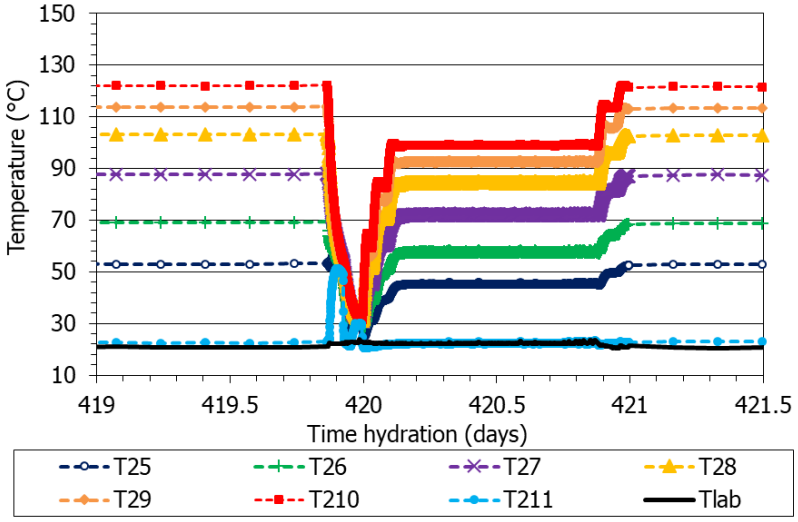

Figure 78. Evolution of external temperatures before and after removal of the RH/T sensors

Along this period several other events took place, such as blackouts or air conditioning failures that were slightly reflected on the cell temperatures (Table *8*). Normally during power outages the heater temperature had to be decreased beforehand (to values 100-120 ˚C) and then stepwise increased to the target value. The scheduled blackouts lasted less than 1 h.

7.3 SUMMARY OF PATTERNS RECORDED

The two cells were disassembled after ~2.5 years of hydration and heating. Before hydration started, the cells had been heating at 150 ˚C for three months, so that to reach steady-state RH conditions. The temperatures reached steady values in few hours. Figure 79 shows these equilibrium values at the end of the heating phase for the two cells. The temperatures measured at the same distance from the heater either inside the bentonite by the capacitive sensors or on the surface of the cells with thermocouples were very similar in the two cells. Also, the thermal gradient generated from the bottom towards the upper part of the bentonite block was linear in both cells, with values around 7 ˚C/cm. The power needed to keep a temperature of 150 ˚C at the heater surface during the heating phase was slightly higher for cell HT2 (10.5 vs. 10.0 W). The movement of water vapour as a result of the thermal gradient was evinced by the increase in relative humidity recorded by the sensors closest to the heater and in the middle part of the cell –followed by a continuous decrease– and the slower increase recorded by the upper sensors, which were in both cells flooded at the end of the heating

phase. The relative humidity gradient at the end of the heating phase was very steep and similar in the two cells.

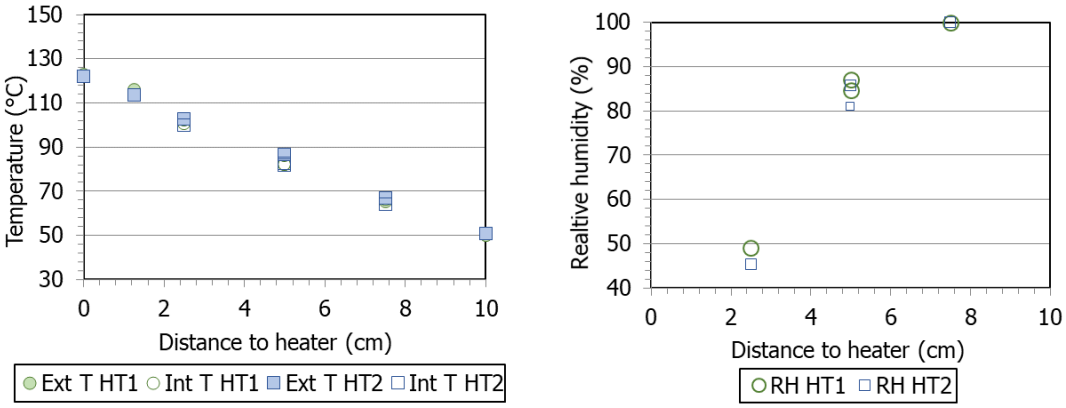

Figure 79. Steady temperatures during the heating phase inside the bentonite and on the surface of the cells (left) and relative humidity at the end of the heating phase (right) for the two cells

The radial pressure during the heating phase remained close to 0.0 MPa in the middle and bottom of the cells, and temporarily increased to values close to 2 MPa in the upper part. The similarity of the pressure development pattern and of the actual values reached in the two cells is rmarkable (Figure 80).

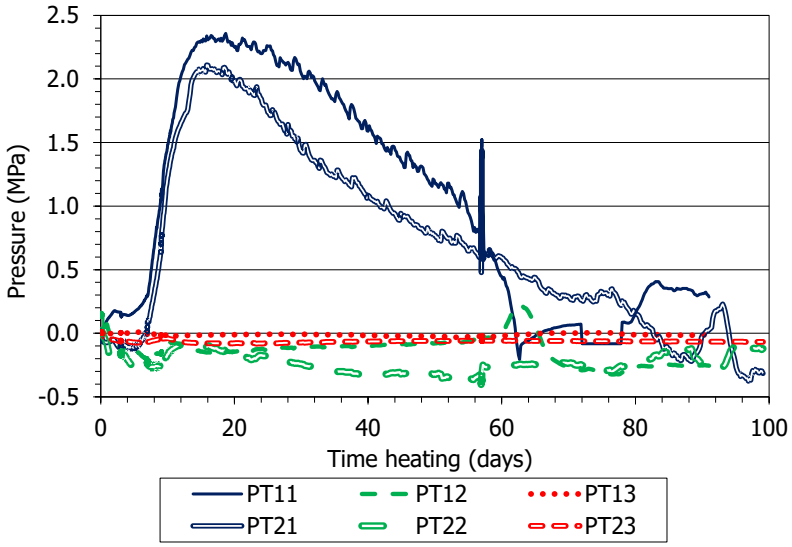

Figure 80. Evolution of radial pressure in the two cells during the heating phase

The temperatures barely changed as a result of hydration and the heater power did not change. The relative humidity inside the cells started to increase in the middle of the bentonite columns one day after the beginning of hydration, and in the bottom part after 2-4 days (Figure 81). This rapidity could suggest that some water transport took place along the cells' wall. The sensors

in the middle part of the cells recorded 100 % after ~25 days. After the overheating event, which took place 80-90 days after the beginning of hydration (described in subchapters 7.1.3.1 and 7.2.3.1), no more information on relative humidity was obtained.

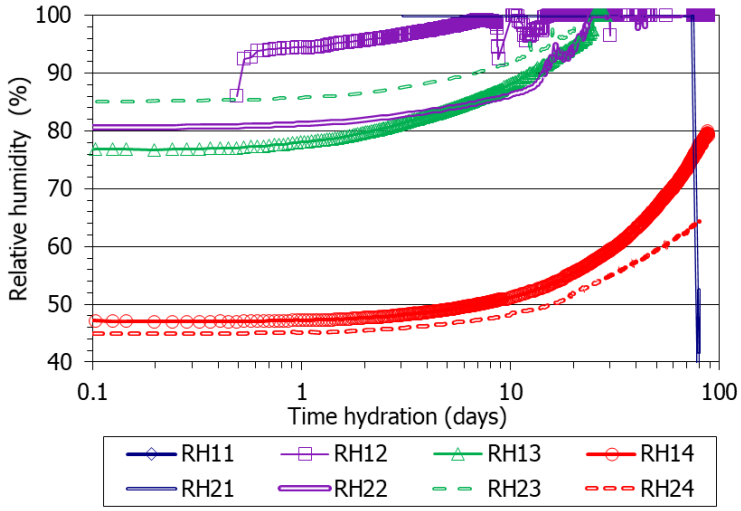

Figure 81. Evolution of relative humidity inside the bentonite in cells HT1 and HT2 before the overheating event (for location of sensors see Table 1)

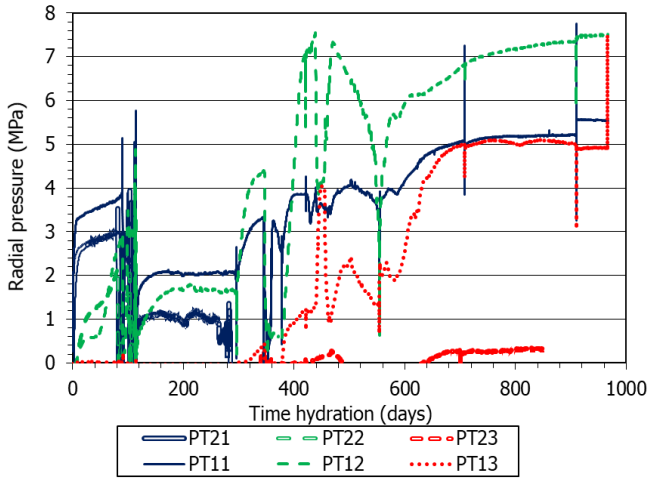

Figure 82. Comparison between radial pressures measured in cells HT1 and HT2 (for location of sensors see Table 1)

The evolution of the pressures measured at the bentonite/cell contact in the two cells is shown in Figure 82. The pressure increased progressively from top (hydration surface) to the middle part of the column. The initial increase on top was quick and simultaneous in the two cells but the quasi-steady values reached were higher in cell HT1 (4 *vs*. 3 MPa), consistent with the low salinity of the hydration water. It took about 7 days for the pressure to increase in the middle part of the column, although the relative humidity in this area had started to increase earlier. In fact, the radial pressure did not increase until the relative humidity reached values of between

78 and 92 %, depending on the location (Figure 83). It took a long time for the bottom sensors (PT13, PT23) to record pressure build-up: ~300 days in cell HT1 and ~440 days in cell HT2. In the latter case the increase was very small and not consistent, only after ~640 days the increase was clearer, but stopped at a steady value of just 0.3 MPa, in accordance with the very low water content reached in this area (see subchapter 9.2.2). The pressure recorded by all sensors was very much affected by the changes in temperature caused by blackouts and by the actions taken to seal leaks, which resulted in pressure increases.

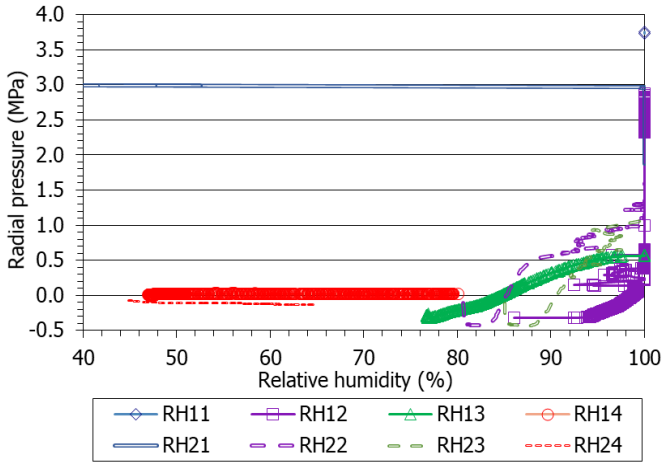

Figure 83. Evolution of radial pressure as a function of the relative humidity measured at the same distance from the heater for the two cells before the overheating event (for location of sensors see Table 1)

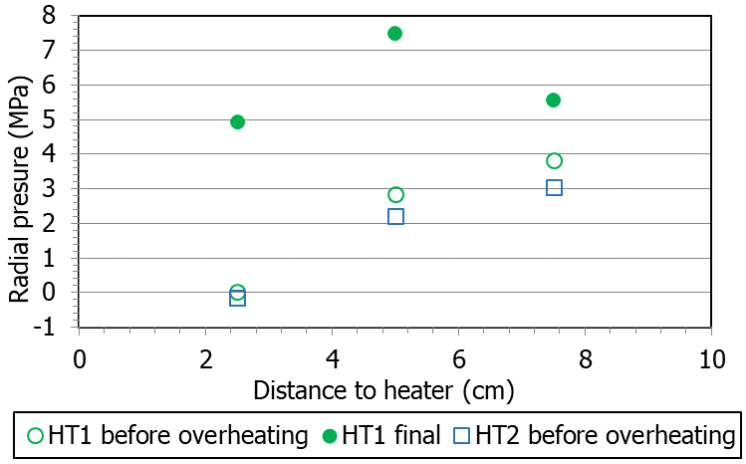

Figure 84. Radial pressures before the overheating event and at the end of the heating+hydration phase for cell HT1

The radial pressure values just before the overheating event and at the end of the test (only for HT1) have been plotted in Figure 84 as a function of the distance to the heater. Before the overheating event the pressure lineally decreased from top to bottom in the two cells but was

slightly lower in the one hydrated with saline water (HT2). After the overall decrease following the overheating event, the pressure measured in cell HT2 never increased above these values. In contrast, they increased in cell HT1 and reached considerably high values through all the column, particularly in the middle part.

The water intake during the hydration phase as recorded by the load cells weighing the water flasks is plotted in Figure 85. The water intake recorded in this way was much higher than the actual water amount taken by the bentonite, which is the one obtained by weighing the bentonite block upon dismantling (see Section 8). The Figure shows these actual water intake values as horizontal lines. The difference between the actual water intake and the one recorded online is considered to be caused mainly by undetected leaks during operation through the sensors' inlets and/or bottom surface, enhanced by the heating/cooling cycles caused by power outages and chiller failures, although other factors could have contributed to a smaller extent. The water intake rate was particularly enhanced after these events. The discrepancy between online measurements and actual water intake was of the same order for the two cells. At the beginning of saturation, the water intake was higher in the cell saturated with glacial water, and it kept so at least for the first year, although the values after the overheating are not very reliable.

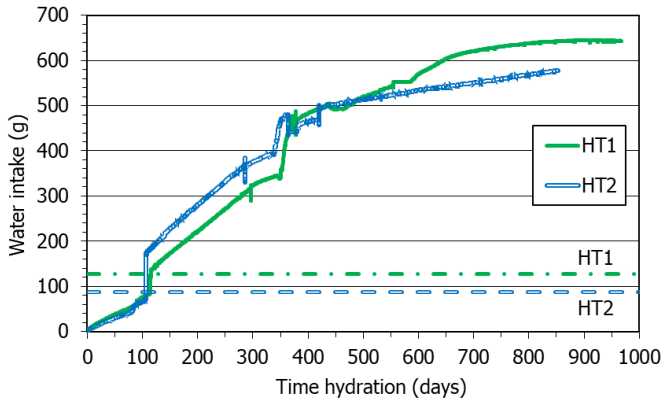

Figure 85. Water leaving the hydration vessels measured online and actual water intake measured at the end of the tests (horizontal dotted lines)

8 DISMANTLING OF CELLS

The two cells were dismantled following the general protocol described below.

1. Changing the time of data acquisition to 1 minute.
2. Closing the water intake.
3. Switching-off the heater.
4. Emptying the upper internal hydration circuit with a syringe and collection of water.
5. Removing of the external insulation (Figure 86). The temperature suitable for manual handling was reached ~1 h after removal of the insulation.

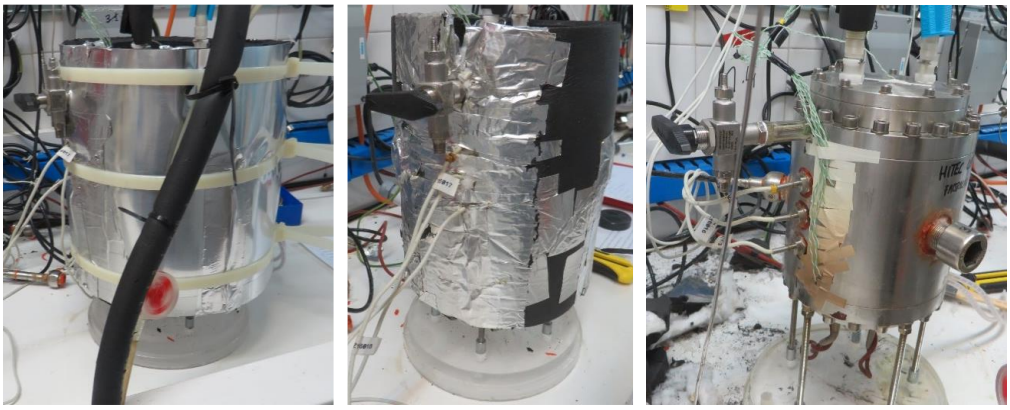

Figure 86. Appearance of cell HT2 (left: external insulation, middle: internal insulation) and HT1 (right: once insulation layers were removed)

6. Extracting the RH/T13 sensor in cell HT1 and closing the openings with bolts. Water outflow through this sensor was observed. The sintering was found broken, oxidised and somewhat displaced (Figure 87). The rest of sensors had been extracted during the operation stage, as described in subchapters 7.1.3.3 and 7.2.3.3.

Figure 87. Extraction of sensor RH/T13

7. Removing the pressure sensors (Figure 88) and closing of the openings with screws.

Figure 88. Extraction of pressure sensors (left: PT13; middle: all PT1x closed with screws; right: PT22, whose screw was not easy to turn)

8. Removing the connection to the cooling circuit.

9. Removing the externally glued thermocouples.

10. Removing the connection to the heater.

11. The hydration vessel was taken from its support to sample the water inside.

12. For the remaining manipulations, moving the cell to the main laboratory. The sensors kept measuring in the air in the same laboratory, to check their performance.

13. Emptying of the cooling chamber and weighing of the cell prior to removing all the external elements of the cell: heater, cooling chamber (Figure 89).

Figure 89. Emptying of the cooling chamber and weighing of cell HT2

14. Extracting the RH/T sinters that remained inside by using the appropriate tools and closing the openings with bolts (Figure 90). In some cases this was not possible and

the filters could not be extracted until the bentonite block was cut in sections (see below).

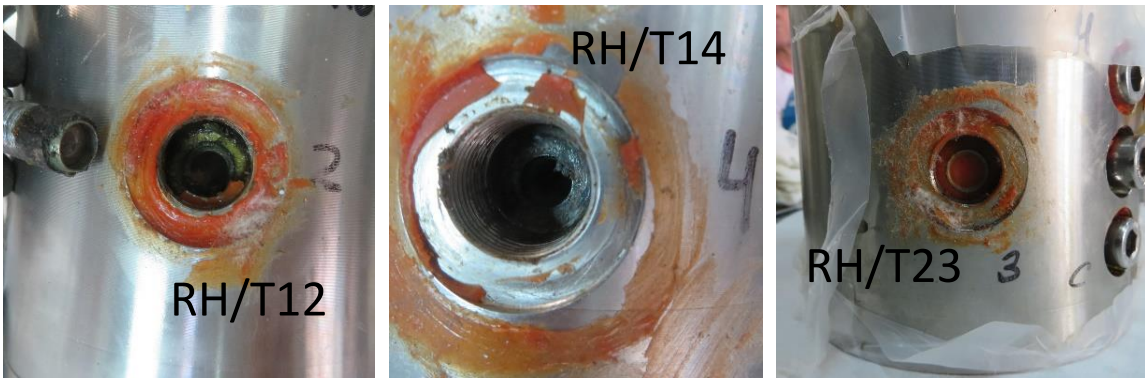

Figure 90. Removing part of sinter of sensor RH/T12 (left). Examples of sensor sinters which had remained stuck inside the bentonite and were broken during extraction (RH/T14, middle and RH/T23, right)

15. Removing both lids and the hydration sinter. Weighing the cell with the bentonite inside and the wet hydration sinter and lids (Figure 91).

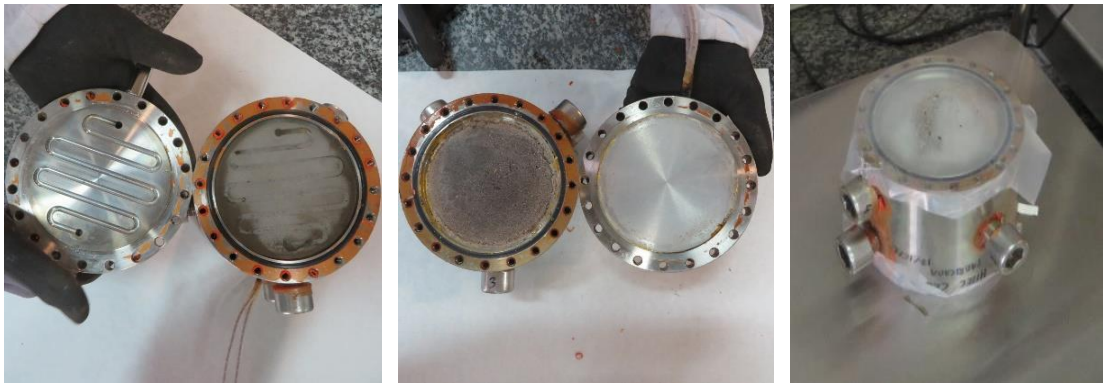

Figure 91. Opening of the hydration (left) and heater (middle) lids in cell HT1. Weighing of cell HT2 (right)

16. Extracting the sample by pressing with a piston from the bottom surface of the sample (Figure 92). Note that the block was able to move upwards during extraction and the pressure applied during this process was much smaller than the compaction pressure, hence no impact of this procedure on the physical state of the block is expected. However, the bottom part of cell HT2 remained stuck to the cell wall (see below in subchapter 8.2).

Figure 92. Extraction of samples HT1 (left) and HT2 (right) by pushing from the bottom

17. Weighing and measuring the bentonite block (Figure 93). Immediately wrapping it with plastic film to preserve water content.

Figure 93. Weighing of entire block of cell HT1 (left) and cohesive part of HT2 (right)

During the dismantling process in the main laboratory, the cell and components were weighed at different phases for crosschecking the final weight obtained once the bentonite block was extracted. The elements susceptible to store water (sinter filter, filter paper, hydration lid…) were weighed immediately after demoulding, and then dried, in order to discount the mass of water that was in the cell, but not in the bentonite. The weight of sinters that could not be extracted from the bentonite was subtracted from the bentonite block weight measured immediately after extraction. Also, all the bentonite that remained adhered to the cell walls, sensors, lids, etc. was recovered and weighed.

The particularities of the dismantling of each cell are detailed in the following subchapters.

8.1 CELL HT1

After 1058 days of heating (2.9 years) and 970 days of hydration (2.7 years) cell HT1 was dismantled following the procedure described above. Figure 94 shows the evolution of

temperature outside the cell and the radial pressures once the heater was switched off and until the external sensors were unglued. No RH/T sensors were working by the time of dismantling.

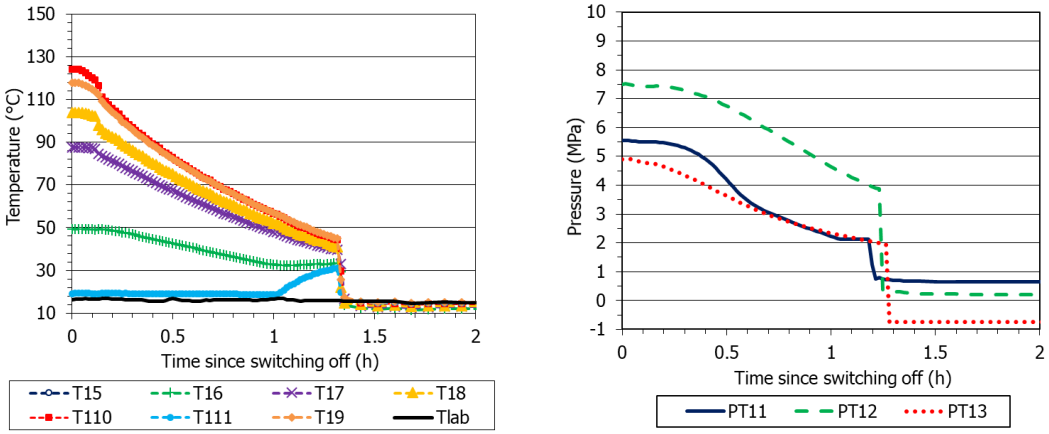

Figure 94. Evolution of external temperatures and radial pressures during the dismantling phase. The sudden drops correspond to the moment the sensors were removed from the cell

The appearance of the pressure sensors was good, they did not seem damaged or corroded (Figure 88). The bentonite block was extracted by applying a pressure from its bottom surface of 1.8 MPa. The block was consistent, looked saturated (because of its dark colour) and presented oxide stains (Figure 95). During dismantling no filter of the RH/T sensors could be extracted, they remained inside the clay (e.g. Figure 87) and had to be extracted when the block was sliced for sampling. Upon slicing, corrosion halos were observed in the external and internal parts of the block, particularly around sensors (Figure 96, Figure 97).

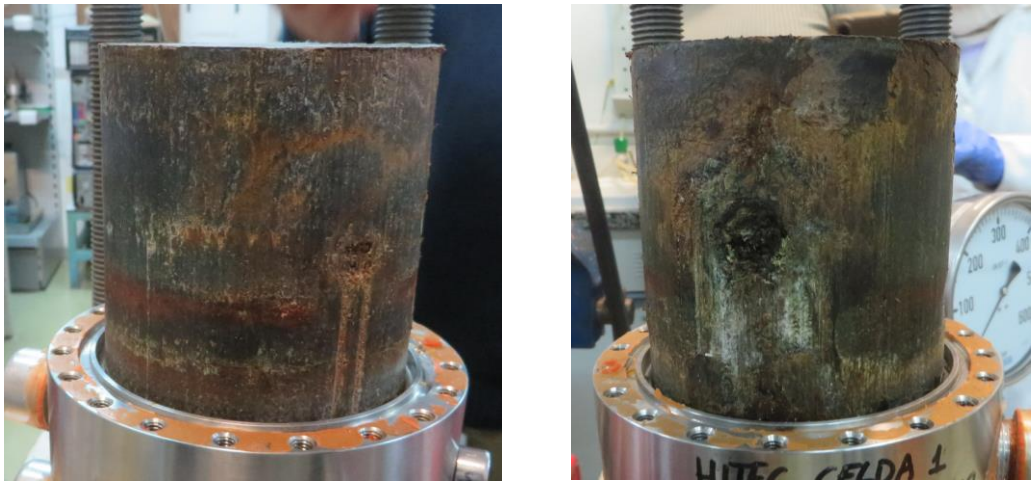

Figure 95. Appearance of HT1 sample once extracted with superficial stains

Figure 96. Corrosion halos between sections 1 (left) and 2 (right) of cell HT1

Figure 97. Halo around sensor RH/T14 (left) and RH/T13 (middle, right)

In sampling section 1 (the one on top), a thin white crust at ~6 mm from the heater was observed (Figure 98) and sampled. It very soon disappeared.

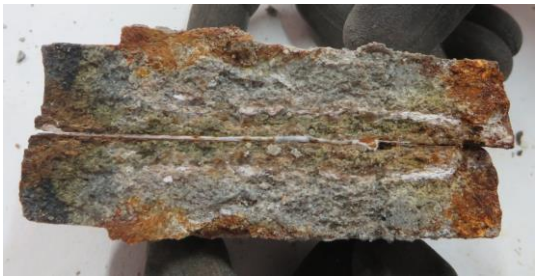

Figure 98. Thin white crust at ~6 mm from the hydration surface of cell HT1 (section 1 was transversally cut and the photo shows the two halves superimposed with the filter paper between them and the white crust above and below)

Figure 99 shows the final appearance of the internal surface of the cell after having been cleaned. Irregular dark stains remain on all the surface, except for the 2 cm closet to the heater. Around sensor RH/T12 a corrosion halo could be observed. The o-ring on the heater lid was flattened and somewhat rigid, but still flexible.

Figure 99. Appearance of the internal surface of cell HT1 just after having cleaned it. On the right-hand side, a corrosion halo around sensor RH/T12 can be seen

The best estimation of the final weight of the block is 1525.5 g, which gives a water intake of 127 g. Considering the initial bentonite weight and assumed initial water content (17.1 %, see Table 5), this would correspond to a final water content of 27.7 %. The measured water intake was of 638 g (Figure 85), which highlights the magnitude of the water leaks during the test.

8.2 CELL HT2

After 952 days of heating (2.6 years) and 853 days of hydration (2.3 years) cell HT2 was dismantled following the procedure described above. Figure 100 shows the evolution of temperature outside the cell and of radial pressure once the heater was switched-off and until the external thermocouples were unglued. Only PT23 was working, but there is uncertainty about its correct behavior. The RH/T sensors had been extracted before the cell was dismantled.

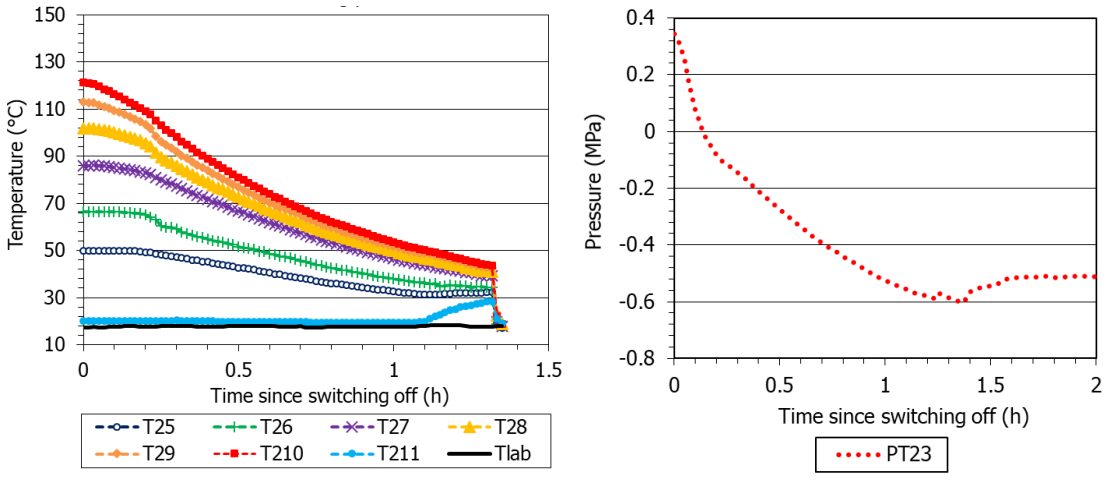

Figure 100. Evolution of external temperature and radial pressure in cell HT2 during the dismantling phase. The final temperature drops correspond to the moment the sensors were unglued from the cell

The sensing elements of the RH/T sensors had been removed in July 2022 (420 day of hydration), hence only the filters were inside the bentonite. The pressure sensors were removed at the beginning of the dismantling works and found very deteriorated (Figure 88), except for sensor PT23, which was only corroded. Their housings on the cell external wall were clean. It was not possible to extract the filters of the RH/T sensors from the bentonite and they had to be retrieved when the block was sliced for sampling.

Once the lower lid of the cell was unscrewed, the bentonite was found very dry, stuck to the heater, and with a darker colour in the periphery (Figure 101, left). The o-ring on the heater lid was flattened and somewhat rigid, but still flexible. The filter paper on top of the block was stuck to the bentonite and could not be totally detached (Figure 101, right). The upper bentonite surface was very wet and dark, but no remarkable stains were observed. The block was extracted by pushing from the bottom applying a pressure of 6.4 MPa, but only the cohesive upper part could be extracted (Figure 92, Figure 93), because the block broke and the rest of it remained stuck to the cell wall (Figure 102). The surface along which the block broke was oxidised and presented black stains close to the sensors' inlets. The bottom part of the block (corresponding to sections 5 and part of 4, i.e. the ~4 cm closest to the heater) had to be sampled with a spoon and other tools because it was not consistent, although some fragments were like cemented (Figure 103).

Upon slicing, corrosion halos and black stains were observed in the external and internal parts of the block (except close to the hydration surface, ~2 cm, where it was black), particularly around sensors (Figure 104). The filter of sensor RH/T24 was broken, and around the other three RH/T sensors crusts had developed. The filters of the sensors were completely deteriorated. Black stains could be observed also in places not related to the presence of sensors (Figure 105). All these particular samples were taken for subsequent analyses. The inner cell surface was heavily corroded, with deep pitting (Figure 106).

Figure 101. Bottom of the bentonite block HT2 and heater surface upon dismantling (left) and top of block with filter paper (right)

Figure 102. Cohesive part of block HT2 extracted from the cell (left) and upper appearance of the part of the block remaining inside the cell (right)

Figure 103. Section 5 (2 cm closest to the heater) of the bentonite block of cell HT2

Figure 104. Appearance of filter of sensor RH/T21 (upper left), filter of sensor RH/T24 (upper right), corrosion halos and crusts around sensors RH/T22 and 23 (bottom left) and RH/T24 (bottom right)

Figure 105. Surface at 6 cm from the heater in block HT2 (between sampling sections 2 and 3)

Figure 106. Appearance of the internal surface of cell HT2 just after block extraction (left, cell upside down) and after having cleaned it (right), showing important pitting corrosion

The best estimation of the final weight of the block is 1488.8 g, which gives a water intake of 88 g. The measured water intake was of 578 g (Figure 85), which highlights the magnitude of the water leaks during the test. As discussed below in subchapter 9.2.2, the incoming water was loaded with salt (with TDS of 10859 mg/L, Table 4), and although most of it evaporated through the sensors inlets until they were completely sealed or removed (see subchapter 7.2.3.3), the salts would have remained inside the cell (except in the case of the water that run along the cables and reached the electronic boxes loaded with bentonite, Figure 76, although it is not possible to assess how much this amount was). A rough computation of this quantity gives a value of 6.3 g of salt. Subtracting this quantity from the final block weight gives a final wet bentonite weight (without salt) of 1482.5 g. Considering the initial bentonite weight and assumed initial water content (17.2 %, see Table 5), this would correspond to a final water content of 24.1 %.

8.3 FINAL ASSESSMENT OF SENSORS' PERFORMANCE

The external thermocouples were left measuring outside the cells to check their proper functioning, as well as the pressure sensors of cell HT1 and sensor PT23, the only one working in cell HT2 (Figure 94, Figure 100). The RH/T sensors had been extracted before the end of operation.

All the external temperature sensors measured properly and the values given under room conditions differed among them in 2.3 °C for cell HT1, which is in the order of the difference found before the beginning of the test (Figure 33). The pressure sensors of cell HT1 gave values between -0.7 and 0.8 MPa, which can be considered a very narrow range.

The temperature sensors of cell HT2 measured in the air values that differed in less than 1.8 °C among them. Sensor PT23 gave a constant value of -0.5 MPa.

9 POSTMORTEM ANALYSES

Once the bentonite blocks were extracted from the cells (Figure 92, Figure 93, Figure 95, Figure 102), they were cut into five 2-cm thick sections with saw and knife (Figure 96, Figure 105). The sections were numbered from 1 (uppermost) to 5 (closest to the heater). This was easily done for cell HT1, because the block was consistent, but the block of cell HT2 was damaged at the bottom, where it was very dry and had little consistency, and sections 4 and 5 could not be clearly defined. Each section was separated in internal and external zones, to check any potential "wall effect" (Figure 107). Subsamples of these two zones were taken for the physical, mineralogical and geochemical characterisation of bentonite. Subsamples for part of the mineralogical and geochemical characterisation of bentonite were taken by staff of the Universidad Autónoma de Madrid (UAM) the same days the cells were dismantled. The subsampling of the sections was performed by sawing or cutting with knives.

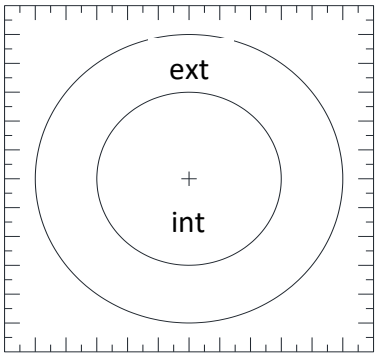

Figure 107. Location of subsamples in each horizontal section

9.1 ANALYSIS OF THE HYDRATION WATER

After the cells were dismantled, an aliquot of about 20 mL from the water remaining in the hydration bottles was taken and analysed. Sodium and potassium were determined by ion chromatography as well as the anions, and the concentration of the rest of major cations was analysed by Inductively Coupled Plasma-Atomic Emission Spectrometry (ICP-AES). The results obtained are shown inTable 9. The initial composition shown in this table corresponds to the actual composition of the water in the hydration bottle of each cell checked just after preparation of the synthetic water (also shown inTable 4), in order to have the exact composition before the initiation of hydration.

In cell HT1, hydrated with glacial water, the amounts of all the ions increased during the test, particularly those of sulphate and bicarbonate. The differences between the initial and final

composition for the cell hydrated with saline water, HT2, were the decrease in the chloride, sodium and calcium amounts and the increase in bicarbonate, sulphate and potassium.

ION	HT1 INITIAL (glacial)	HT1 FINAL	HT2 INITIAL (saline)	HT2 FINAL
F^-	-	<0.1	-	<0.10
Br^-	-	0,41	-	0,15
Cl^-	2,94	15	6.689	6.200
I^-	-	<0.5	-	<0.10
SO_4^{2-}	0,12	79	-	0,31
HCO_3^-	-	98	-	32,94
Al^{3+}	-	<0.03	-	<0.03
Ca^{2+}	0,86	5,6	1.628	1.300
Mg^{2+}	0,68	0,66	0,14	0,13
Na^+	0,83	60,00	2.542	2.200
K^+	0,74	3,3	0,36	0,83
Sr^{2+}	-	<0.03	-	0,23
Fe	-	0,67	-	<0.03
SiO_2	-	4,49	-	0,68
B^{3+}	-	0,25	-	<0.03
Si	-	2,1	-	0,32
pH	5,7	7,3	6,9	6,1
I.S. (mol/L)	$1.7 \cdot 10^{-4}$	$4.5 \cdot 10^{-3}$	0,23	0,20
E.N. (%)	29	-9	1	-4

Table 9. Initial and final composition of the hydration water of cells HT1 and HT2 (units in mg/L, I.S.: ionic strength, E.N.: electronegativity)

9.2 DRY DENSITY AND WATER CONTENT

9.2.1 METHODOLOGY

The gravimetric water content (*w*) is defined as the ratio between the mass of water and the mass of dry solid expressed as percentage. Consequently, all the values given in this report are weight percentages. The mass of water was determined as the difference between the mass of the sample and its mass after oven drying at 110 ˚C for 48 hours (mass of dry solid). The samples used for the water content determination had masses between 6 and 23 g, with an average of 13±4 g for cell HT1 and 12±5 g for cell HT2.

Dry density (ρ_d) is defined as the ratio between the mass of the dry sample and the volume occupied by it prior to drying. The volume of the specimens was determined by immersing them in a recipient containing mercury and by weighing the mercury displaced, considering a density of mercury of 13.6 g/cm^3. The absolute error of this measurement is in the order of 10^{-2} g/cm^3. The volume of the samples used for this determination ranged between 5 and 12 cm^3, with an average of 10±2 cm^3 for cell HT1 and 8±2 cm^3 for cell HT2. The same samples whose volumes had been determined were used for an additional water content determination. However, this value was only used as a cross-check and is not presented here.

The balance used was an AND GF2000, with a capacity up to 2,100 g and a precision of 0.01 g.

9.2.2 RESULTS

The results of water content and dry density for the internal and external subsamples of each section are shown in Table 10 for block HT1 and Table 11 for block HT2. In each section two kinds of subsamples were considered: external (e) and internal (i), corresponding to the part in contact with the cell wall and the core one (Figure 107). The degrees of saturation (S_r) have been computed considering a water density of 1 g/cm^3 and a density of solid particles of 2.82 g/cm^3. The weighted average values of water content have been computed considering the dry density of each section. It was difficult to take samples for water content, and especially dry density, determinations in cell HT2; for this reason, it was not possible to obtain external and internal parts of each section. In some sections the sample obtained did not clearly correspond to the internal or external parts, and those are the samples labelled as “Ind” in Table 11 . Other samples were suitable for water content determination but not dry density.

SECTION	DISTANCE TO HEATER (cm)	EXTERNAL w (%)	INTERNAL w (%)	EXTERNAL ρ_d (g/cm^3)	INTERNAL ρ_d (g/cm^3)	EXTERNAL S_r (%)	INTERNAL S_r (%)
1	9,0	32,8	36,1	1,41	1,36	93	95
2	7,0	27,1	33,1	1,50	1,39	87	91
3	5,0	23,8	24,8	1,61	1,61	90	93
4	3,0	23,5	22,1	1,63	1,65	91	88
5	1,0	23,7	21,2	1,64	1,67	92	87
Average	-	26,2	27,5	1,56	1,54	91	91
Weighted average[a]	-	26,0	27,0	-	-	91	91
Average[b]	-	26,6	-	1,55	-	91	-

Table 10. Final water content and dry density at different sampling positions of block HT1 (a considering the density of each section; b weighted average considering the volume of external and internal parts)

SECTION	DISTANCE TO HEATER (cm)	INT w (%)	EXT w (%)	INT w (%)	INT ρ_d (g/cm^3)	EXT ρ_d (g/cm^3)	INT ρ_d (g/cm^3)	S_r (%)	EXT S_r (%)	INT S_r (%)
1 sup	9,5	34,5	-	-	1,41	-	-	97	-	-
1	9,0	-	31,9	-	-	1,44	-	-	94	-
1 inf	8,5	31,3	-	-	1,48	-	-	97	-	-
2	7,0	-	27,6	27,6	-	1,53		-	92	-
3	5,0	25,8	-	26,0	1,55	-	1,58	89	-	94
3-4	4,0	-	23,6	-	-	-	-	-	-	-
4	3,0	9,8	17,5	-	1,66	1,62	-	39	66	-
5	1,0	2,3	-	-	1,67	-	-	10	-	-

Table 11. Final water content and dry density at different sampling positions of block HT2 (Ind: indistinct; Ext: external; Int: internal)

As discussed below, the values for cell HT2 are likely affected by the amount of salt accumulated during operation, because of the continuous saline water supply and leakage through sensors openings. Since there is not a straightforward way of telling apart dry soil from salt content, the latter is inaccurately considered as soil mass in the final computation of dry density and water content. This would have caused to compute higher dry densities and lower water contents than the actual ones for cell HT2.

Figure 108 and Figure 109 show the final water content and dry density values along the bentonite blocks of cells HT1 and HT2, respectively. There were relevant gradients between top and bottom of the blocks both in terms of water content and of dry density, particularly in the case of HT2. In cell HT1 the water content increased from the hydration surface to approximately the middle of the column whereas the dry density decreased. Then both parameters remained almost constant in the lower half of the block. In contrast, in cell HT2 the water content continuously decreased from top to bottom whereas the dry density increased, with much sharper gradients than in cell HT1. The top parts of the two blocks had water contents well above 30 % and dry densities around 1.4 g/cm^3, which reveals the swelling of the part of the blocks that was first saturated.

There were significant differences between the external and internal parts of each section in cell HT1: in the upper part of the block the water content of the external part was lower than that of the internal part and consequently, the dry density was higher. In the bottom half of the block it was the other way round, but the differences between external and internal parts were smaller than in the upper part of the block. Although no clear patterns can be established in cell HT2, the few data available are consistent with those found in cell HT1.

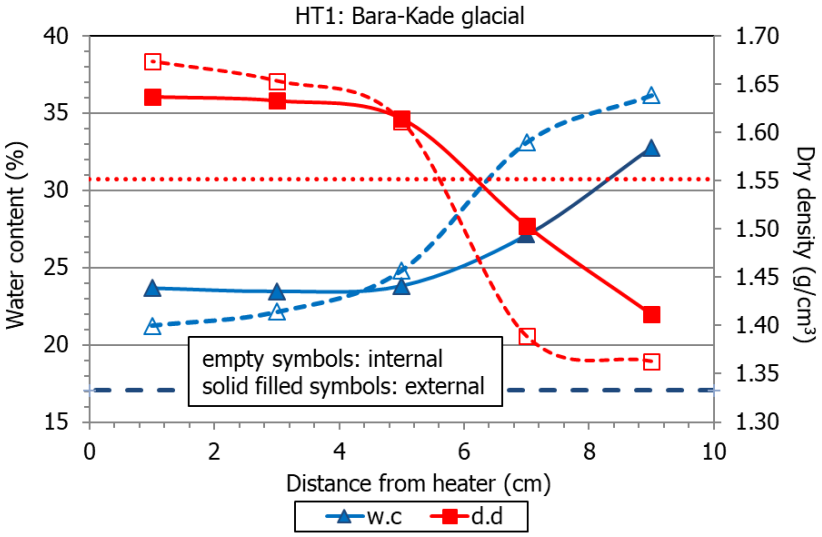

Figure 108. Final water content (w.c.) and dry density (d.d.) in external and internal parts of the sections of cell

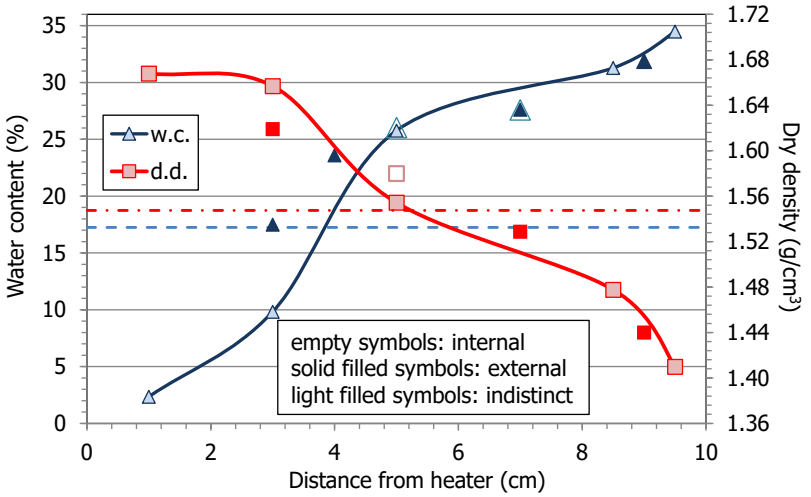

Figure 109. Final water content (w.c.) and dry density (d.d.) in external, internal and indistinct parts of the sections of cell HT2

A direct comparison of the results obtained in the two cells is shown in Figure 110: the water content in the upper half of the two blocks was similar but greatly differed in the 4 cm closest to the heater. As for the dry densities, it is remarkable that the overall dry density seems to be higher for block HT2, although the initial bentonite dry density was the same in the two cells (Table 5). This is likely a consequence of the increase of salt content during operation because of hydration with highly saline water and continuous evaporation until all the leaks were sealed and the RH/T removed. In fact, the water that left the hydration vessel was ~578 g, whereas the weight increase of the bentonite block was of only 88 g (Figure 85). This means that a large quantity of water entered the cell and evaporated, but the salt would have remained inside (see subchapter 8.2 for a rough computation of this quantity). This was already observed in another set of related tests using the same setup and saline water (Villar et al. 2023).

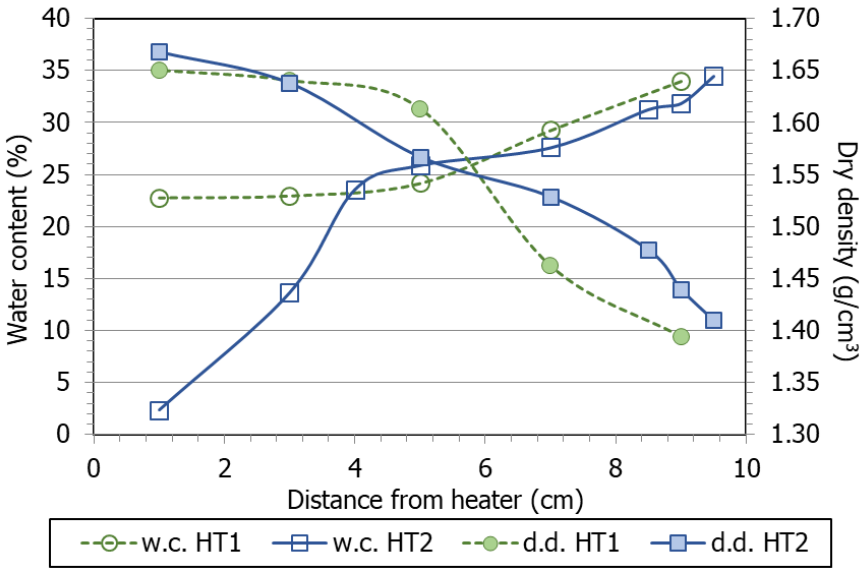

Figure 110. Water content and dry density (average values per section) along the bentonite blocks of cells HT1 and HT2

Figure 111 shows the final degree of saturation for the two cells. In the upper half of the blocks the degree of saturation was homogeneous and higher than 90 % (slightly higher for cell HT2, in agreement with the inaccurate higher dry densities computed because of hydration with saline water). In the bottom half of cell HT1 the degree of saturation kept high and constant. In contrast, in cell HT2 the degree of saturation in the lower half of the block sharply decreased towards the heater, reflecting the sharp decrease in water content (Figure 109).

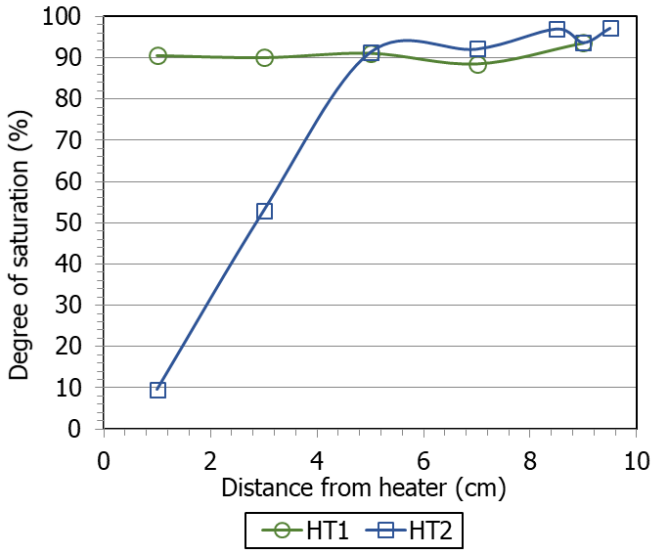

Figure 111. Final degree of saturation in cells HT1 and HT2

Figure 112 relates the final pressure values measured by the sensors in cell HT1 (Figure 84) to the final dry density and water content of the bentonite measured at the same level. The lowest

value (measured by sensor PT13 at the bottom of the cell) corresponds to an area where the dry density was high, but the water content was lower than in the rest of the block. The highest pressure was measured in the middle part of the cell, where the density was highest, although the water content was lower than in the upper part. This would indicate that, for samples that had remained very close to full saturation for a long time, pressure developed completely in accordance with the dry density; whereas in areas where saturation was slightly lower or had not been high for so long, pressure had not reached yet the equilibrium value corresponding to the dry density in the area.

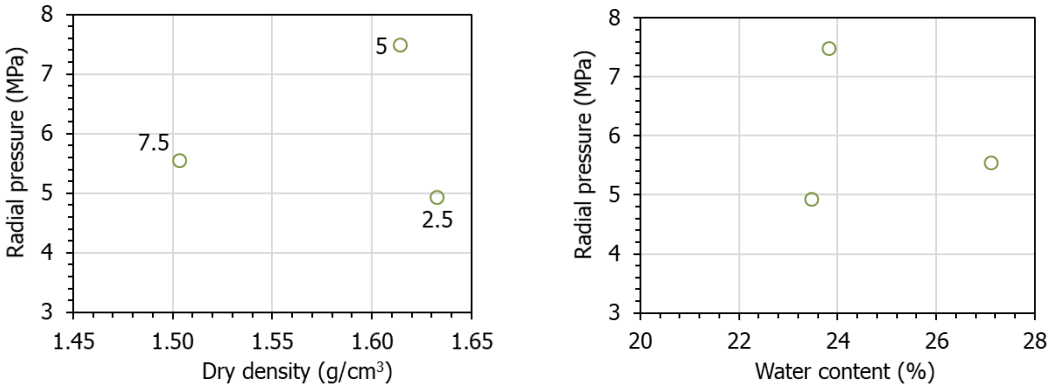

Figure 112. Final pressure measured by sensors in cell HT1 as a function of the final dry density and water content measured at the same locations (the distance of the sensor to the heater is indicated in cm)

10 COMPARISON WITH TESTS AT LOWER TEMPERATURE

As explained in the Introduction, tests HT1 and HT2 were performed in the same setup used in a previous research, the MAB (Mineralogical Alteration of Bentonite) project, carried out in collaboration with Amphos 21 for Posiva, the Finnish nuclear waste agency. In the framework of this project two tests were performed following the same procedures and using Wyoming-type bentonite (MX-80 instead of Barakade) compacted with the same initial conditions (reported in Villar et al. 2020). The bentonite was hydrated using the same solutions as in cells HT1 and HT2 (glacial for test C5 and saline for test C4), and the hydration phase lasted 2.5 years, as for the cells reported here. However, in those tests the heater temperature was set to 110 ˚C (with an initial period at 90 ˚C). Hence the only difference between the two sets of tests (C4-C5 and HT1-HT2) was the heater temperature. Consequently, the comparison between them can help to identify the effect of high temperature on the THM behaviour of the bentonite. A summary of the characteristics of both set of tests is given inTable 12.

TEST	HT1	HT2	C5	C4
Heating phase *T* (°C)	150	150	90	90
Heating phase duration (days)	91	99	132	54
Hydration solution	Glacial	Saline	Glacial	Saline
Hydration phase duration (days)	967	853	329 (90 ˚C) + 602 (110 ˚C)	490 (90 ˚C) + 448 (110 ˚C)

Table 12. Characteristics of the two sets of tests performed

TEST	HT1	HT2	C4	C5
Bentonite	Barakade	Barakade	MX-80	MX-80
Initial water content (%)	17,1	17,2	17,7	17,1
Sample mass (g)	1.422	1.425	1.451	1.442
Compaction pressure[a] (MPa)	8,5	8,2	9,2	10,2
Sample mass after drilling (g)	1.399	1.400	1.423	1.413
Theoretical dry mass (g)	1.195	1.194	1.209	1.207
Dry density (g/cm^3)	1,55	1,55	1,57	1,56
Porosity	0,449	0,451	0,437	0,437
Void ratio	0,816	0,822	0,775	0,777
Degree of saturation (%)	59	59	64	61

Table 13. Characteristics of the bentonite samples of the two sets of tests after compaction (a Average value for the five layers)

The granular bentonite was mixed with deionised water to reach the target initial water content of 17 % and it was compacted to a dry density of 1.57 g/cm^3 following the procedure described in subchapter 4.2. The characteristics of the blocks obtained are shown in Table 13, and the dry densities along the blocks as computed from the weight and dimensions of each of the five layers are plotted in Figure 113.

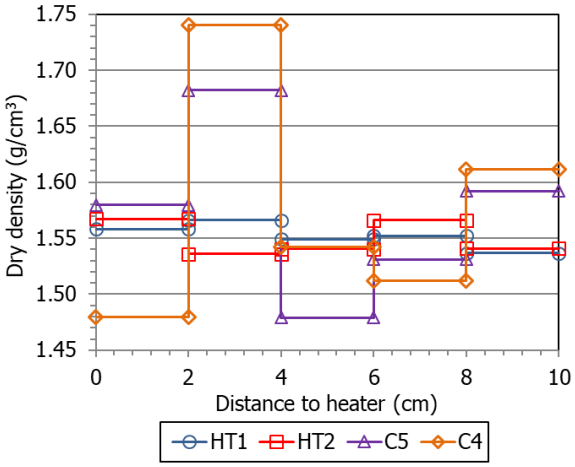

Figure 113. Estimated initial dry densities along the bentonite blocks of the two sets of tests

10.1 THERMO-HYDRO-MECHANICAL EVOLUTION

During the heating phase the temperature of the heater in cells C4 and C5 was set at 90 °C, hence the steady temperatures at the end of this phase were considerably different between the two sets of tests (Figure 114). Consequently, the movement of water vapour was much more intense in the cells with heater at 150 °C, and at the end of the heating phase, the relative humidity in the upper half of the blocks was higher in cells HT1 and HT2, and in fact the top RH sensors in these cells were flooded at the end of the heating phase. This was reflected in transient radial pressure build-up (Figure 80) that was not observed in the cells heated at lower temperature.

In cells C4 and C5, the heater temperature was increased to 110 °C after hydration had been going on for 329 and 490 days, respectively. The steady temperatures inside the bentonite and on the cell surface after the increase in heater temperature are shown in Figure 114 (right).

As hydration started, the relative humidity in the middle part of the blocks increased more quickly in tests HT1 and HT2, in which it was already higher (Figure 115), and the sensors in the area were flooded earlier than in the tests performed at lower temperature (Figure 116, Figure 117). Also at the bottom of the cells the relative humidity increased more quickly and sharply in the tests under higher temperature. However, the initial water intake was slightly lower in the

tests under higher temperature, but after ~80 days the rate was very similar in both sets of tests (Figure 118). As it had been observed in all the tests performed within the MAB project (Villar et al. 2023), the water intake was higher in the cells saturated with glacial water, irrespective of the temperature. After the overheating event in cells HT1 and HT2 the water intake measurements reflected also leaks through the cell elements and are not comparable with the measurements in cells C4 and C5. In these cells there was a discrepancy between the actual water intake and the weight recording of the vessel of about 100 g (Villar et al. 2020), whereas in the case of tests HT1 and HT2 it was of ~500 g (Figure 85). This water was probably entering the cells, but it evaporated once inside through the sensors' inlets.

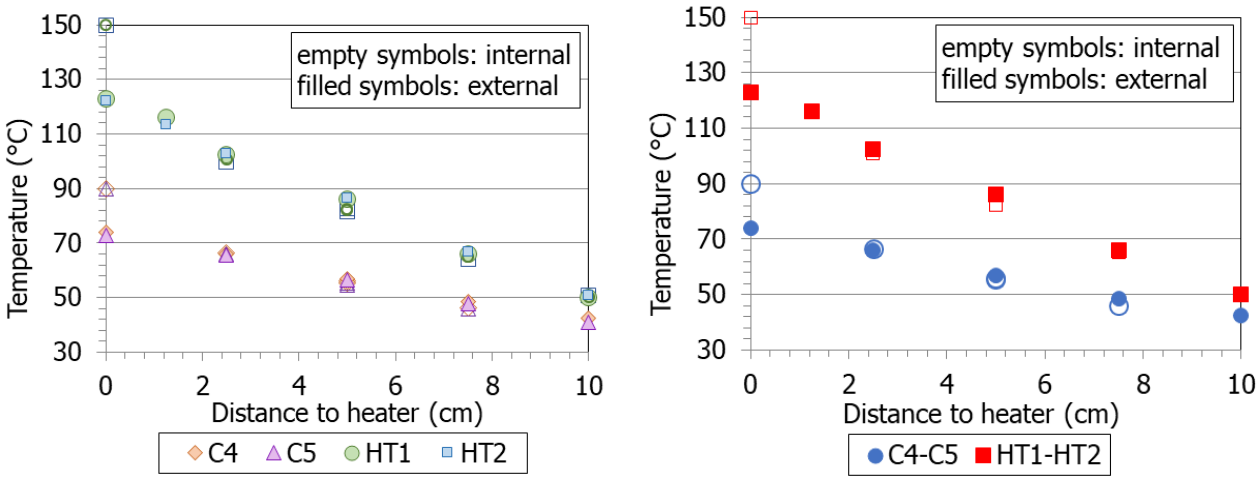

Figure 114. Steady external and internal temperatures during the heating phase of the two sets of tests (left, heater T in HT1-HT2: 150 ˚C; in C4-C5: 90 ˚C), and during the hydration phase (right, heater T in HT1-HT2: 150 ˚C; in C4-C5: 110 ˚C)

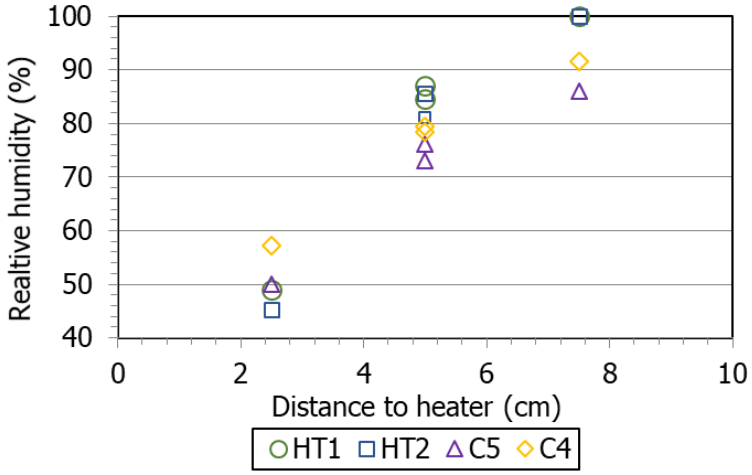

Figure 115. Relative humidity of the bentonite at the end of the heating phase of the two sets of tests (heater T in HT1-HT2: 150 ˚C; in C4-C5: 90 ˚C)

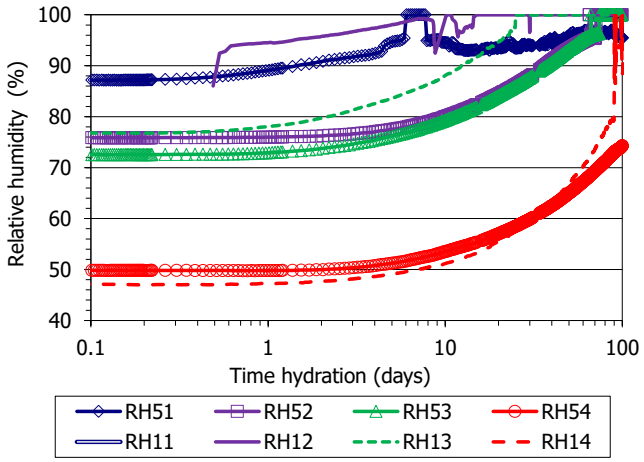

Figure 116. Evolution of relative humidity at the beginning of the hydration phase in the cells saturated with glacial water. Sensors RH5x in cell C5, sensors RH1x in cell HT1. Heater T in HT1: 150 °C, in C5: 90 °C

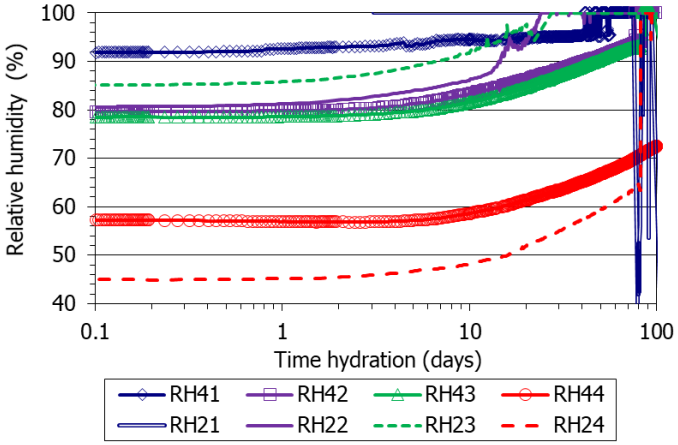

Figure 117. Evolution of relative humidity at the beginning of the hydration phase in the cells saturated with saline water. Sensors RH4x in cell C4, sensors RH2x in cell HT2. Heater T in HT2: 150 °C, in C4: 90 °C

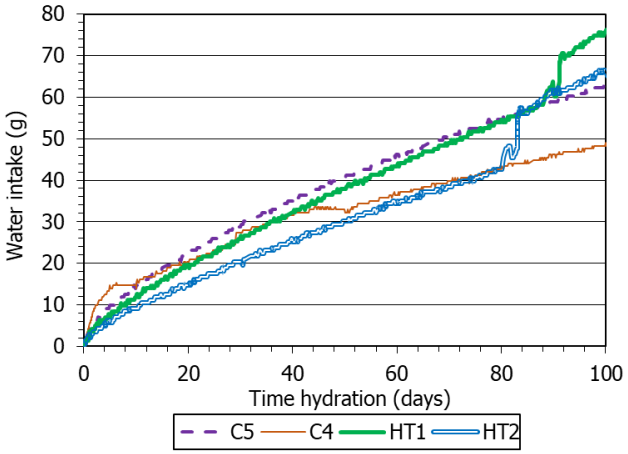

Figure 118. Water leaving the hydration vessels at the beginning of tests performed under different thermal gradient (heater T in HT1-HT2: 150 °C, in C4-C5: 90 °C)

Figure 119 and Figure 120 show the evolution of radial pressure at the beginning of hydration for the tests with glacial and saline water, respectively. Beyond that time it is not straightforward to compare the two sets of tests because of the overheating occurred in the HT cells (described in 7.1.3.1 and 7.2.3.1), which affected irreversibly the evolution of pressure. Nevertheless, the radial pressures measured until the end of the tests performed with glacial water is shown in Figure 121. In the first stage of hydration radial pressure developed faster in the tests hydrated with glacial water, and for a given water salinity, they built up faster at higher temperature and reached higher values. Despite the different events in the HT cells that altered the natural evolution of radial pressure, the values reached at the end of test HT1 were higher than those reached in test C5, except close to the heater (Figure 122).

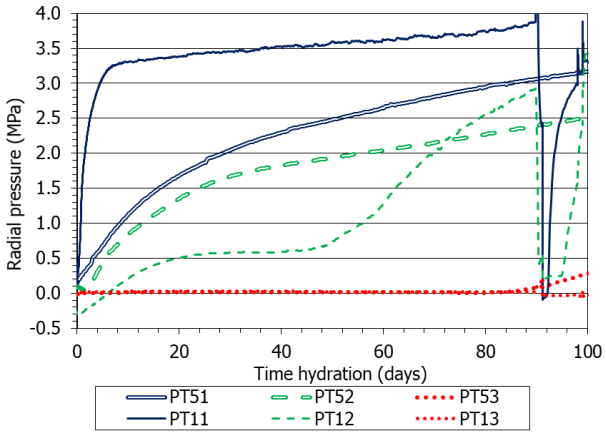

Figure 119. Evolution of radial pressure at the beginning of the hydration phase in the cells saturated with glacial water. Sensors PT5x in cell C5, sensors PT1x in cell HT1. Heater T in HT1: 150 °C, in C5: 90 °C

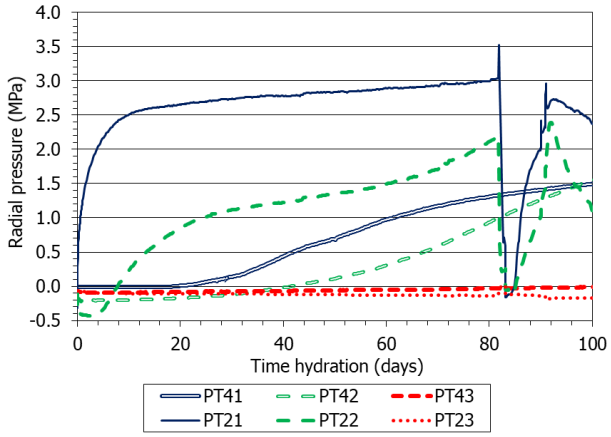

Figure 120. Evolution of radial pressure at the beginning of the hydration phase in the cells saturated with saline water. Sensors PT4x in cell C4, sensors PT2x in cell HT2. Heater T in HT1: 150 °C, in C5: 90 °C

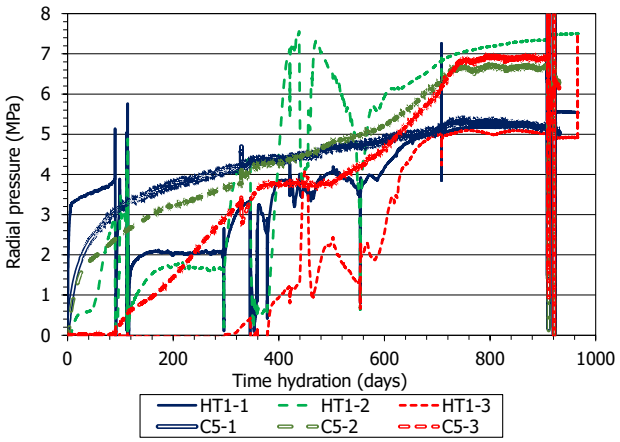

Figure 121. Evolution of radial pressure during the whole hydration phase in the cells saturated with glacial water. Sensors 1 at 7.5 cm from the heater, sensors 2 at 5 cm from the heater, sensors 3 at 2.5 cm from the heater. Heater T in HT1: 150 ℃, in C5: 90 ℃ (until day 329)-110 ℃

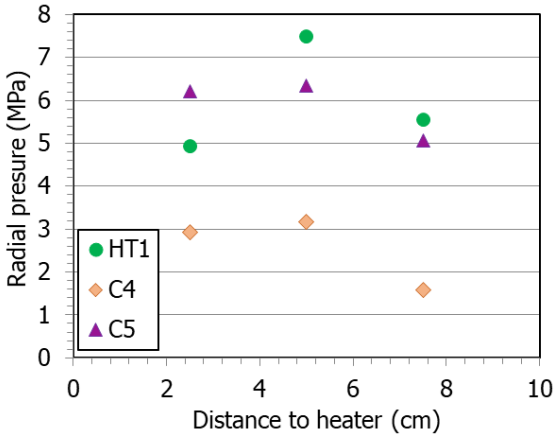

Figure 122. Radial pressures after 2.5 years of hydration in different tests

10.2 FINAL STATE

When the cells were dismantled after 2.5 years of hydration under thermal gradient, except for test HT2, all the bentonite blocks were consistent and looked homogeneous. The main difference among them was the abundance of corrosion stains, internal and external, in block HT1 (Figure 123). Block HT2 looked considerably different, not only because of the red, black and white stains, but also because the bottom part was very dry and inconsistent. Likely, this would have not been the case if the overheating event and resulting leaks had not occurred. In fact there were no significant differences among the final water contents of the three other cells, although they were higher towards the hydration surface and lower towards the heater in cell HT1 (Figure 124), pointing perhaps to a more difficult saturation of the areas submitted to higher temperature. This was more accentuated in cell HT2, in which the leaks through the sensors hindered the saturation of the lower half of the block. The dry density gradient at the

end of the tests was steeper in the two tests performed under higher temperature, mainly because of the significant reduction in dry density close to the hydration surface, which can be related to the higher initial swelling resulting from the quicker relative humidity increases in the area (Figure 116, Figure 117). The final degree of saturation was homogeneously high in all cells except HT2 (Figure 126).

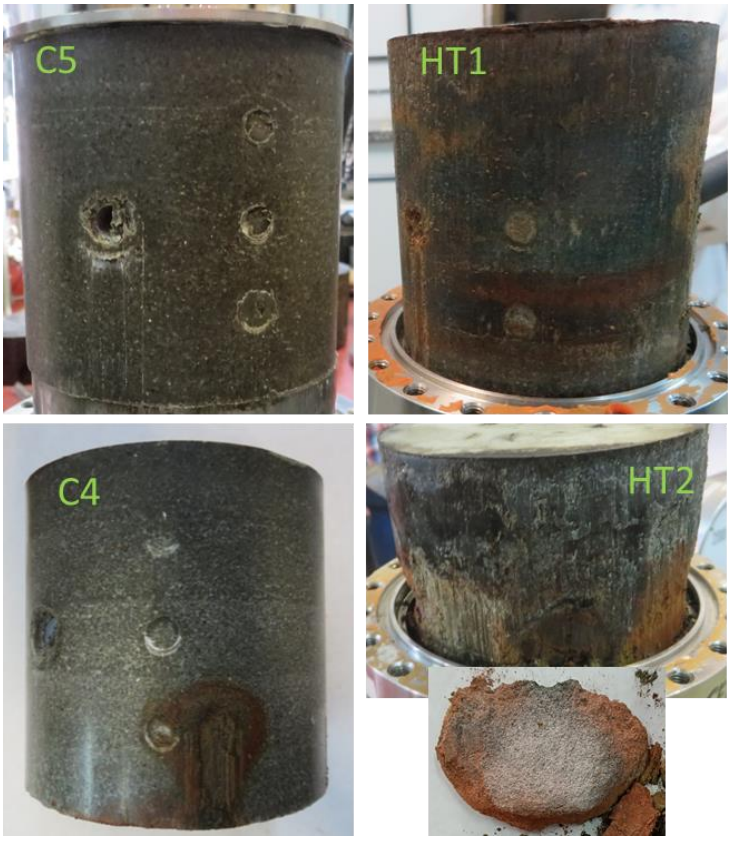

Figure 123. Final appearance of the four cells hydrated for 2.5 years

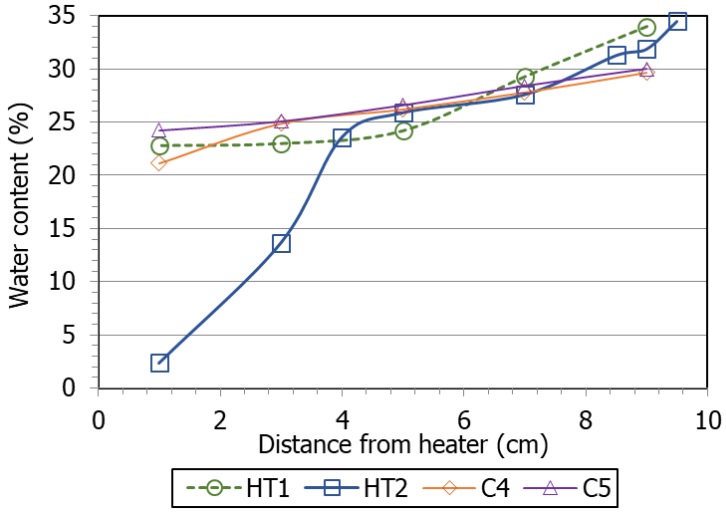

Figure 124. Final water content along the bentonite blocks of tests performed under different thermal gradients (heater T in HT1-HT2: 150 °C, in C4-C5: 90 °C)

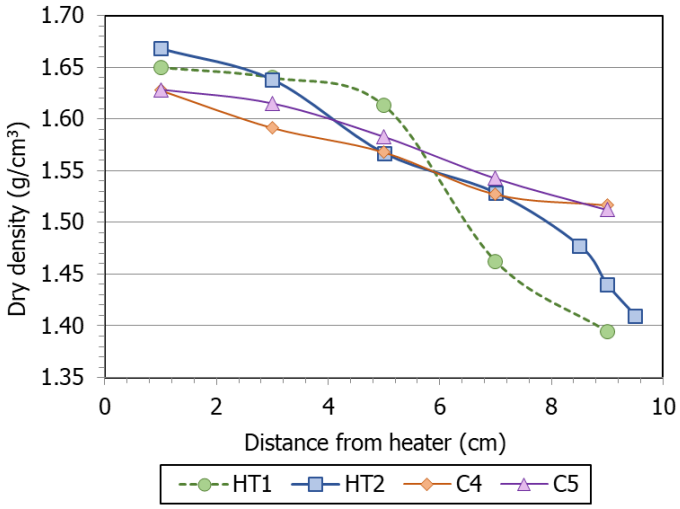

Figure 125. Final dry density along the bentonite blocks of tests performed under different thermal gradients (heater T in HT1-HT2: 150 °C, in C4-C5: 90 °C)

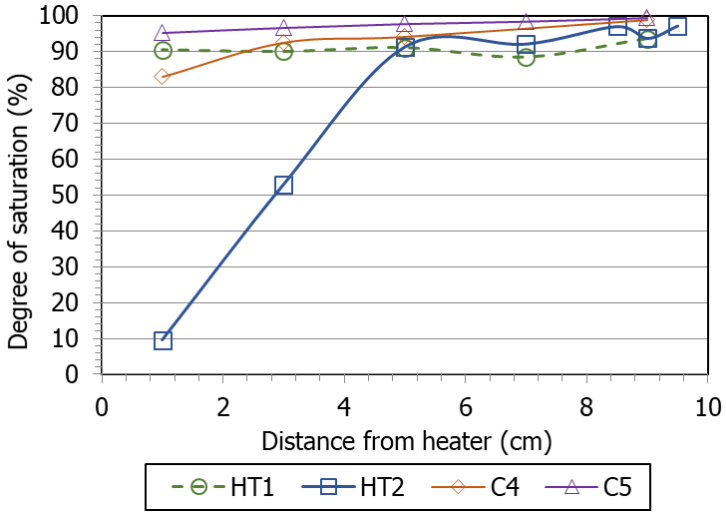

Figure 126. Final degree of saturation along the bentonite blocks of tests performed under different thermal gradients (heater T in HT1-HT2: 150 °C, in C4-C5: 90 °C)

11 SUMMARY AND CONCLUSIONS

Two thermo-hydraulic tests were carried out in stainless steel cylindrical cells using Barakade bentonite compacted to a dry density of 1.55 g/cm^3 with a water content of ~17 % (HT1 and HT2). The cells were instrumented with relative humidity (RH/T), temperature and pressure sensors. At the bottom of the cells, a heater was placed and set initially at 150 ˚C. The temperatures inside the bentonite quickly stabilised, defining an almost linear thermal gradient (7 ˚C/cm) across the length of the blocks. The temperatures measured at the same distance from the heater either inside the bentonite or on the surface of the cells were very similar. The relative humidity close to the heater and in the middle part of the block decreased, because of the water vapour transport to cooler areas. Opposite to the heater, relative humidity continuously increased, triggering a transient increase in radial pressure. The relative humidity gradient at the end of the heating phase, which lasted three months, was very steep and similar in the two cells, with relative humidity of 100 % at least in the 2.5 cm closest to the hydration surface.

Afterwards, hydration of the bentonite through a porous filter placed on the surface of the block opposite to the heater started with water coming from a vessel hanged 1 m above the cells. The composition of the water in cell HT2 reproduced that of saline groundwater, mainly containing chloride, sodium and calcium, whereas in cell HT1 quite dilute glacial water was used. During the hydration phase, the temperatures barely changed. The relative humidity inside the bentonite increased very quickly along the axis of the bentonite blocks, and the sensors in the middle part of the cells recorded 100 % after a few days. This rapidity could suggest that some water transport took place along the cells' wall. An overheating event, during which the temperatures inside the bentonite increased to values between 120 and 150 ˚C, took place 80-90 days after the beginning of hydration. As a result of it, no more information on relative humidity was obtained because the sensors were flooded or damaged, and vapour leaks through the sensors inlets were triggered, which hindered the proper online measurement of water intake. The RH/T sensors had to be eventually removed to effectively seal the inlets.

The pressure at the bentonite/cell interface built up progressively from top (hydration surface) to the middle part of the columns, delayed with respect to the RH changes. Before the overheating event the pressure lineally decreased from top to bottom in the two cells, but was slightly lower in the one hydrated with saline water. After the overall decrease in radial pressure following the overheating event, the pressure measured in cell HT2 never increased above these values. In contrast, they increased in cell HT1 and reached considerably high values through all the column, particularly in the middle part. The pressure recorded by all sensors was very much affected by the changes in temperature caused by blackouts, likely because of

the water leaks through the sensors' inlets prompted by sudden heating-cooling of the system, and by the actions taken to seal leaks, which resulted in pressure increases. Hence, final values between 5 and 7.5 MPa were measured in cell HT1. The final assessment of these values indicates that, in areas that had remained very close to full saturation for a long time (upper half of the bentonite block), pressure developed completely in accordance with the dry density; whereas in areas where saturation was slightly lower or had not been high for so long (bottom of the blocks), at the end of the tests pressure had not reached yet the equilibrium value corresponding to the dry density in the area (or else, could not develop further because of the higher temperature).

The water leaks also caused that the online measurement of water intake did not correspond just to the amount of water taken by the bentonite, but to the amount that entered the cell and either remained inside or left the cell. The discrepancy between online measurements and actual water intake was of the same order for the two cells.

After 2.5 years of hydration the heaters were switched-off and after a short cooling period the cells were dismantled. The bentonite blocks were extracted, weighed, measured and cut into five sections to obtain samples for the different postmortem determinations that will be reported elsewhere. The block from cell HT1 had a consistent state, with no cracks, but in cell HT2, the bottom half of the block was very dry and brittle, so the 4 cm closest to the heater were difficult to sample. The two blocks showed internal and external corrosion stains and halos and crusts around the sensors, particularly in cell HT2.

The two cells presented water content and dry density gradients at the end of operation, steeper in the case of cell HT2. The water content in the upper half of the two blocks was similar but greatly differed in the 4 cm closest to the heater, where the block of cell HT2 was much drier. The overall final dry density was higher for block HT2, which is likely a consequence of the increase of salt content during operation because of the hydration with highly saline water and continuous evaporation until all the leaks were sealed. In the upper half of the blocks the degree of saturation was homogeneous and higher than 90 %, but whereas in the bottom half of cell HT1 the degree of saturation kept high and constant, in cell HT2 the degree of saturation in the lower half of the block sharply decreased towards the heater (reflecting the sharp decrease in water content). It is considered that this difference was caused by the worst performance of cell HT2 (likely because the saline water under high temperature was very aggressive and damaged more the cell elements, promoting continuous evaporation), but not by the incapability of the bentonite to reach full saturation when saline water is used.

The comparison with similar tests performed under lower temperature (tests C4 and C5, heater set at 110 °C) showed that the movement of water vapour during the initial heating phase was

much more intense in the cells under higher temperature, and at the end of it, the relative humidity in the upper half of the blocks was higher in cells HT1 and HT2. When hydration started, the relative humidity in the middle and bottom part of the bentonite blocks increased more quickly in tests HT1 and HT2. The water intake rate until the overheating event mentioned above was very similar in both sets of tests. The water intake was higher in the cells saturated with glacial water, irrespective of the temperature, which was unexpected (but already observed in previous related investigations), given the higher permeability to saline water. In the first stage of hydration, radial pressure developed faster in the tests hydrated with glacial water, and for a given water salinity, it built up faster at higher temperature and reached higher values. Despite the different events in the HT cells that altered the natural evolution of radial pressure, the values reached at the end of test HT1 were higher than those reached in test C5, except close to the heater.

The final degree of saturation was homogeneously high in all cells, except HT2. There were no significant differences among the final water contents of the three other cells, although they were higher towards the hydration surface and lower towards the heater in cell HT1, pointing to a more difficult saturation of the areas submitted to higher temperature. This was more accentuated in cell HT2, in which the leaks through the sensors hindered the saturation of the lower half of the block. The dry density gradient at the end of the tests was steeper in the two tests performed under higher temperature, mainly because of the significant reduction in dry density close to the hydration surface, which can be related to the higher initial swelling resulting from the quicker relative humidity increases in the area.

These results indicate that the increase of temperature to values in the bentonite higher than 100 °C does not hinder saturation, neither the development of swelling pressure to the same values expected for lower temperatures. However, the final inhomogeneity of the barrier can be enhanced by saturation under higher temperature. The comparison between the final appearance of the bentonite saturated under different temperatures suggests that corrosion and alteration processes would be more intense under higher temperature, but this will have to be confirmed by the postmortem chemical and mineralogical analyses.

12 REFERENCES

[1] Hellä, P., Pitkänen, P., Löfman, J., Partamies, S., Vuorinen, U., Wersin. P. 2014. Safety Case for the Disposal of Spent Nuclear Fuel at Olkiluoto. Definition of Reference and Bounding Groundwaters, Buffer and Backfill Porewaters. POSIVA 2014-04.

[2] Idiart, A., Villar, M.V., Martín, P.L., Gutiérrez-Álvarez, C., Iglesias, R.J., Pękala, M., Korkeakoski, P., Vuorio M. 2017. Laboratory experiments of thermo-hydro-geochemical evolution of compacted bentonite. 7th International Conference on Clays in Natural and Engineered Barriers for Radioactive Waste Confinement, Davos. Book of Abstracts, pp 559-560.

[3] Martín, P.L., Gutiérrez-Álvarez, C., Barcala, J.M., Iglesias, R.J., Villar, M.V., Melón, A.M. 2017. Project MINALBEN. Experimental procedures. Preparation of the experimental setup and initiation of tests in cells. Informe Técnico CIEMAT/DMA/2G219/1/17. Madrid, 34 pp.

[4] Schatz, T. 2011. Preparation of Posiva Reference Solutions. Standard Operating Procedure SOP-L-PRS v. 3.0. B+TECH. 9 pp.

[5] Villar, M.V., Gutiérrez-Álvarez, C., Iglesias, R.J., Martín, P.L. 2020. Project MINALBEN. Report on dismantling of cells running for 2.5 years (C3, C4 and C5). Technical Report CIEMAT/DMA/2G219/1/20. Madrid, 84 pp.

[6] Villar, M.V., Gutiérrez-Álvarez, C., García-Herrera, G., Iglesias, R.J., Martín, P.L., Barcala, J.M. 2023. Project MINALBEN. Online evolution and final state of cells running for 5 years (C6, C7 and C8). Technical Report CIEMAT/DMA/2G219/1/23. Madrid, 64 pp.


2695-8864